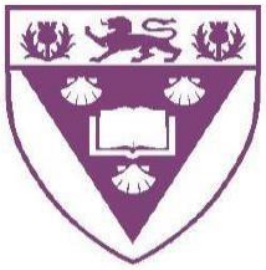

RHODES UNIVERSITY

Grahamstown • 6140 • South Africa

Mineralogical, Geochemical and Lead Isotopic Analysis of the Lead Mineralization of the Skorpion Deposit, South Western Namibia

By

Kakunauua Uazeua

A thesis submitted in partial fulfilment of the requirements for the degree of
Master of Science (Cwk/Thesis)
(Economic Geology)
MSc Exploration Geology Programme
Geology Department
Rhodes University
P.O. Box 94
Grahamstown 6140
South Africa

12 February 2018

Acknowledgements

Firstly, I would like to thank the Almighty for giving me the necessary strength, persistence and confidence I needed throughout this endeavor. I would also like to thank my son, Mbazuvirua Uazeua, for being Mommy's motivation. This MSc is dedicated to you.

On an academic level, I would like to thank my supervisor Prof Steve Prevec for the significant contribution to the attainment of this degree as well as my co-supervisor Prof Jock Harmer for the valued assistance. Lastly, I would like to thank Ashley Goddard for always being a helping hand that never wearies as well as Rhodes University for access to the Electron Microprobe (partially funded by NRF National Equipment Program grant UID 74464).

A special thanks goes out to Mr. Callum Kerr, Mr. Stefanus Sitoka and Mr. Cedric Joseph for encouraging me to conduct this study and thereby add value to the Skorpion Zinc Deposit knowledge base. Additionally, gratitude is due to the Skorpion Zinc 2014 Exploration team for their assistance with sample collection which was quite a laborious job.

Lastly, thanks is due to my parents, Adronikus and Rudolfine Uazeua and my siblings for your valuable support during my studies.

Declaration

I, Kakunauua Uazeua, declare this thesis to be my own work except where due acknowledgement has been made. It is submitted in partial fulfillment of the Degree of Master of Science at Rhodes University. It has not been submitted before for any degree or examination in any other University or tertiary institution.

Signature of the candidate: …….

Date: ……

Abstract

The Skorpion none-sulphide Zinc Deposit is located in the para-autochtonous Port Nolloth Zone of the Gariep Belt, which overlays the Lower-Proterozoic Orange River Group basement rocks (Corrans et al., 1993). Situated in close proximity to the larger Rosh Pinah Zn-Pb deposit, the Skorpion Deposit contained a resource of 24.6 Mt at 10.6 % Zn and unquantified Cu and Pb prior to mining. To date, zinc has been the only metal exploited, with minor amounts of copper as a by-product.

This study aims at understanding the mineralogical composition of the Skorpion lead mineralization and understanding the relationship between lead and the major metals such as zinc and copper in order to form a basis for further work that could determine the potential of processing lead as a by-product.

As part of the study, work was also done on lead isotopes mainly with the aim of understanding the mineralization genesis and to determine the differences between the Skorpion and Rosh Pinah deposit which rationalize the inferior economic potential of the Skorpion lead mineralization.

Results of the study have shown that majority of the lead mineralization is hosted by the felsic metavolcanics as galena and subordinately in the metasiliciclastics as pyromorphite, a lead manganese phosphate. In terms of the mineral textures, the lead minerals appear to be mainly secondary phases that have been remobilized and reprecipitated around pyrite, within pyrite cracks and intergrown with minerals such as chalcocite and greenockite. Lead has been mainly concentrated along fault zones. The elevated pyromorphite concentrations tend to occur within gossanous zones in close association with iron and manganese oxides. These textures represent supergene enrichment of a sulphide proto ore. However, contrary to copper and zinc mineralization, lead was not remobilized far from the proto ore merely as a function of its poor mobility in acidic fluids (Reddy et al., 1995). This substantiates the concentration of secondary lead in the felsic metavolcanics and to a much lesser extent, in the metasiliciclastics. Both secondary zinc and copper were reprecipitated in the metasiliciclastics, further away from the sulphide proto ore, hosted mainly by the felsic metavolcanics.

The average lead isotope ratios of $^{206}Pb/^{204}Pb$ (17.26), $^{207}Pb/^{204}Pb$ (15.60) and $^{208}Pb/^{204}Pb$ (37.42) resemble results provided by Frimmel (2004) for both the Skorpion and Rosh Pinah deposits. For the Skorpion samples from Frimmel (2004) had the following average ratios: $^{206}Pb/^{204}Pb$ (17.29), $^{207}Pb/^{204}Pb$ (15.59) and $^{208}Pb/^{204}Pb$ (37.51). The Rosh Pinah samples had the following average ratios: $^{206}Pb/^{204}Pb$ (17.17), $^{207}Pb/^{204}Pb$ (15.61) and $^{208}Pb/^{204}Pb$ (37.45). These results indicate lead derivation from the lower 2.0 Ga Eburnean pre-Gariep basement in agreement with and Frimmel et al. (2004). The host felsic metavolcanics might have been derived from melting of the basement rocks during the formation of the Adamastor Ocean. In comparison to the Rosh Pinah deposit lead isotope signatures, the Skorpion lead isotopes overlap with the Rosh Pinah deposit isotopes, but have a much narrower range. This is an indication of a much shorter lived and potentially faster mineralization event contrary

to the SEDEX type Rosh Pinah deposit. The smaller tonnage of the Skorpion deposit, its inferior lead concentrations and the elevated radiogenic lead isotopes point toward a VMS deposit which was formed in a small graben fed by shallow conduits during a short lived mineralization event. Sedimentary rocks covered the forming deposit at a fast rate and impaired the deposit advancement. The interaction between the upper crustal rocks and the mineralizing fluids is what may have resulted in the elevated radiogenic lead signature. In contrast to this, SEDEX deposits such as the Rosh Pinah Deposit, are generally fed by deep seated conduits that allow more longer lived leaching of metals from the underlying basement rocks and generally allow minor influence from upper crustal rocks.

Table of Contents

List of Figures

List of Tables

List of Abbreviations

BSE – Backscattered Electron

Co. Ltd – Company Limited

EMPA – Electron Microprobe Analysis

ICP-AES – Inductively Coupled Plasma Atomic Emission Spectroscopy

ICP-MS - Inductively Coupled Plasma Mass Spectrometry

LME – London Metal Exchange

Ma – Million Annum

Mt – Million Tonnes

SEDEX – Sedimentary Exhalative

TAS – Total Alkali Silica

VHMS – Volcanic Hosted Massive Sulphide WDS – Wavelength Dispersive Spectrometry

XRD – X-ray Diffraction

1 Introduction

The largely none sulphide Skorpion Zinc Deposit is situated within the para-autochtonous Port Nolloth Zone of the Gariep Belt which overlays the Lower-Proterozoic Orange River Group basement rocks (Corrans et al., 1993). The deposit is hosted mainly by banded shaley meta-arkose and is believed to have formed from the near surface low temperature supergene oxidation of a Late Proterozoic sulphide ore body (Kärner, 2003). Meteoric fluids are believed to be the cause of the seemingly protracted oxidation which post-dates the Pan African deformation as indicated by the major north-south faults that host the deposit. Sulphide minerals of the proto ore are preserved mainly in the felsic metavolcanics, and to a smaller extent in the deeper meta-sediments (Kärner, 2003). As indicative of the name, the major element of economic importance at Skorpion is zinc. Prior to commencement of production in 2003, the Skorpion deposit contained a resource of 24.6 Mt at 10.6 % Zn with unquantified amounts of copper and lead. However, based on grade control sampling and estimation, a substantial amount of copper ore has been mined and stockpiled separately throughout the life of mine. Moreover, there is a significant overlap of zinc and copper concentrations in the western ore zone. Lead containing minerals have been encountered in several exploration boreholes at various depths. Both non-sulphide and sulphides lead minerals have been encountered. However, since the discovery of the deposit, no work has been dedicated to the understanding of the lead mineralization of the deposit. In addition to this, lead has not been modelled in both the Resource and Grade Control Models of the mine implying that the opportunity of enhancing the understanding of the orebody and consequently the depositional environment of the ore has remained unexploited. Regionally, the Skorpion Zinc deposit is situated within the Port Nolloth Zone, which is an autochthonous passive continental margin zone of the Gariep Belt (Frimmel et al., 2004). Within the Port Nolloth Zone, the Skorpion Zinc deposit occurs with other major ore deposits, namely the Rosh Pinah Zinc deposit and the Gergarub deposit which are both dominantly Zn, Pb sulphide deposits. The Rosh Pinah deposit is believed to be situated at approximately the same stratigraphic position as the Skorpion deposit (Frimmel et al., 2004).

Both the Gergarub and Rosh Pinah deposits have been described as SEDEX deposits and are situated less than 50km away from the Skorpion Zinc deposit. Various workers have shown that SEDEX deposits generally do not occur in isolation, but normally occur in a district of numerous deposits due to their mode of genesis (Borg, 2000). Borg (2000), described the Pb-Zn Gariep deposits as being associated with the hinge line of the basin and having been deposited through fluids that migrated through graben bound faults formed during rifting associated with the formation of the Adamastor Ocean.

The Rosh Pinah Mine has been in production since 1969 and produces 2000 milled tonnes per day of zinc and lead sulphide and minor amounts of silver, copper and gold (Anon, 2018).

The undeveloped Gergarub deposit contains 11.36 Million tonnes of indicated resource at 9.13% Zn, 2.48 % Pb, 43.39 g/t Ag (Anon, 2018).

Of these three major base metal deposits within the Gariep Belt, the Skorpion Zinc deposit is the only one without economical lead mineralization. Moreover, this deposit is the only one that has been described as VHMS by various studies and the only one that has been oxidized to an economical supergene zinc deposit.

However, due to the diminishing zinc resource, the possibility treating lead mineralization as a byproduct could assist with prolonging the Skorpion life of mine and provide an extra source of revenue that can potentially assist with funding life extension projects currently planned. The increase in lead price seen particularly from 2014 to 2017 justifies the potential value add of lead mining to the company (Figure 1).

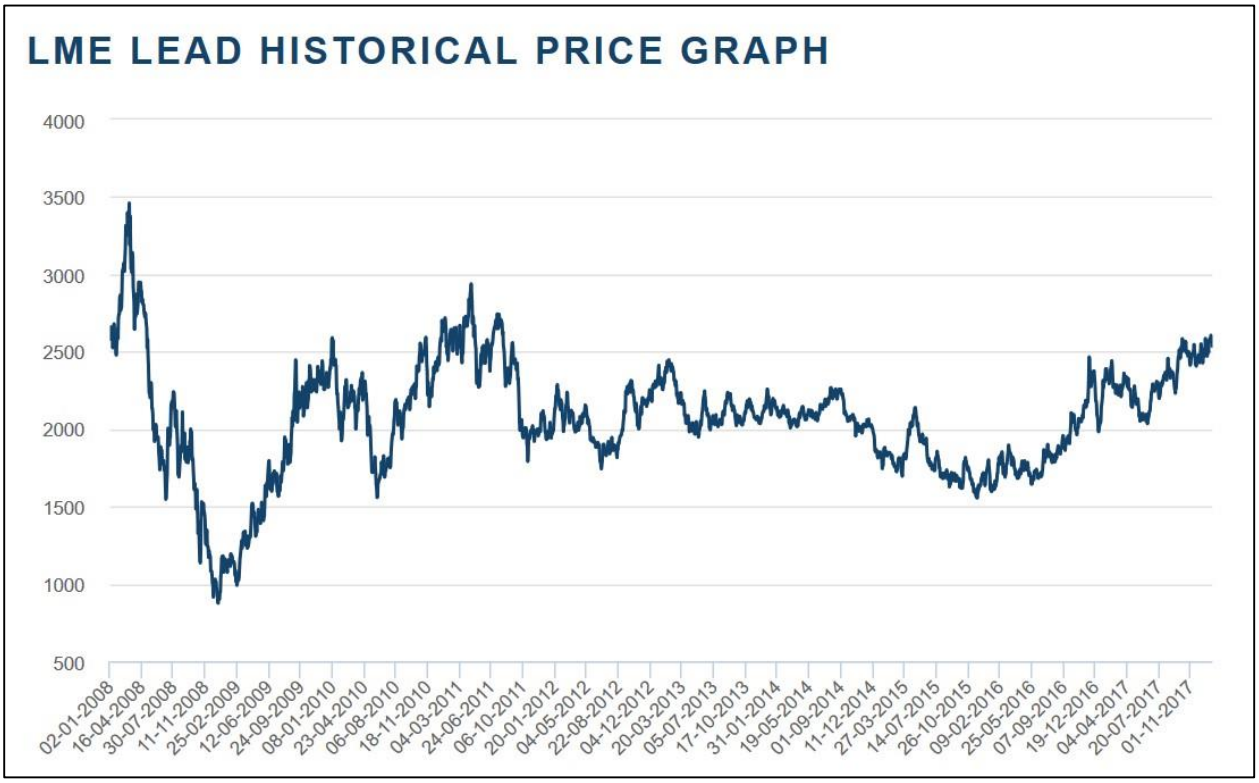

Figure 1: Historical lead prices form London Metal Exchange (LME) (Anon, 2018)

This study aims at understanding the mineralogical composition of the Skorpion lead mineralization as well as the relationship between lead and the major metals such as zinc and copper in order to form a basis for further work that could determine the potential of processing lead as a by-product.

As part of the study, work was also done on lead isotopes mainly with the aim of understanding the mineralization genesis and to determine the differences between the Skorpion and Rosh Pinah deposit which justify the inferior economic potential of the Skorpion lead mineralization.

1.1 Project Aims and Objectives

Since commencement of mining, the Skorpion deposit has only been exploited for zinc and minor zinc associated copper as copper cake. Zinc devoid copper material has also been mined and stockpiled separately and currently stands at a tonnage of 5.6 Million Tonnes at 0.46% Cu. Although, the exact composition of this material is not well understood, the mined material generally occurs within the gossanous zones of the deposit, which with exploration boreholes, have been proven to contain elevated lead grades. Therefore the potential exploitation of lead lies within the further mining of these gossanous zones, and/or the processing of the stockpiled copper rich gossanous material. However, these two scenarios can only occur once the composition of this material is well understood and the potential for the existence of economic lead mineralization has been proven.

It is therefore against this background that this study is undertaken to serve as the baseline for further analysis of the possible exploitation of the Skorpion lead mineralization. The aim of this study is to:

- Study the mineralogy of the lead mineralization, lead's association with elements such as zinc, copper, cadmium, silver, iron and manganese as well as the host lithologies of lead in order to assist in characterisation of the Zn-Pb-Cu deposit (Mineralisation System)
- Study lead isotope ratios and compare with the Rosh Pinah deposit to aid in the understanding of the genesis of the mineralisation and the rest of the Skorpion deposit
- Analyse how the lead mineralization, elemental associations and isotopic signatures justify the lack of economical lead mineralization with respect to the adjacent deposits
- Recommend further work that can be conducted to enhance the possibility of mining and processing lead as a by product

2 Detailed Review of Study Area: Skorpion Zinc Deposit

2.1 Regional Geology: The Gariep Belt

The Skorpion Zinc Mine is situated in the para-autochtonous Port Nolloth Zone of the Gariep Belt which overlays the Lower-Proterozoic Orange River Group basement rocks (Corrans et al., 1993). Covering a small portion in Namibia and South Africa along the South Atlantic coast, the Gariep Belt extends from Lüderitz in south western Namibia to Kleinsee in the north western coast of South Africa. The Gariep Belt is arcuate, north-south trending (Alchin & Moore, 2005), has a strike length of 400 km and extends inland by 100 km (Coward & Davis, 1982). Moreover, the Gariep Belt is considered to be an extension of the Pan African Damara Orogenic Belt in central Namibia and thus forms part of the network of orogenic belts in western Gondwana, which are of late Proterozoic to early Palaeozoic in age (Frimmel, 1996). Besides the Skorpion Zinc Deposit, the Belt also hosts the economically significant Rosh Pinah Zn-Pb-Ag and the undeveloped Gergarub Pb-Zn deposits. Despite the limited amount of work focused on Gergarub, both Gergarub and Rosh Pinah deposits have been described as SEDEX deposits. It is postulated that the exploration potential of discovering similar sediment hosted deposits elsewhere within the Gariep Belt is high (Frimmel, 2008).

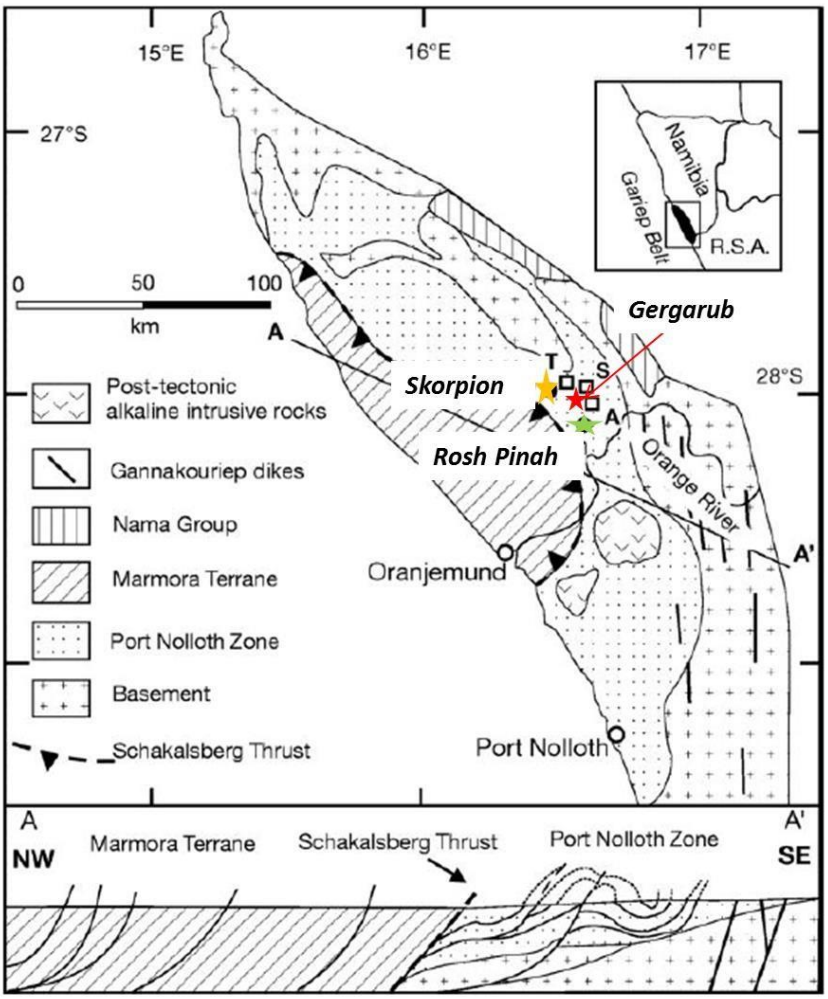

Figure 2: Map displaying the location of the Gariep Belt in South Western Namibia and the significant base metal deposits (Skorpion as an orange star; Gergarub as a red star and Rosh Pinah as a green star); Other base metal prospects are indicated on the map as open squares (A = Aus Road, S= Spitzkop; T= Trekpoort); Adapted from Frimmel and Frank, 1998

Formation of the Gariep Belt is believed to have been initiated by the break-up of the Supercontinent Rodinia along a triple point craton junction at around 741 Ma (Alchin & Moore, 2005). This was a result of continental uplift and separation and resulted in the formation of the southern Adamastor Ocean and thus the separation of the Rio de la Plata craton and the Angola and Kalahari cratons (Frimmel & Frank, 1998). Inversion from extensional to compressional tectonics led to the closure of the Adamastor Ocean and thus the subduction of the ocean floor at around 575Ma (Frimmel & Frank, 1998). This was followed by continent-continent collision between the South American continent and the southern African continent, the subsequent formation of southern western Gondwana and the peak of metamorphism that occurred around 500 to 545Ma (Frimmel & Frank, 1998). An extended period of tectonic stability preceded the break-up of Gondwana and the eventual formation of the Southern Atlantic Ocean (Kärner, 2006).

The Gariep Belt is divided into two tectonic zones, namely the eastern Port Nolloth zone and the western Marmora Terrane,which are separated by a major thrust fault, the Schakalsberge Fault (Frimmel, 2008). The Port Nolloth zone is an autochthonous passive continental margin zone and extends from the west coast of South Africa, south of Alexander Bay to south of Luderitz through Rosh Pinah in south western Namibia (Frimmel, 1996).

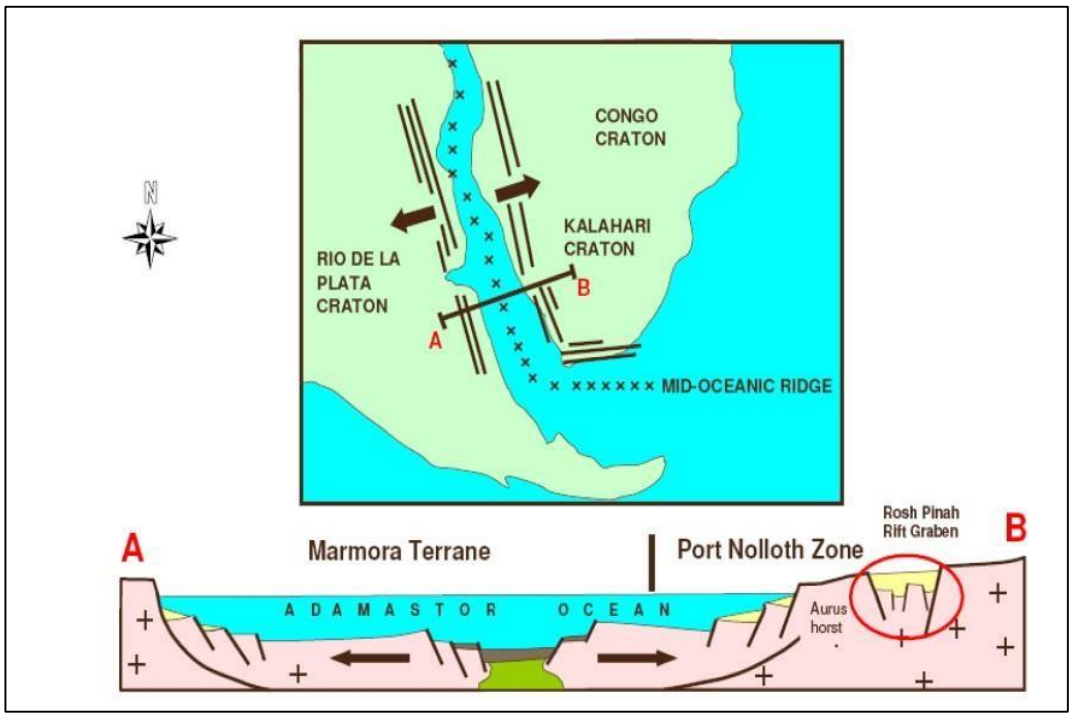

Figure 3: Map showing the rifting that occurred during the formation of the Adamastor Ocean and subsequent Marmora Terrane and Port Nolloth Zone; Cross-section A-B shows ocean floor development now preserved as ophiolites in the Marmora Terrane and the Rosh Pinah Rift Graben and associated depositional environments of the Port Nolloth Zone (Adapted from Alchin and Moore, 2005)

Rocks of the Pickelhaube and Rosh Pinah formation dominate the area of the Skorpion Zinc and Rosh Pinah Mines. The stratigraphic interpretation of the Port Nolloth Zone, (Alchin et al, 2005), predominantly indicate a rift setting. The Marmora Terrane is an allochthonous zone consisting of mafic rocks of oceanic crust that were thrusted onto the Port Nolloth Zone during continent-continent collision (Frimmel & Frank, 1998). The Port Nolloth Zone is overlain by rocks of the Nama Group.

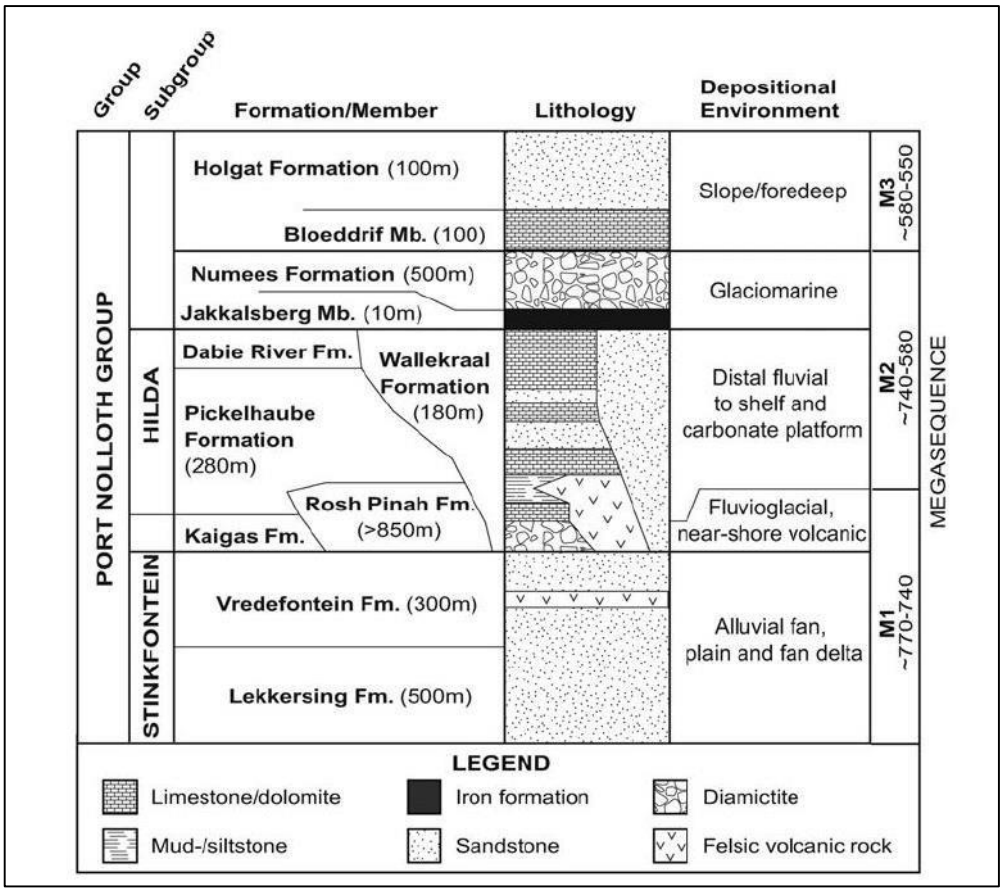

Figure 4: Stratigraphic Interpretation of the Port Nolloth Zone (After Alchin et al, 2005)

2.2 Geography

Located 40 km north of the Orange River and 25 km North West of Rosh Pinah, the Skorpion Zinc Mine is situated adjacent to the Sperrgebiet 1, within the south eastern part of the Namib Desert (Borg et al., 2003). The mine is located 100 km west of the Great Escarpment (Kärner, 2006) and lay at 670 m above mean sea level prior to mining.

2.3 History

The Skorpion Zinc deposit was first discovered by Erongo Exploration and Mining Co. Ltd (Borg et al., 2003). This was achieved by sampling of drainage sediments and gossans in 1976 to 1977. Elevated concentrations of Zn, Pb, Cu, Mn and Ag were seen in some samples from both the gossans and the sediments and this led to the establishment of a drilling programme (Borg et al., 2003). Due to the structural complexity of the area, low core recovery was a norm. Moreover, the lack of technology to extract Zn from non-sulphides made the Zn economically unrecoverable. For these reasons, the deposit

was abandoned and was considered uneconomic (Borg et al., 2003). At the time the deposit was abandoned, measured and indicated resources of 8.3Mt at 10.9% Zn were known (Corrans et al., 1993). In 1996, Anglo American and Reunion Mining initiated another exploration phase in which Reunion established a drilling programme which increased the proven resource to 17.5Mt at 10.4% Zn by 1998 (Borg et al.,2003). This resource was converted into a reserve after Reunion Mining investigated solvent extraction and electrowinning treatment processes with the aid of Technicas Reunidas and Union Miniere of Spain and Belgium respectively (Borg et al., 2003). Anglo American became the sole owner of the Skorpion Zinc Mine in 1999, mining started in 2001 and the first zinc metal was produced in

2003. Vedanta Resources plc, India's largest non-ferrous metals and mining company, took ownership of Skorpion Zinc Mine in November 2010.

2.4 Geology

2.4.1 Lithotypes

The rocks of the Skorpion deposit form part of the Hilda subgroup of the Port Nolloth group. The grey marble exposed in the Skorpion Mine Pit is part of the Pickelhaube formation member whereas the siliciclastics and volcanics are part of the Rosh Pinah formation (Corrans et al., 2003).

Lithologies exposed in the Skorpion Mine open-pit include mafic metavolcanics, a calcitic dark gray marble, highly weathered siliciclastics and felsic metavolcanics (Borg et al., 2003). The mafic metavolcanic is currently exposed in the southern part of the pit and has also been encountered in some drill cores. Being the second oldest unit in the local stratigraphy, the gray marble rests structurally on top of the younger felsic metavolcanics due to shear zones with a reverse sense of movement (Borg et al., 2003). The marble generally contains no mineralization, but minor mineralization, in the form of smithsonite, along its contacts with the overlying mineralized siliciclastics, has been observed by the mine geologists. The siliciclastics include meta-arkoses, metaquartzarenites, volcaniclastites, quartzites and accretionary lapilli tuffs (Borg et al., 2003). Currently, the marble is exposed in the eastern to the central and northern part of the pit with intercalations of the metamorphosed felsic metavolcanics, locally known as the quartz sericite schist. This felsic metavolcanic is prominent in the north eastern part of the pit but a similar lithology has also been observed on the south western part of the pit at greater depths, bordering the mafic metavolcanics. The siliciclastics cover most of the western area and a myolinitic sericite schist runs through the centre of the pit from south to north. The planar relationships of most of these lithologies are indicated in Figure 5 below. Van Schalkwyk (2016) has interpreted the contacts between the main lithologies as thrusts and has consequently divided the pit area into six different thrust imbricate domains (Figure 5).

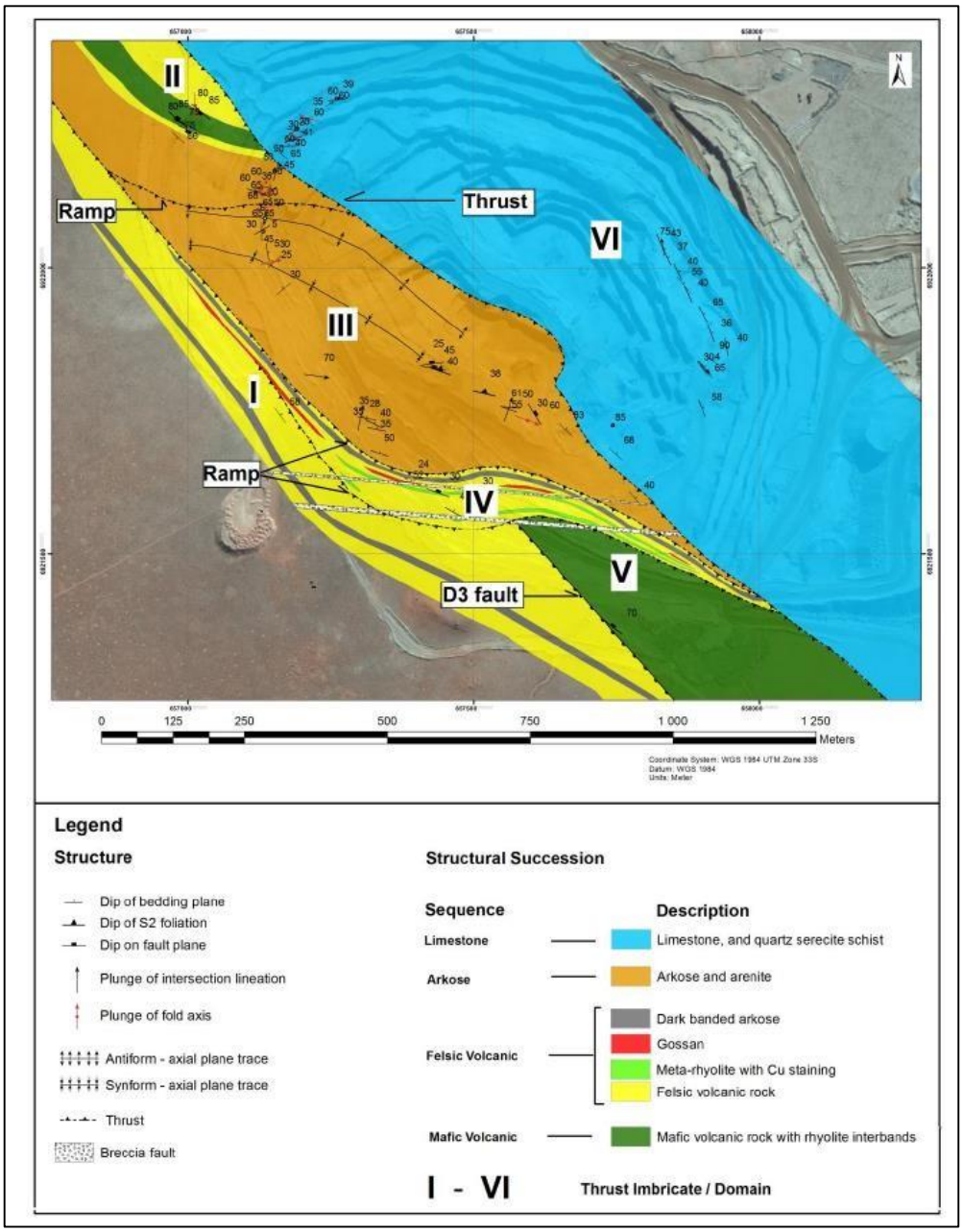

Figure 5: Map showing Skorpion Mine area geology (Lithologies on map are named as per unmetamorphosed equivalents); Gossanous areas and important structures are also indicated on the map as per the legend);
Taken from Van Schalkwyk (2016)

2.4.2 Structure and Tectonics

Owing to the bi-modal volcanic rocks and the presence of siliciclastics and carbonate rocks, the Skorpion area is believed to have been formed in a continental rift to passive rift continental margin setting. The area has been strongly affected by vertical tectonism, local horst and half-graben structures as well as synsedimentary and synvolcanic growth faults (Borg et al., 2003). Pan-African ductile deformation and late stage brittle deformation are also believed to have affected the area (Borg et al., 2005). Ductile high strain domains, rodding, sheath folds and SSE-ward thrusting within the area are manifestations of the Pan-African deformation (Borg et al., 2005). Moreover, the rocks experienced uppermost greenschist to lower amphibolite facies metamorphism at the peak of tectono-metamorphism at 540 Ma. Anastomosing fault arrays, which trend NNW-SSE, seen within the pit are believed to be related to the development of the Skorpion Fault System during the late stage brittle deformation (Borg et al., 2005). The fault planes dip moderately to steeply towards ENE and various structures such as sigmoidal folds, extensional veins and slickensides suggest a transpressional regime (Borg et al., 2005). The Skorpion area is generally believed to have been affected by four deformational events. The summary of the deformational events below was obtained from work done by Dirks (2004).

- D1 was characterised by extensional deformation during sedimentation → relating to opening of the Adamastor Ocean and related sedimentation in half graben structures
- D2 was characterised by transpression and SSE directed thrusting → due to closure of the Adamastor Ocean
- D3 was due to compressional tectonics which imparted brittle-ductile shearing → due to oblique collision of the South American plate and the Southern African plate
- D4 occurred in an extensional setting and is seen in forms of NW and NE trending normal faults → related to opening of the Atlantic Ocean

2.4.3 Mineralization

The Skorpion zinc deposit is hosted by arkosic meta-arenites and subordinately by volcaniclastic metasediments (Borg et al., 2003). The orebody forms a sharp contact with the gray marble on the east and the zinc grades generally increase towards the east. Sauconite (a zinc smectite), hemimorphite and smithsonite are the main ore minerals (Borg et al., 2003 and Boni, 2003) within the supergene zone currently being exploited.

This supergene, bowl-shaped and irregular zone is believed to have formed from the oxidation of a sulphide protore by circulating meteoric water (Borg et al., 2003). Breakdown of minerals such as albite and calcite cement, by the acidic water, increased the permeability of the metasediments and allowed the deposition of the zinc minerals in unhindered open spaces resulting in delicate euhedral

crystals (Borg et al., 2003). Sauconite and hemimorphite are believed to have replaced some feldspars and mica in pore spaces whereas smithsonite and some hemimorphite precipitated in fractures and breccias.

In addition, a metal zonation pattern has been identified within the deposit. The western end is composed of a zone of mixed Fe-oxihydroxides and Mn-hydroxides, followed by a Cu zone to the east then by a weak Pb zone before grading into a Zn zone in the far east closest to the gray marble (Borg et al., 2005). Based on metal mobility, it has been suggested that the mineralising fluid flowed from the west to the east through fractures and deposited metals as the feldspar buffer reduced its acidity. Furthermore, the grey marble acted as a hydrological barrier (Borg et al., 2005) and most of the zinc was thus deposited at the contact with the marble. Vertical supergene zoning was also recognised by Kärner (2006) and interpreted it as the result of the oxidation of the sulphide protore due to fluctuation of the water table. Due to the presence of metal rich gossans with meta-siliciclastics, as well as primary ore mineral assemblages within felsic-metavolcanics and metavolcaniclastics, the primary zinc sulphides ore body seems to have been hosted by both metasediments and felsic meta-volcanics (Kärner, 2006). Work conducted by Theron and Carter (2001), on various samples from the Skorpion Area and surrounding outcrops revealed that the Skorpion proto ore can be classified as a sediment hosted volcanic massive sulphides. The workers concluded that the ore body formed from volcanic activities which had a hiatus period during which banded iron formations, barite and cherts continued to be extruded on the sea floor with associated sulphides mineralization. Sedimentation onto the sea floor followed the hiatus and continued with the sulphides mineralization from hydrothermal cells within the underlying volcanics. This resulted in sulphide mineralization occurring in both the volcanics and sediments. Work conducted by Van Schalkwyk (2016) indicate that the stratifom Zn, Cu, Pb sulphide mineralization believed to be the proto-ore of the oxide mineralization occurs within the felsic metavolcanic sequence as thrusted ramp-like lenses above the mafic meta-volcanics. This is illustrated in the Figure 6.

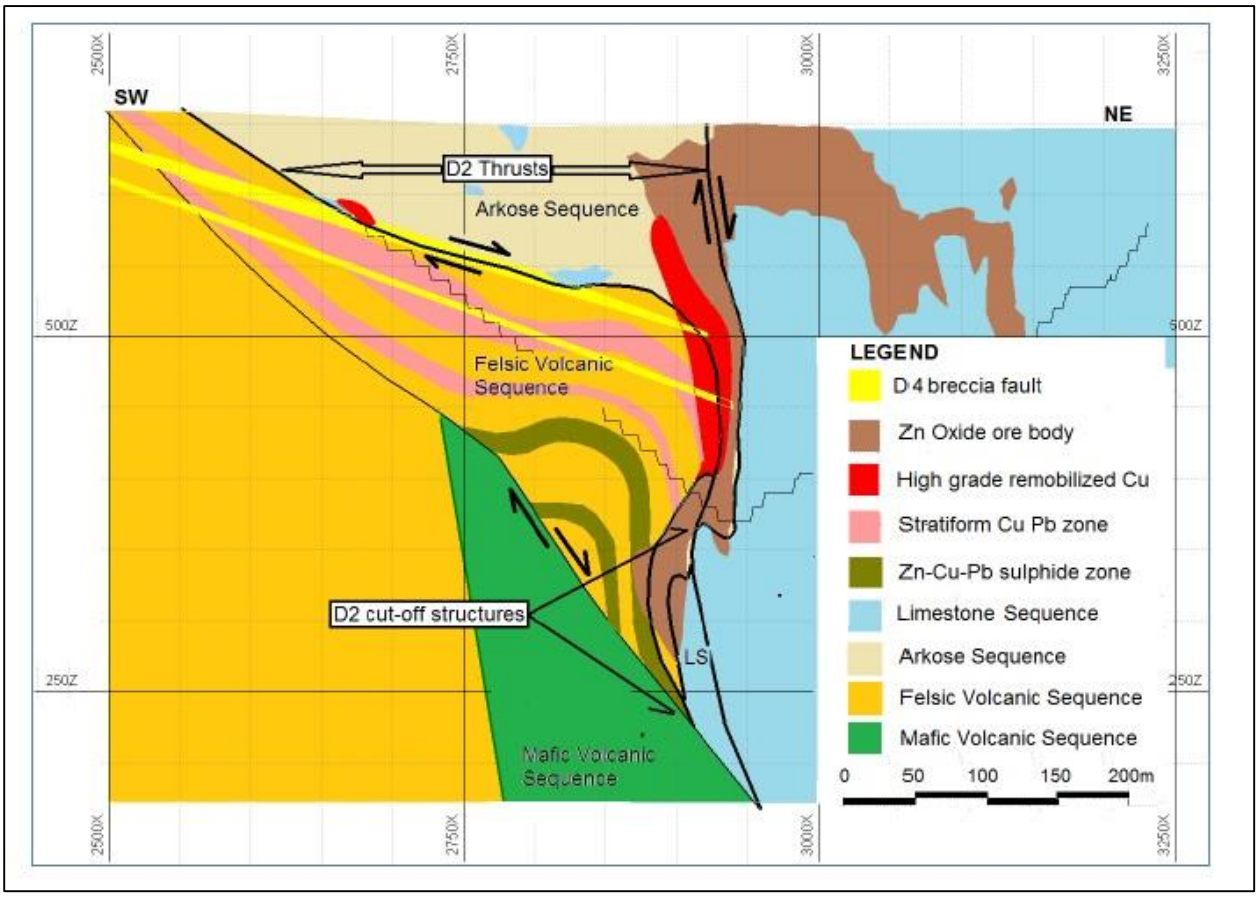

Figure 6: Cross-section illustrating the different lithologies in the Skorpion pit area as well as the position of the sulphide and oxide mineralization and associated structures (adapted from Van Schalkwyk, 2016)

Gutzmer (2004) studied the age of the mineralisation using Ar-Ar laser step-heating of microcrystalline manganomelane. Three dates which correspond to the evolution of the Southern African climatic and tectonic conditions, and thus the development of the African planation surface, were obtained. The older date (34-47 Ma) coincides with tectonic stability and warm humid conditions in Southern Africa which occurred after the break-up of Gondwana. This allowed advanced and deep chemical weathering of the Skorpion sulphide protore. The younger date (19-20 Ma) corresponds with the tectonic uplift of the African continent whereas the youngest date (11-13 Ma) is believed to correspond to semi-arid to arid conditions that occurred after the establishment of the Post African I erosion surface which allowed changes of the Zn deposit.

2.4.4 Background on Skorpion Lead Mineralization

Elevated lead grades were first encountered in coarse fraction gully sediment samples obtained by Anglo American in June 1976 in an area extending from Eccles Ridge, situated 9km south of the Skorpion Exploration Camp, to about 1km north of the Camp (Corrans et al., 1993). The general background concentration in the area was 20-40 ppm lead but the highest values obtained from the samples was 250 ppm. Follow up samples of the anomalous areas obtained grades as high as 2500 ppm lead against a background of 20-60 ppm (Corrans et al., 1993). These elevated lead grades were also associated with high Zn, which was the commodity being sought after, as well as Cu. Mapping of the available outcrops in the exploration area located three types of gossans. The most important one was SKC which was a Pb, Zn, Cu, Ba, Sn, Au gossan (Corrans et al, 1993). Having an exposed area of 1 x 1.5m, this gossan had values of 0.1-0.3% Cu, 0.1-2.9% Pb, 0.1-4.1% Zn, 2-50ppm Ag and 0.3-13% Mn. Drilling about 600m east of this gossan is what led to the discovery of the Skorpion Zinc Deposit under sands and calcretised gravels of up to 12m thick (Corrans et al, 1993). Initial drilling intersected oxidized Pb-Zn mineralization which led to the abandonment of the SKC in July 1982, as sulphides is what was being explored for.

Besides lead grades intersected during various drilling campaigns, not much information has been gathered regarding the lead mineralization type and extend. Kärner (2006) conducted a limited amount of work on galena within a few selected study samples. Thin section and electron microprobe analysis showed that primary galena occurs in foliated felsic metavolcanics (the SSS) in the footwall of the zinc mineralization and occurs in association with sphalerite. It mainly occurs in open pore spaces or along grain boundaries of sphalerite (Kärner, 2006). The presence of Ag and Bi in galena, which is a common feature in galena formed away from a feeder zone in a hydrothermal environment, has been shown by electron microprobe analyses (Kärner, 2006). Contrary to primary galena, secondary galena does not contain any Ag. The association of Ag with primary galena can thus be used to generally distinguish between overall primary mineralization (or Skorpion protore) and the supergene enrichment zones. Further details on the postulated genesis of the Skorpion ore body and its sulphides proto-ore are summarized in the Mineralization review in 3.3.3.

3 Methodology

3.1 Sample Selection Process

For the study, 12 core samples were selected from different generations of exploration boreholes. The samples with the highest lead grades were selected to ensure that lead minerals are encountered in all the samples with all analysis methods used. Moreover, the selection was partly also based on the content of the elements that are commonly associated with lead in VHMS and SEDEX deposits, namely Mn, Zn, Cu, Ba, Fe and S. At least 10cm of HQ half core or quarter core samples were collected on selected intervals and then divided into two or three samples on the basis of inhomogeneity to result in a total of 26 samples. All the samples were described in terms of their rock types, visible minerals, major textures as well as intensity of weathering. These details are provided in Appendix 1.

Table 1: Samples selected for the study, with location and elements that formed as the basis for selection (location using Mine local coordinate system)

Selected Samples							
Sample ID	**Original Borehole**	**Interval**	**Weight Kg**	**Major Elements**	**Easting**	**Northing**	**Depth**
MBHPb01	SK_204	166-167	1.48	Zn,Pb,S	2844.68	16072.51	409.52
MBHPb02	SK_206	334-336	1.20	Zn,Pb,S	2749.98	16370.87	320.49
MBHPb03	SK_207	314-315	0.76	Zn,Pb,S	2764.94	16323.73	353.75
MBHPb04	SK_203	214-217	0.56	Zn,Pb,S,(Mn,Ba?)	2854.72	16113.73	379.34
MBHPb05	TC605v	314-313	1.36	Mn,Pb,Ba	2784.69	16100.03	587.59
MBHPb06	SK_204	186-187.6	1.00	Pb,S	2853.05	16071.94	391.36
MBHPb07	SK_204	225-227	1.66	Zn,Pb,S,Mn	2869.59	16071.01	356.05
MBHPb08	SK_204	145-146	1.50	Pb	2835.98	16073.18	428.62
MBHPb09	SK_212	155-158	1.64	Mn,Pb,Fe,Zn,Ba,Cu	2840.12	16072.84	419.52
MBHPb10	SKSDD05	343-347	1.82	Zn,Mn,Pb,Fe,Ba	2700.67	16267.15	284.63
MBHPb11	SK_204	217.5-218.16	1.26	Pb,S	2866.20	16071.19	363.30
MBHPb12	SK_237	184-186	0.38	Mn,Pb,Fe	2710.44	16314.37	424.34

3.2 Thin Sections and Polished Sections

Sixteen thin sections of mainly the translucent minerals were prepared and studied using a Leica EC3 with an input of 5Volts and 500milli ampere. Another 10 sections were polished and studied using an electron microscope. These were meant to identify the opaque minerals but due to the extreme weathering of the rocks, the polishing was not successful with majority of the samples. Seven of the best polished samples were then used for electron microprobe analysis which had better resolution.

3.3 Lead Assays for Geochemical Analysis

The trace metal assays used for the geochemical analysis of the mineralization was obtained from the Skorpion Zinc Exploration Database. These assay were obtained during various exploration campaigns from 2008 to 2013. The trace elements were analyzed from pulverized samples of either Reverse Circulation or Diamond Drilling, using a certified ALS Chemex MEICP-61A or OG-62, where assays exceed 10 000 ppm. These methods both involve four acid digestion followed Inductive Coupled Plasma Mass Spectrometry (ICP-MS) analysis.

3.4 Electron Microprobe Analysis

Quantitative mineral chemical analyses were obtained by using four wavelength dispersive spectrometers on a JEOL JXA-8230 electron probe micro-analyzer at Rhodes University in 2014. The beam was generated by a Tungsten cathode; 15 kV accelerating potential, 20 nA current, and a focused beam were applied. Counts for Si, Al, Fe, Mn, P, Zn, Cu, Ti, Co, Ni, S, and Sm were measured on Kalpha peaks. Counts for Zr, La, Ce, Nd were measured on L-alpha peaks and Th and Hf were measured on the M-alpha peaks. Counting times were 10 seconds on the peak, and 10 seconds total on the background, for all elements. Commercial "SPI" standards were used. The data was collected with JEOL software. To correct for differential matrix effects, an automated ZAF matrix algorithm was applied to sulphide analyses and a Phi-Rho-Z algorithm (JEOL XM-27450-PRZ) to zircon analyses. Oxygen was calculated by stoichiometry. Analysis was done on the seven best polished sections.

3.5 X-Ray Diffraction

All twelve samples were sent for X-ray diffraction to ALS Minerals Lab in Johannesburg, South Africa. This was mainly to assist in determining lead minerals and confirm associated elements. Associated rock types could also be confirmed using the major minerals identified.

The samples were prepared using a backloading preparation method. They were analysed with a

PANalytical Empyrean diffractometer with PIXcel detector and fixed slits with Fe filtered Co-Kα radiation. The phases were identified using X'Pert Highscore plus software. The relative phase amounts were estimated using the Rietveld method. The technique is unable to detect amorphous or poorly crystalline material. Minerals present in trace amount <2mass% may not be detected using an XRD.

3.6 Lead Isotopes

The twelve samples were also sent for lead isotope ratios analysis to ALS Minerals Lab in Johannesburg, South Africa. All the samples were first crushed to 70 % < 2mm, riffle split and then pulverized to 85 % < 75µm. The samples were then analyzed using 33 element four acid ICP-AES to determine the lead concentrations. Samples with lead concentrations more than 1% were then analyzed using a four acid ICP-AES method. The isotope analysis method, PbIS-RAT61 which uses ICP-MS was then used. The precision of the method is +- 2%.

4 Results

4.1 Petrography

4.1.1 Thin Sections and Polished Sections

The host lithologies for the lead of the study samples can generally be divided into four main rock types, namely metasiliciclastics, felsic metavolcanics, graphitic schist and carbonatized metasiliciclastic. Most of the samples were very fine grained and highly weathered. Due to these reasons, the preparation of the thin sections was a challenge due to minerals being easily plucked out during grinding and polishing. The mineralogy was therefore not easily identifiable from the sections. However, all the 12 samples were also sent for XRD, which aided in major rock mineral identification. The best possible descriptions of these lithotypes based on the hand specimen and the thin sections are summarized below (for the purpose of shortening the sample ID on images, the first three letters (MBH) are removed from the sample ID's in this section).

Felsic Metavolcanic Rocks

In hand specimen this rock appears very fine grained (coarse silt on Udden-Wentworth Grain-size scale), light grey with graded bedding and containing thin bends of lighter material (Images A, B and C in Figure 7). In thin section, the bands appear slightly folded and contain some bigger lithic fragments (Image K and L in Figure 8). Disseminated pyrite is also visible. In thin section, quartz grains and quartz and feldspar rich lithic fragments, wrapped by disseminated pyrite, dominate the rock. The fragments show a vague preferred orientation and most are slightly elongated. The grains and fragments are cemented by clay which appears dark grey in thin section and is visible in hand specimen. In polished section, subhedral disseminated pyrite grains are visible with anhedral sphalerite within a matrix of quartz grains and clay. Pyrite grains contain sphalerite inclusions. Galena, sphalerite and chalcocite are intergrown and contain irregular shapes (Images D to F in Figure 8). Galena appears to be irregular, elongate and contains triangular cleavage pits (Image D in Figure 8). Galena also recrystallized along chalcocite and sphalerite grains. Chalcocite is also visible in some areas and is intergrown with galena. These sulphides occur mainly in veins showing that most are secondary minerals.

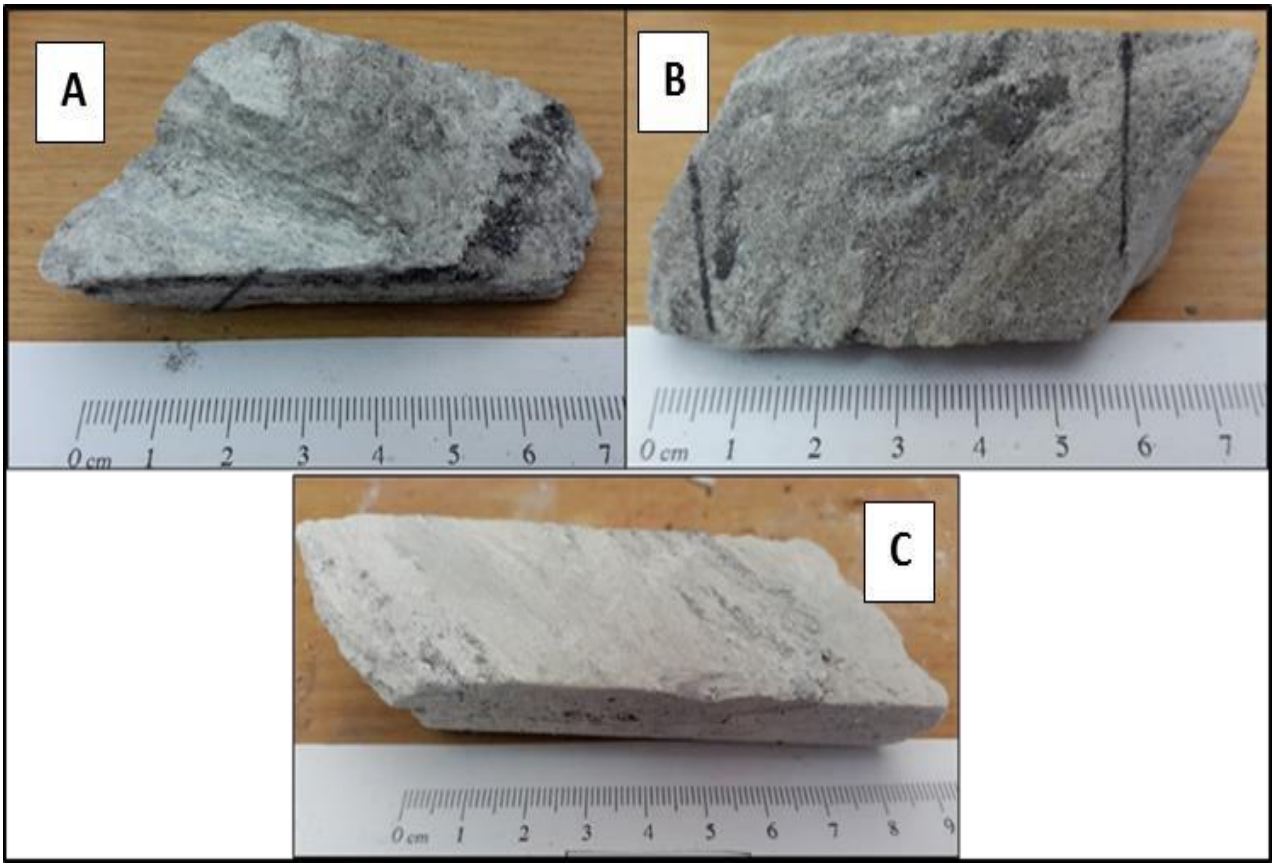

Figure 7: Photographs of hand specimens of the felsic metavolcanics (Image A shows the bands of the light felsic material and the darker sulphides with some mafic minerals); Image B shows the dark mineral grains of galena; Image C shows the schistose nature of the rock with some dark veins of sulphides; All lengths are in centimetres

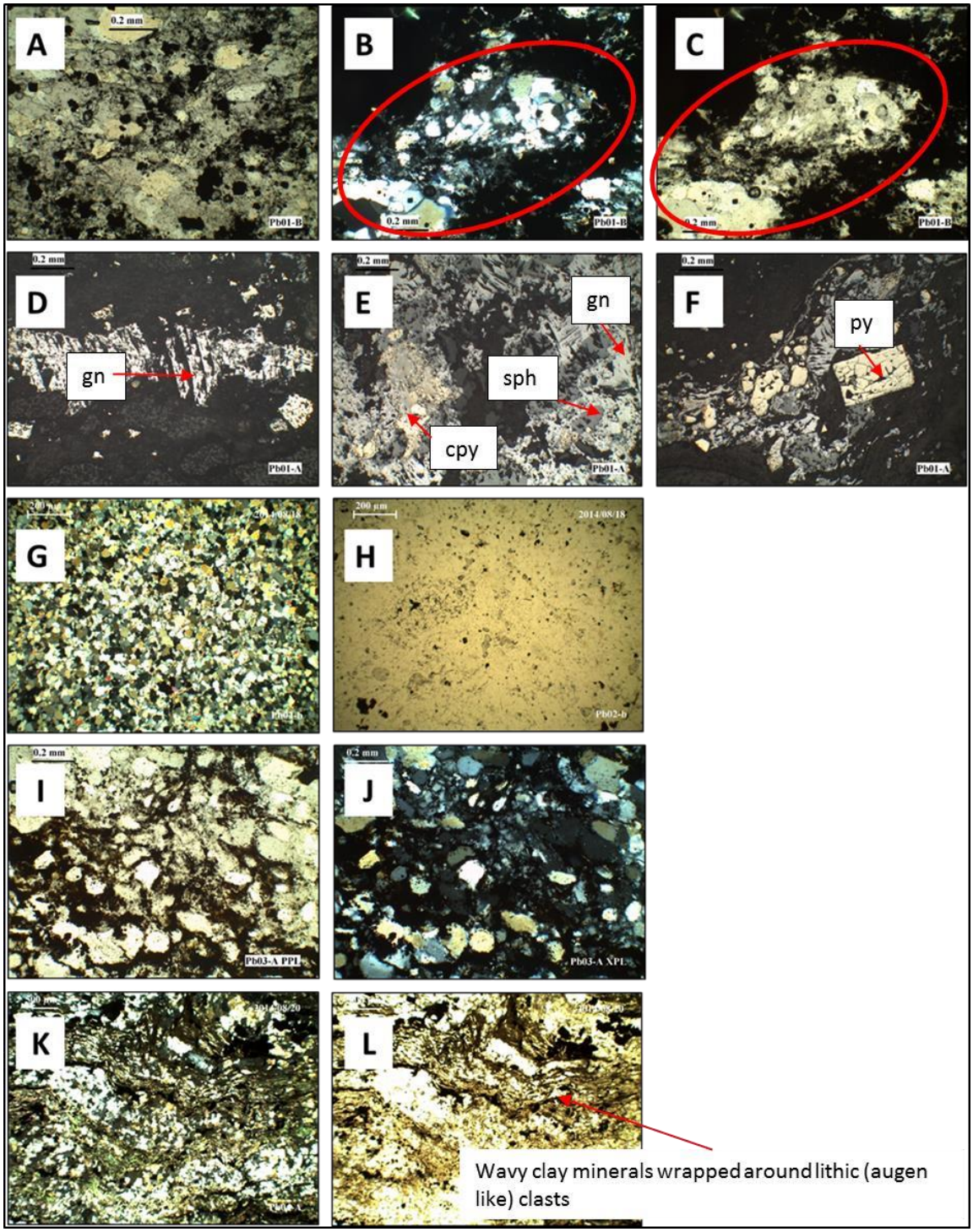

Figure 8: Images of Thins sections and polished section under Plane Polarized Light (PPL) and Cross Polarized Light (XPL); Images A to C showing lithic fragments wrapped by clay minerals. These are shown by the red oval shape on the image (A and C under PPL; B under XPL); Images D to F show images from the electron microscope (D= galena (gn) with its characteristic triangular pits), (E= galena (gn) intergrown with chalcocite (cpy) and sphalerite (sph)), (F= showing pyrite (py) growing over the wavy intergrown sulphides appearing unaffected by deformation; Images H to I show the fine grained quartz and feldspars with fine grained opaque minerals along quartz grain boundaries (G and J under PPL, and H and I under XPL); Images K and L show the wavy clay mainerals wrapped around augen of lithic clasts (K is under XPL and L under PPL)

Metasiliciclastics

This rock is a gritty, fine to medium grained, light brown with a red brown mineral within veins making it look banded (A and B in Figure 9) . Some varieties of the rock appear darker, most probably due to the presence of manganese oxides (image D in Figure 9). In thin section the rock is composed of quartz, sericite and feldspar. In some areas, the quartz shows an interlocking texture. All these minerals show no preferred orientation and the specimen is generally poorly sorted. Iron oxides form irregular veins within the rock as well as anhedral patches. Veins within the rock contain sericite (Figure 10). The iron oxides show a box work structure and some patches of sulphides with disseminated euhedral pyrite are visible. A euhedral dark brown mineral with high birefringence, detected by EMPA as zircon, was identified. The rock is highly weathered and fractured and very few sections could be polished well enough for a polished section and EMPA.

Some samples appear more fine grained, pale orange and with small vugs of oxidized minerals (B in Figure 9). Poorly defined banding is visible. This is defined by bands of coarser oxidized minerals within quartz augen and bands of finer quartz.

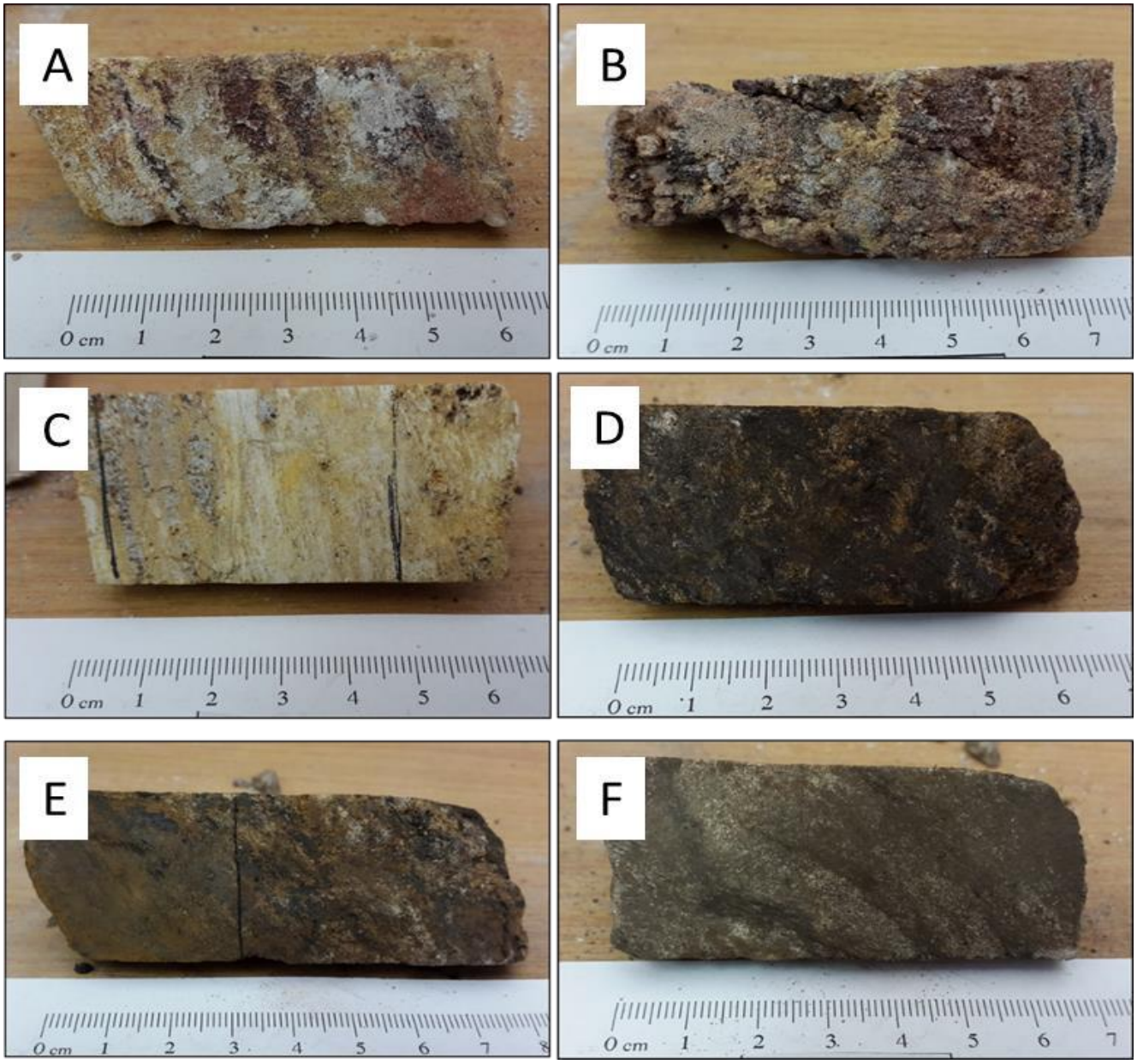

Figure 9: Metasiliciclastics hand specimen pictures (A and B show vuggy variety; C shows slightly more silicified and less vuggy specimen; D to F show darker manganese rich variety that is slightly banded in F); All lengths are in centimetres

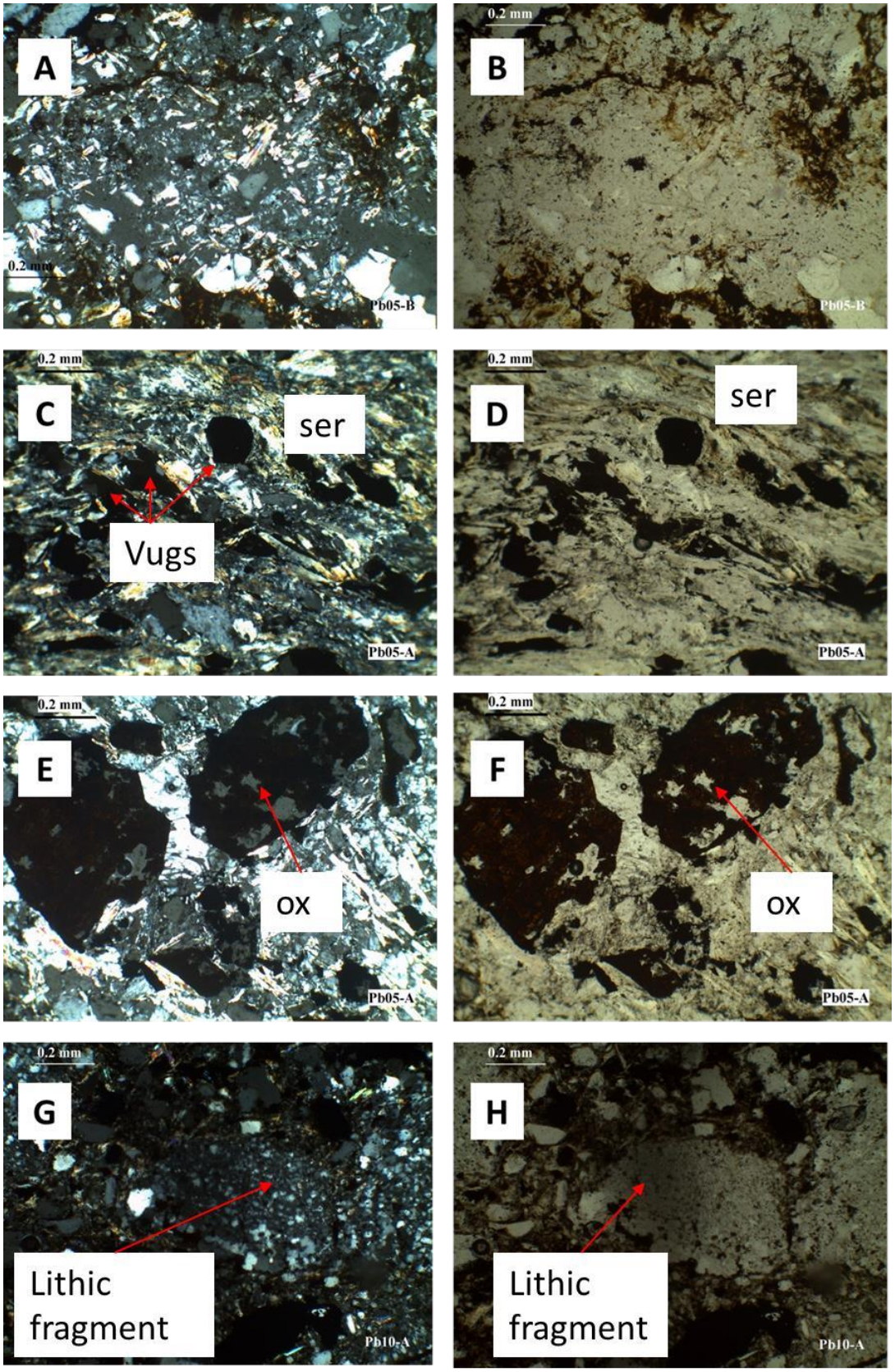

Figure 10: A and B showing poorly sorted sandstone with grains (quartz, feldspar and sericite) with no preferred orientation; Images C and D show vugs (black areas) and sericite within slightly deformed veins; E and D show partially plugged and vuggy iron oxides that appear to be have replaced sulphides (probably pyrite?); G and H show fine grained quartz rich lithic fragments surrounded by iron oxides in veins and random quartz grains

Graphitic Schist

The hand specimen is composed of a fine grained dark grey graphitic rock (Figure 11) with fine disseminated pyrite and a talc like mineral in areas. The rock gives off a black staining on hands and paper, which is indicative of the presence of graphite.

In thin section the sample is highly altered and is composed of mainly quartz and sericite with a poorly defined preferred orientation (A in Figure 12). The rock appears to be cemented by silica and sulphides. Some disseminated euhedral grains of pyrite, other sulphides and another unidentifiable mineral with high birefringence are visible in areas. Boxwork forming oxides and sulphides are also visible in some areas of the rock.

Figure 11: Photograph showing dark graphitic schist with disseminated pyrite; All lengths are in centimetres

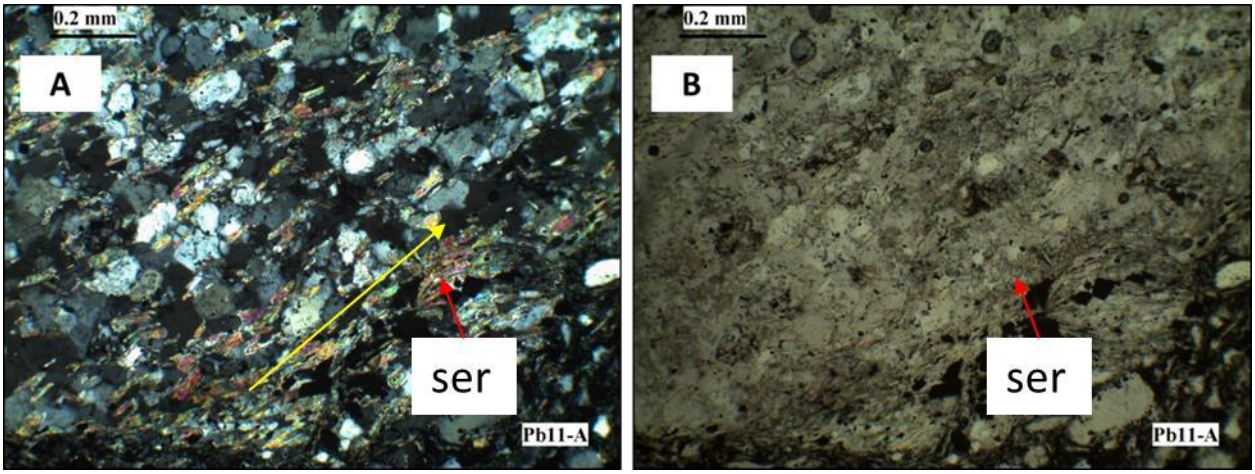

Figure 12: Images A and B showing quartz, feldspars and sericite (ser) in XPL (A) and in PPL (B); Yellow arrow shows preferred orientation of grains that define a schistosity

Carbonatized Sediment

The hand specimen is a grey hard fine grained rock containing quartz, as well as smithsonite in vugs and veins (B and C in Figure 13). Some stains of iron oxides are visible in areas. In thin section, there is a presence of fine grained interlocking carbonate mineral grains with a rhombohedral cleavage in areas (A, B, C and D, Figure 14). The carbonate mineral is also present in other areas within a fine grained mass composed of quartz, feldspars and undifferentiated clay minerals (E and F, Figure 14). Iron and manganese oxides and a phosphate mineral grow along the coarser grains. The phosphate mineral, identified as pyromorphite by EMPA, grows over the coarser grains but also in a network composed of rounded grains within the finer grained areas (G, H, I and J Figure 15). The carbonate mineral was identified as smithsonite which is also visible in the hand specimen.

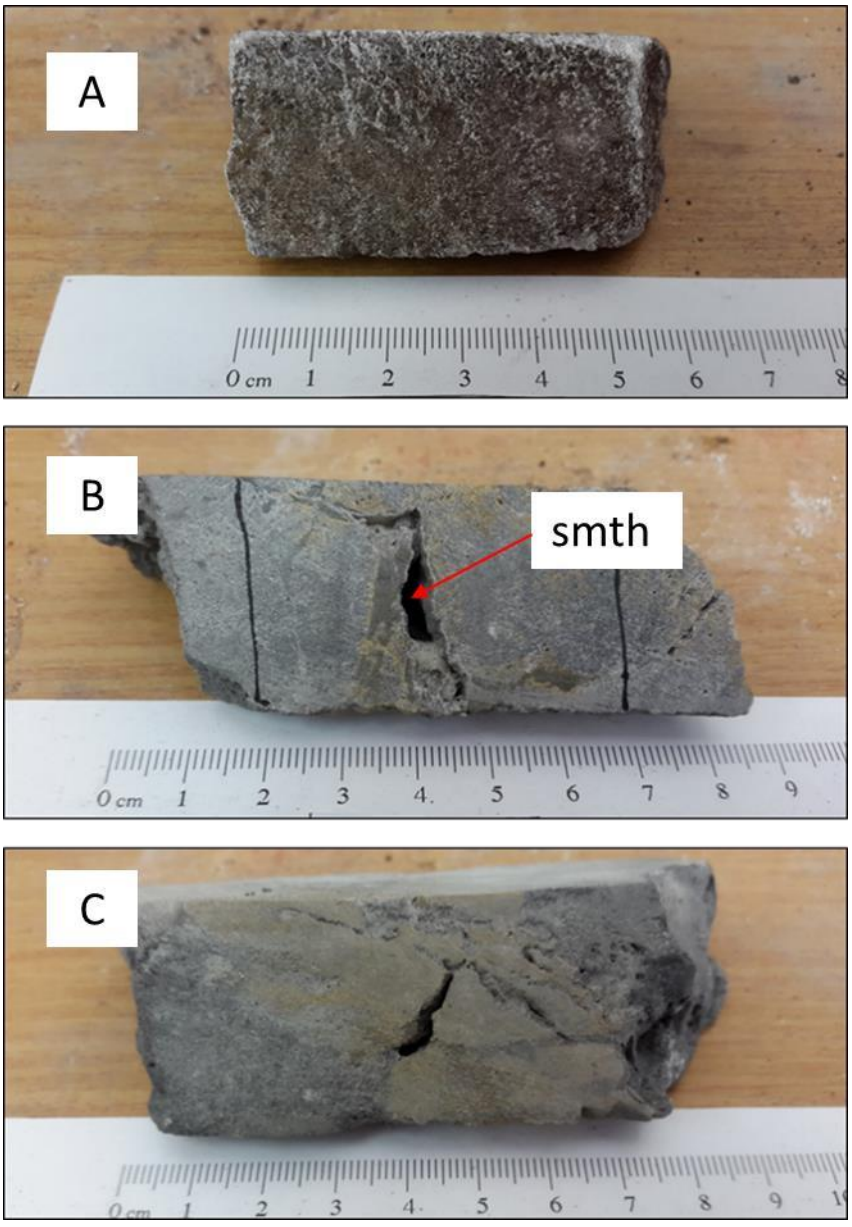

Figure 13: Images of Carbonatized Sediment; A shows less vuggy variety; B and C show vuggy variety with smithsonite (indicated by arrow as smth) filling vugs; All lengths are in centimetres

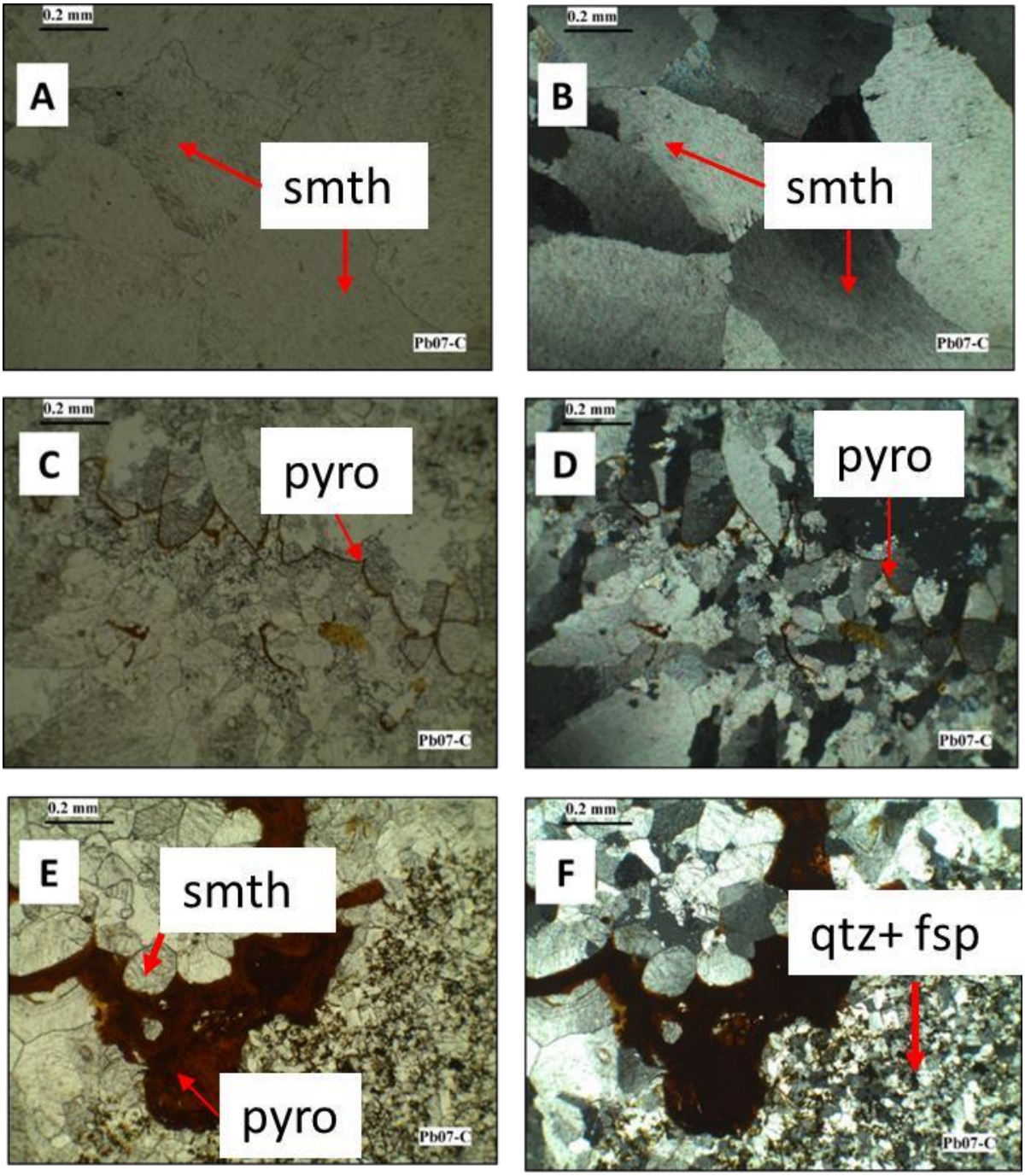

Figure 14: Images of Carbonatized Sediment in thin section; A and B show coarse grained smithsonite; C and D show less coarse smithsonite with pyromorphite growing along grain boundaries; E and F show smithsonite grains with irregular pyromorphite growing around the grains; the right portion of the two images show the quartz and feldspars that constitute the major part of the rock; G and H show colliform textured pyromorphite forming on quartz and feldspar; I and J show more massive pyromorphite

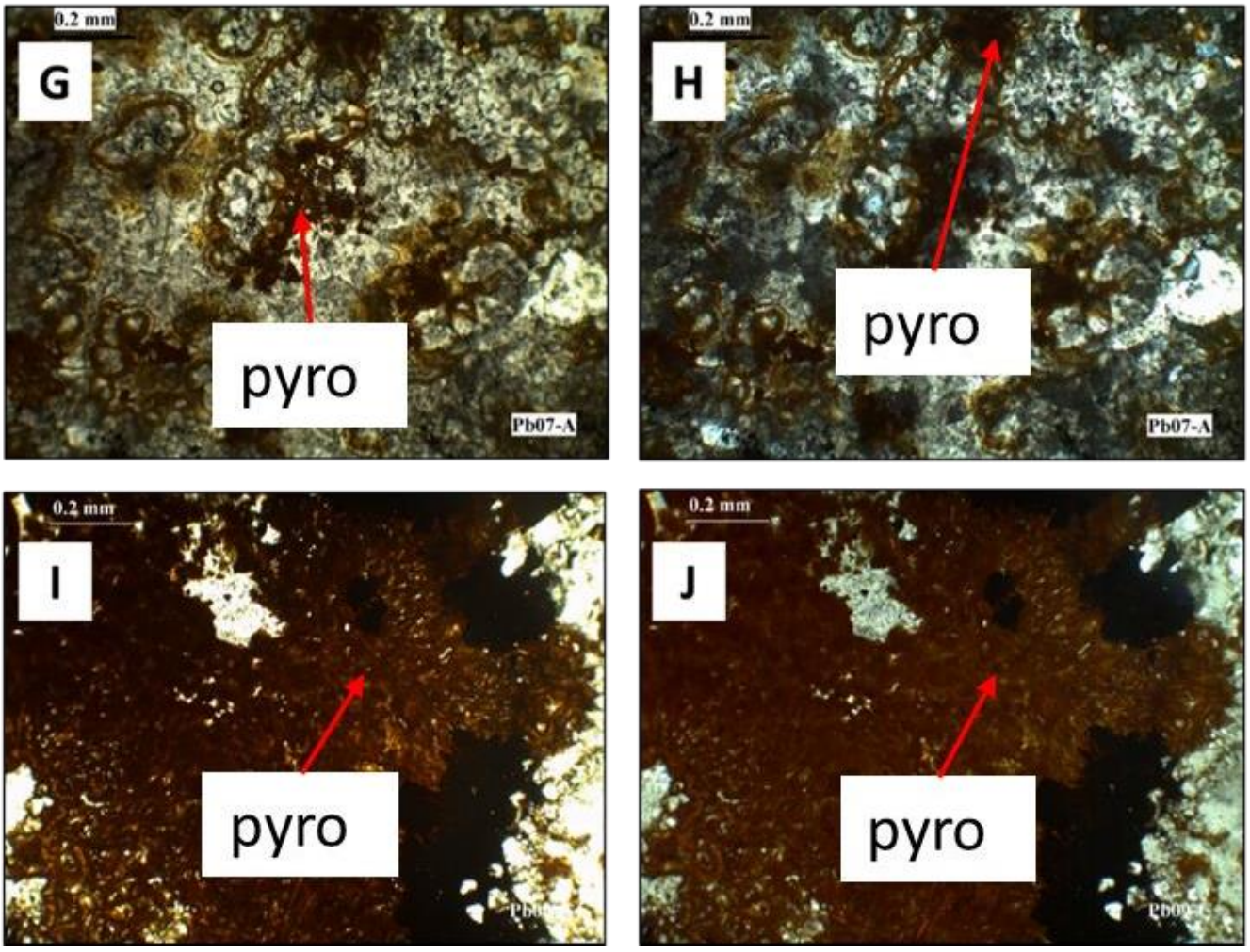

Figure 15: Images of Carbonatized Sediment in thin section; G and H show colliform textured pyromorphite forming on quartz and feldspar; I and J show more massive pyromorphite

4.1.2 X-ray Diffraction for Study Samples

The twelve study samples were sent to ALS Minerals Lab for X-ray diffraction. This was mainly to assist in determining lead minerals and confirm associated minerals. This was also aimed at confirming the lithologies identified using thin sections.

The results of the XRD are summarized in the graph and tables below:

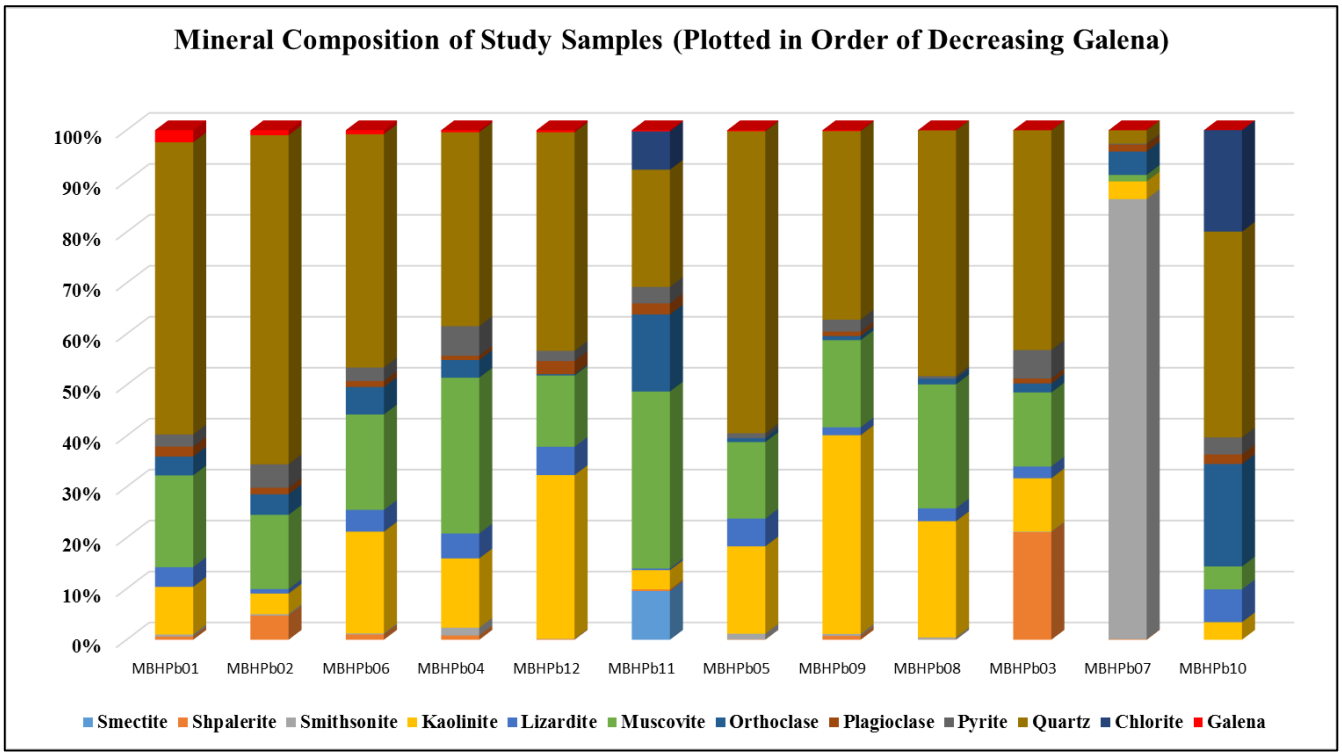

Figure 16: Figure 15: Graph of study samples XRD results (indicating the presence of quartz, kaolinite, muscovite and orthoclase in majority of the samples with the exception of MBHPb12)

The major minerals identified by XRD that are common in all the samples are quartz (ranging between 35% and 65%) with the exception of the graphitic schist (sample MBHPb11) and the carbonatized sediment (sample MBHPb07); and muscovite ranging between 30% and 15% again with the exception of the previously mentioned samples. Kaolinite and lizardite are the other minerals that are also common in the majority of the samples and again with the exception of the MBHPb11 and MBHPb07. The graphitic schist is composed mainly of muscovite, quartz, orthoclase, chlorite and smectite, making it more of a clay rich rock. Sample MBHPb10 is the only other sample that contains a high content of chlorite. The presence of chlorite and smectite in these two highly weathered samples imply a mafic photolith as chlorite and smectite from the alteration of olivine, pyroxene and amphiboles

(Churchman, 2012). MBHPb07, classified as carbonitized sediment from thin section, is composed mainly of smithsonite (87%) and subordinately orthoclase, quartz, kaolinite, muscovite and plagioclase. The actual compositions of all the samples are summarized in Table 2 below.

Ore minerals identified by XRD include galena, sphalerite, pyrite and smithsonite. Galena is the major lead bearing mineral.

Table 2: XRD mineralogical composition of study samples

	Galena	Shpalerite	Smithsonite	Kaolinite	Lizardite	Muscovite	Orthoclase	Plagioclase	Pyrite	Quartz	Chlorite	Smectite	Total
MBHPb01	2.36	0.65	0.39	9.35	3.86	18.01	3.69	1.96	2.37	57.37			100.01
MBHPb02	0.98	4.74	0.27	4.05	0.89	14.56	4.04	1.30	4.58	64.61			100.02
MBHPb03	0.02	21.11	0.11	10.47	2.31	14.53	1.76	0.99	5.58	43.11			99.99
MBHPb04	0.40	0.83	1.53	13.61	4.89	30.57	3.46	0.85	5.80	38.06			100.00
MBHPb05	0.21	0.07	1.12	17.14	5.44	15.02	0.78	0.00	0.95	59.26			99.99
MBHPb06	0.78	1.03	0.21	19.97	4.27	18.73	5.40	1.16	2.65	45.80			100.00
MBHPb07	0.01	0.11	86.38	3.46	0.00	1.28	4.59	1.37	0.20	2.60			100.00
MBHPb08	0.03	0.02	0.43	22.81	2.53	24.32	1.13	0.00	0.50	48.22			99.99
MBHPb09	0.18	0.74	0.39	39.00	1.54	17.11	0.79	0.88	2.35	36.99			99.97
MBHPb10	0.00	0.00	0.00	3.45	6.44	4.49	20.10	1.88	3.33	40.37	19.90		99.96
MBHPb11	0.22	0.31	0.00	3.77	0.32	34.75	15.12	2.18	3.23	23.00	7.53	9.57	100.00
MBHPb12	0.39	0.11	0.09	32.13	5.55	14.00	0.25	2.60	2.00	42.92			100.04

4.2 Mineralogy

4.2.1 Electron Microprobe Analysis

Wavelength-dispersive spectrometry scans, backscattered images and X-ray element maps were produced for the seven best polished sections. These were mainly to determine the dominant lead minerals, elemental and mineralogical associations, as well as for the textural analysis of the lead minerals.

EMPA quantitative analyses, done on selected spots on the well-polished samples, are summarized in the Table 3 and Table 4 below and graphs for galena and greenockite spots identified are provided in Figure 17 and Figure 18, respectively.

Table 3: Normalized stoichiometry of analysed lead containing spots of MBHPb06 and MBHPb11

MBHPb06 EMPA Quantitative							Mineral
Pb(Norm%)	Fe(Norm%)	Zn(Norm%)	Cu(Norm%)	Cd(Norm%)	S(Norm%)	Total(Norm%)	
87.37	0.00	0.00	0.00	0.10	12.529	100.0	Galena
87.75	0.05	0.00	0.03	0.08	12.089	100.0	Galena
88.68	0.39	0.03	0.02	0.09	10.795	100.0	Galena
96.91	1.01	0.00	0.07	0.02	1.992	100.0	Lead Sulphate (Cerussite?)
MBHPb11 EMPA Quantitative							
83.11	0.12	0.06	0.57	2.92	13.214	100.0	Galena
1.78	0.15	0.61	9.82	63.00	24.632	100.0	Greenockite
0.12	0.03	0.01	1.24	74.94	23.668	100.0	Greenockite
0.26	0.22	0.48	23.74	48.04	27.26	100.0	Greenockite; Cu bearing
84.34	0.30	0.23	0.23	0.26	14.626	100.0	Galena
91.88	0.06	0.00	0.06	0.18	7.822	100.0	Lead Sulphate (Cerussite?)
87.78	0.01	0.00	0.04	0.07	12.092	100.0	Galena
0.16	1.07	0.38	10.31	62.27	25.811	100.0	Greenockite; Cu bearing

Table 4: Normalized stoichiometry of lead containing spots within MBHPb08, MBHPb04 and MBHPb07

MBHPb08 EMPA Quantitative							Mineral
Pb(Norm%)	Fe(Norm%)	Zn(Norm%)	Cu(Norm%)	Cd(Norm%)	S(Norm%)	Total(Norm%)	
86.82	0.02	0.11	0.05	0.01	12.99	100.00	Galena
MBHPb04 EMPA Quantitative							
85.39	0.25	0.51	0.00	1.23	12.62	100.00	Galena
87.29	0.06	0.00	0.00	0.07	12.58	100.00	Galena
MBHPb07 EMPA Quantitative							
85.77	1.32	0.04	0.52	0.17	12.19	100.00	Galena

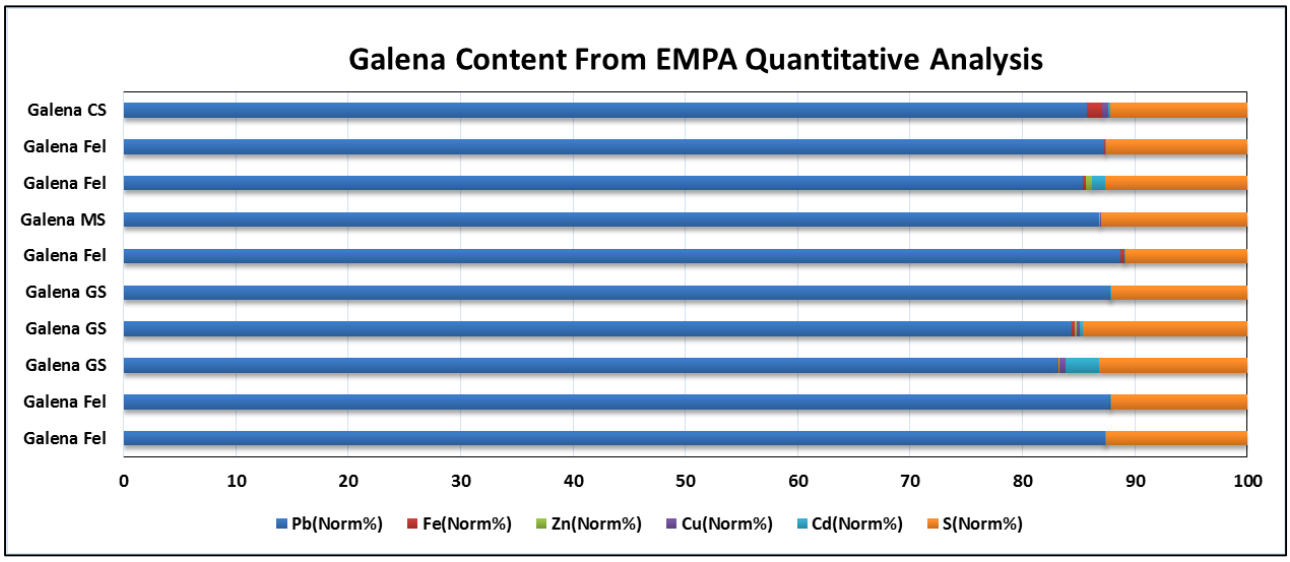

Figure 17: Normalized galena from EMPA quantitative analysis in the different lithologies (CS = Calcified Metasediment; Fel = Felsic Metavolcanics; MS = Metasiliciclastics; GS = Graphitic Schist)

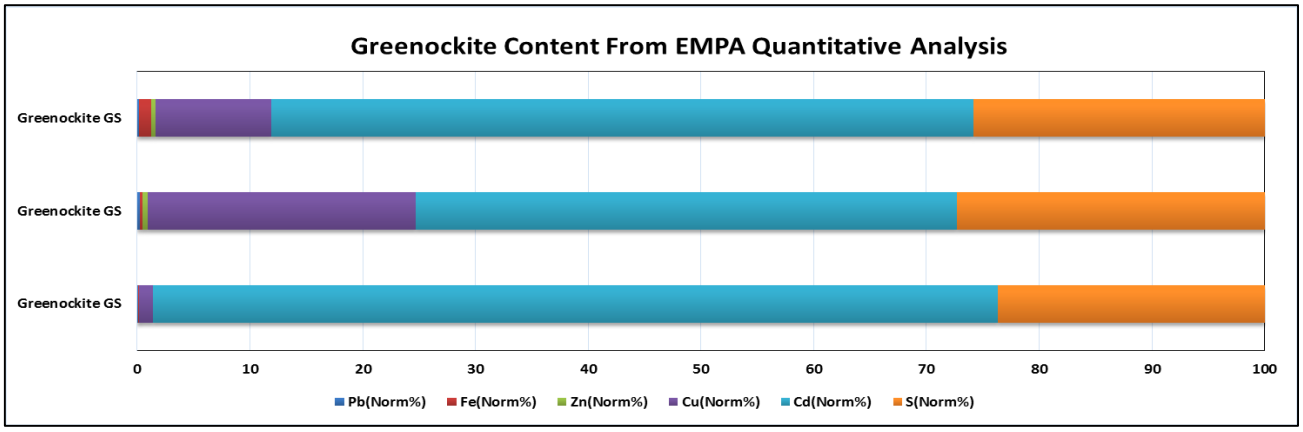

Figure 18: Normalized greenockite from EMPA quantitative analysis in the different lithologies (GS = Graphitic Schist)

Ore minerals identified with the EMPA are galena, chalcocite, pyrite, copper bearing greenockite and a lead bearing sulphate, which is probably cerrusite. These are mainly concentrated in the felsic metavolcanics.

A cryptocrystalline mineral containing Pb was detected in a few samples. Analysis using calibrations for the sulphides minerals mainly detected lead in the mineral. Using silicate calibrations, the mineral was confirmed to contain phosphate, barium, chloride, calcium, iron, manganese, sodium and silica. The mineral appears to be anhedral in shape and fills veins, particularly in the carbonitized metasiliciclastic.

This mineral was identified as pyromorphite. An interesting notable mineral identified is zircon. Grains of zircon were visible in a few of the study samples. The main elements in the zircon are zirconium and hafnium. The zircon appears to be a detrital mineral in the metasiliciclastics.

WDS Scans also produced graphs that show the presence of the various elements within scanned mineral grain spots (Appendix 2). These confirmed the ore minerals in the different rock types. Element maps produced from selected mineral grains containing lead were also produced to assist in identifying elemental associations and understanding the texture of lead containing phases. These are also shown in the sections focused on the various rock types below.

Felsic Metavolcanic Rocks

Minerals identified within the felsic metavolcanic rock are galena, chalcocite, sphalerite, a Zn, Fe (oxide), titanite, a Mn, Ca and Fe mineral and pyrite. Galena seems to have grown around pyrite (Figure 20), within cracks in pyrite (Figure 20) as well as within pore spaces (Figure 20). Chalcocite occurs as inclusions within galena (
Figure **21**). Titanite grows around galena in a semicircular manner (Figure 19). This occurs in openings within clay minerals.

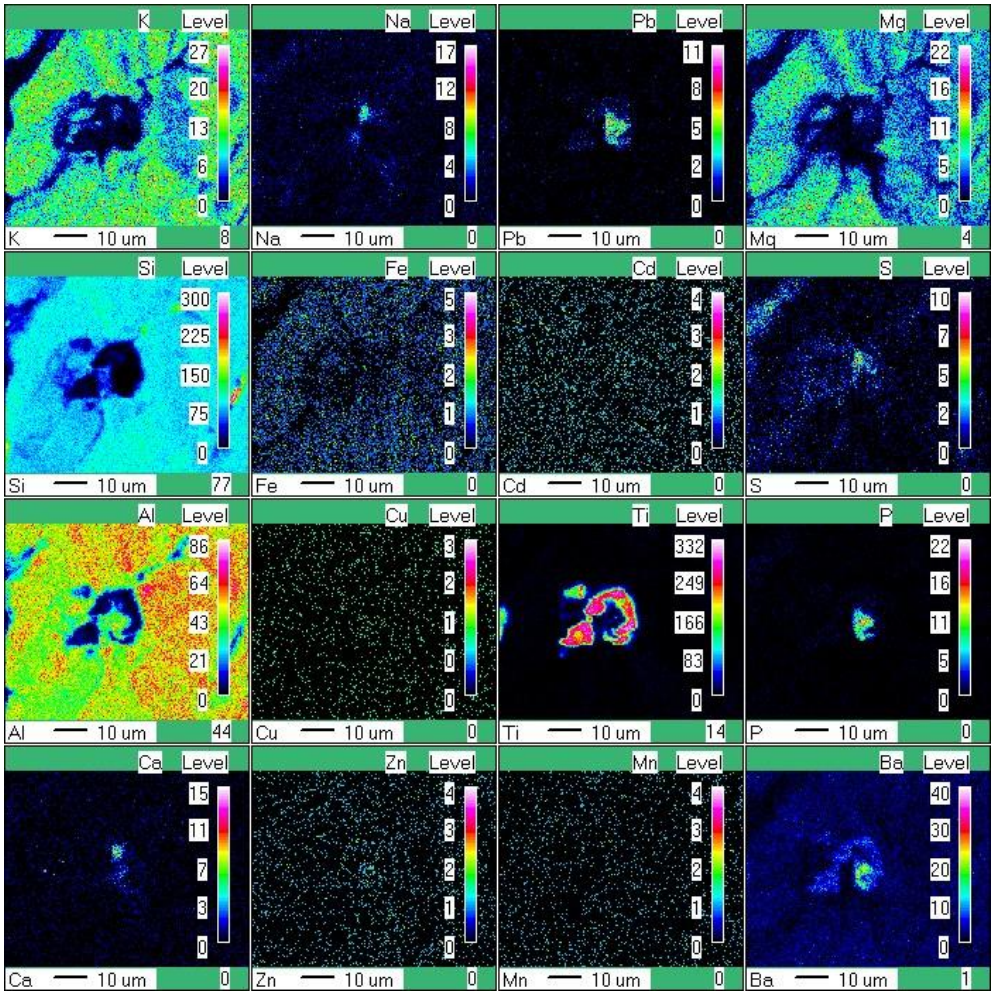

Figure 19: Galena overgrown by rutile; both surrounded by clay minerals (containing K, Si, Al, and Mg); (The Y-axis is in X-ray Counts)

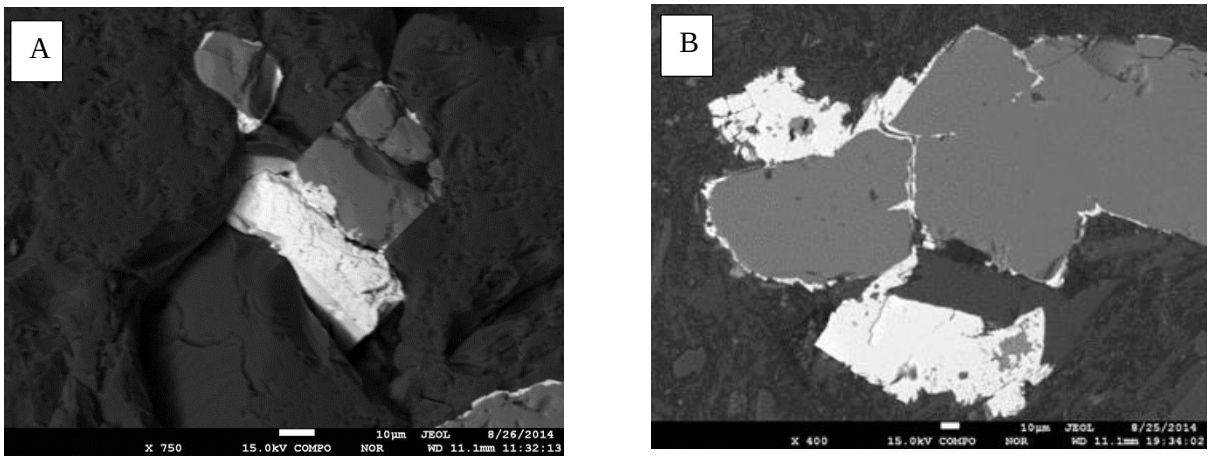

Figure 20: A: Galena (white) growing within pore spaces and around other mineral grains (Backscatter Electron Image); B: Galena (white) growing around pyrite grains, within pyrite cracks and containing chalcocite inclusions (Backscatter Electron Image)

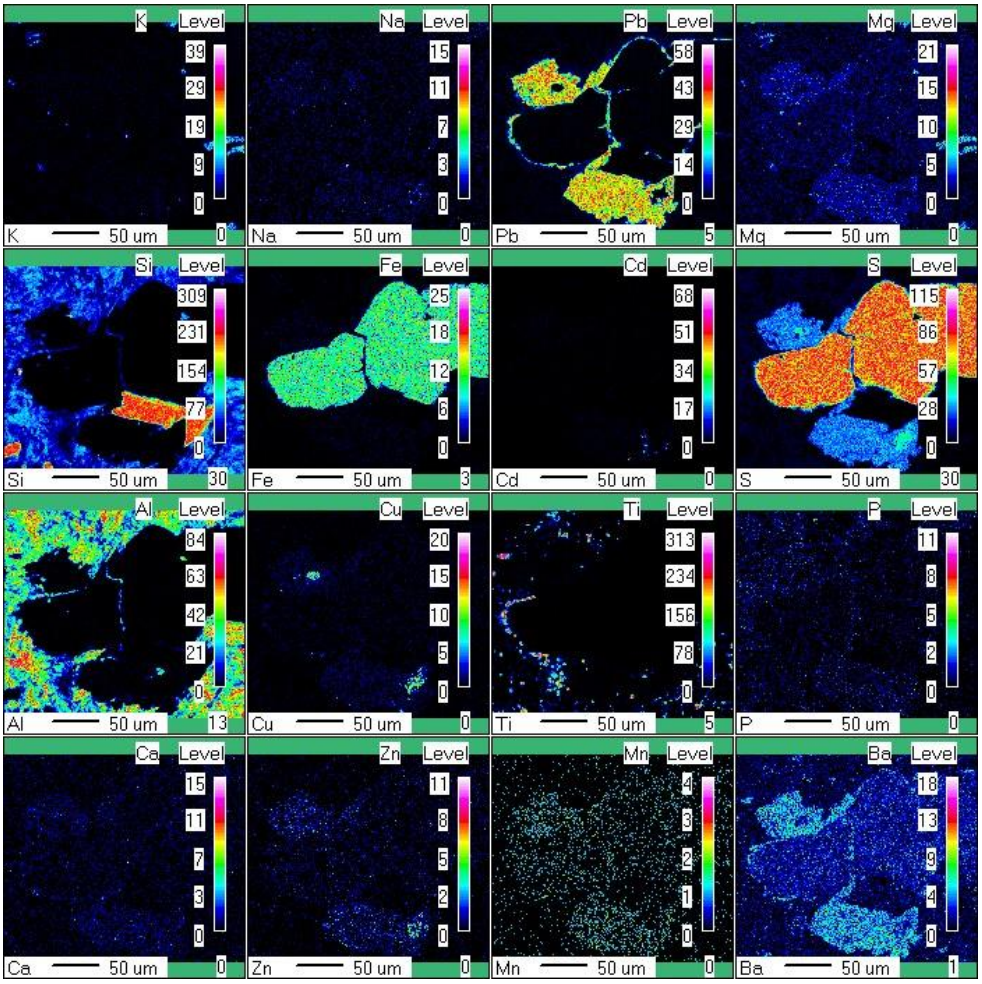

Figure 21: Element map showing rutile grains along galena boundary as well as chalcocite inclusions in galena, represented by copper occurrence; Galena also grows around pyrite grains; (The Y-axis is in X-ray Counts)

Metasiliciclastics

The main lead phase within the weathered sandstone is a manganese and lead containing non-sulphide, identified as pyromorphite. The mineral occurs as an anhedral phase closely surrounded by clay minerals and associated with a barite mineral identified as barrylisite with the Quantitative Analysis (Figure 24). Pyromorphite also occurs intergrown with clay minerals within veins, with a preferred orientation, and surrounding augen quartz grains (Figure 22). In some areas, pyromorphite appears more competent and is associated with iron oxides with which it forms augen wrapped by quartz and clay minerals (Figure 23). Galena, which occurs as a secondary lead phase in some weathered sandstone samples, has grown along sphalerite grain boundaries where it is intergrown with greenockite and subordinately clay minerals (

Figure **25**). All these feature are shown in the elemental maps referenced.

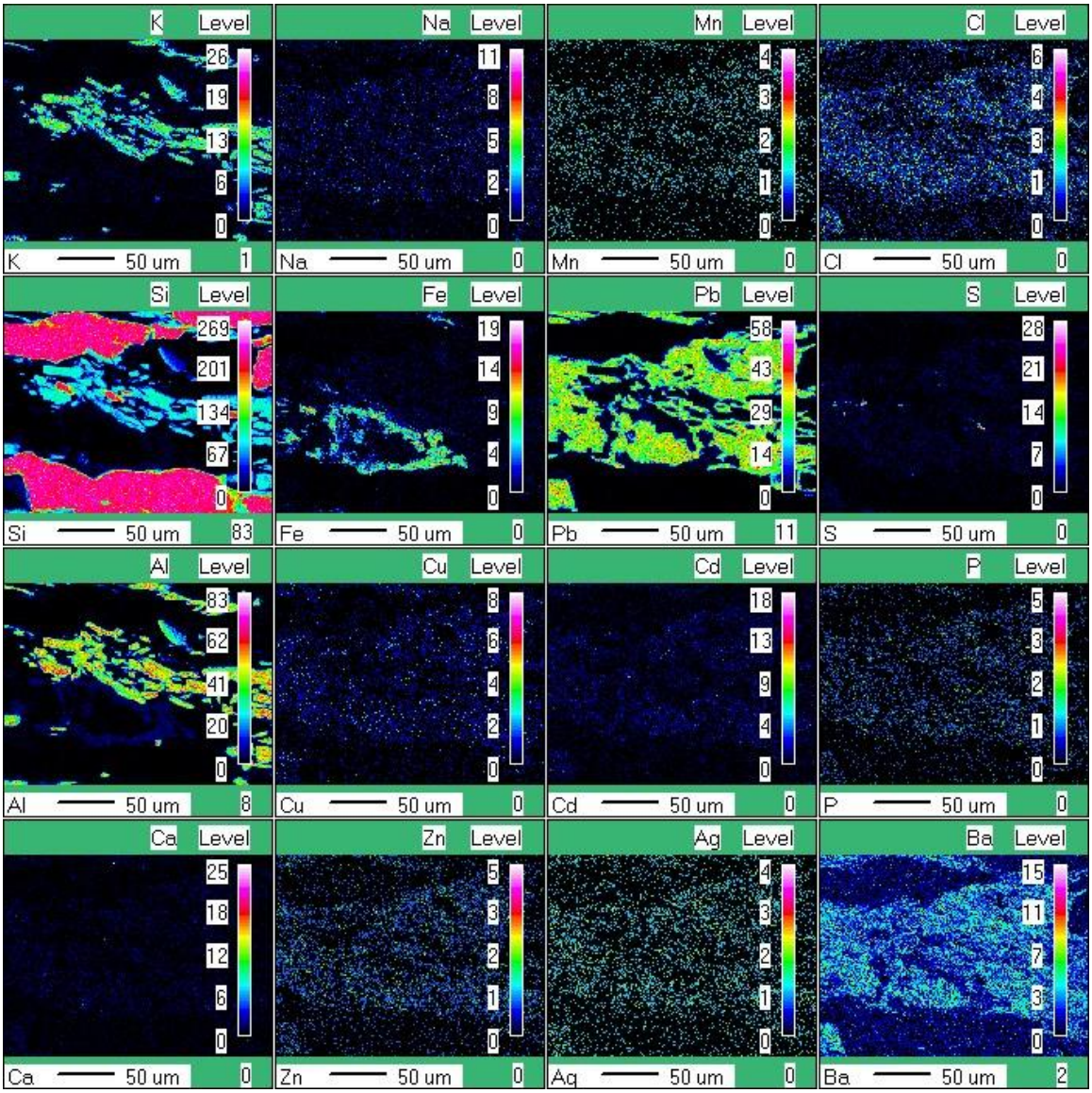

Figure 22: Pyromorphite intergrown with clay minerals and iron oxides; all showing a preferred orientation ((The Y-axis is in X-ray Counts)

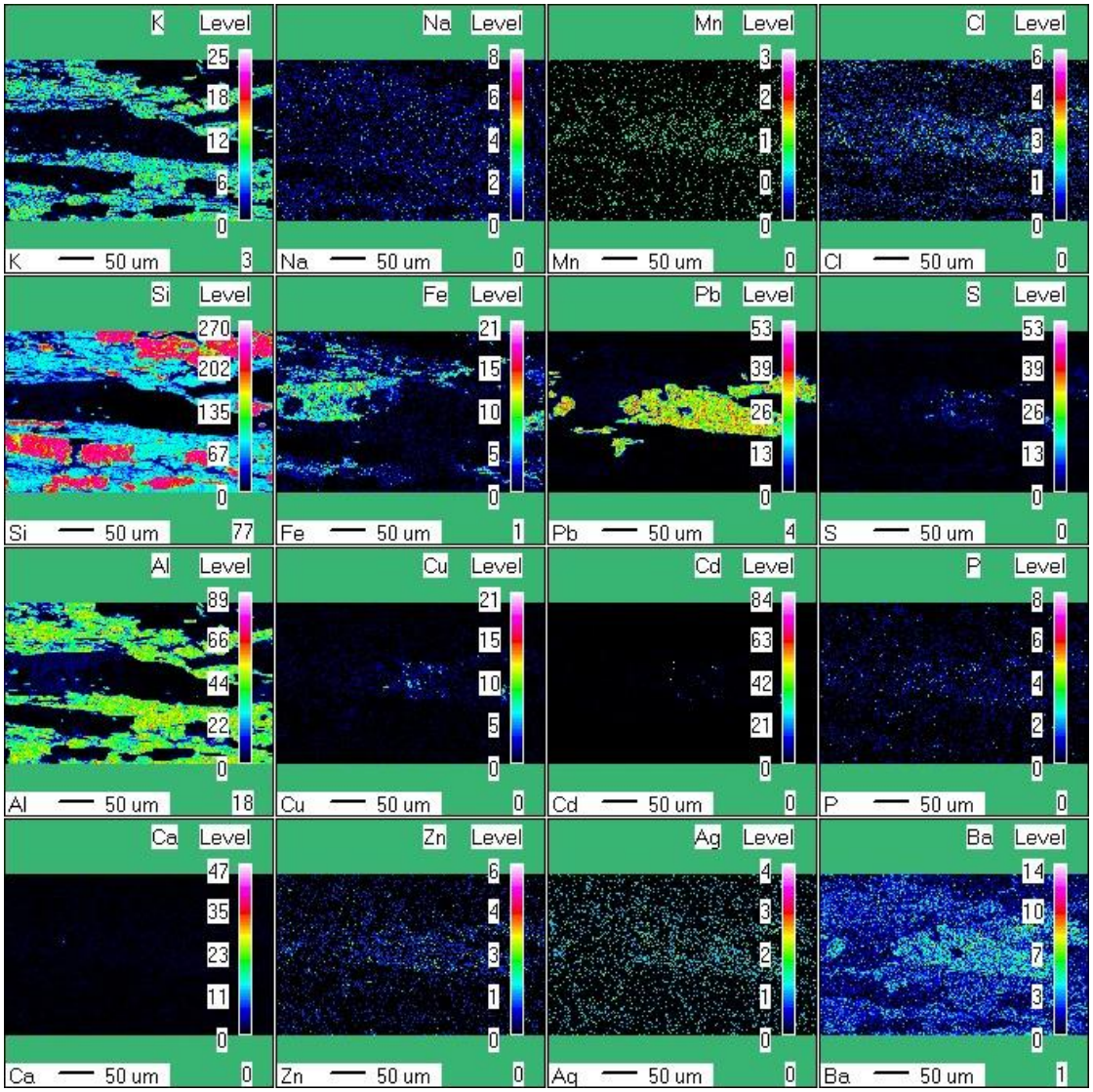

Figure 23: Pyromorphite occurring as augen within intergrown clay minerals and quartz; partly intergrown with iron oxides; Remnants of galena are visible within pyromorphite; (The Y-axis is in X-ray Counts)

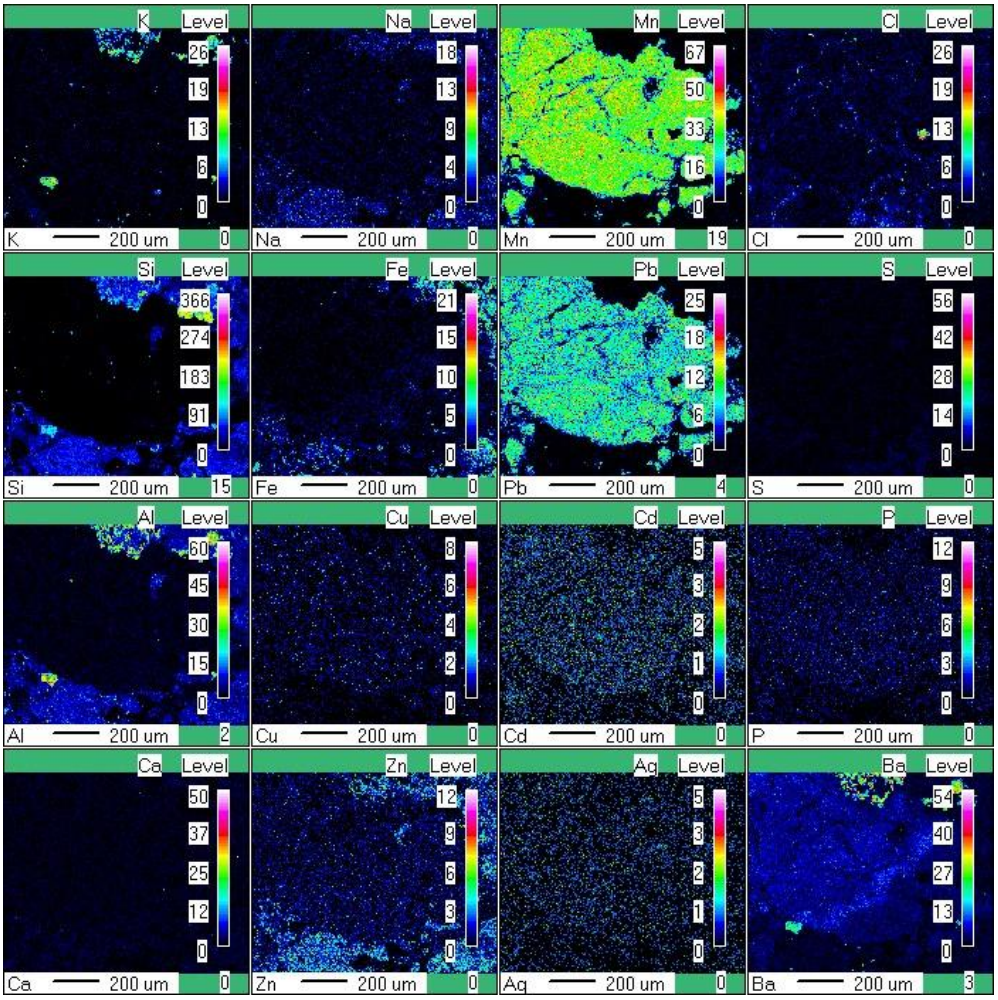

Figure 24: Pyromorphite appearing more massive with cracks and baryllisite grains growing on the edges of pyromorphite ((The Y-axis is in X-ray Counts)

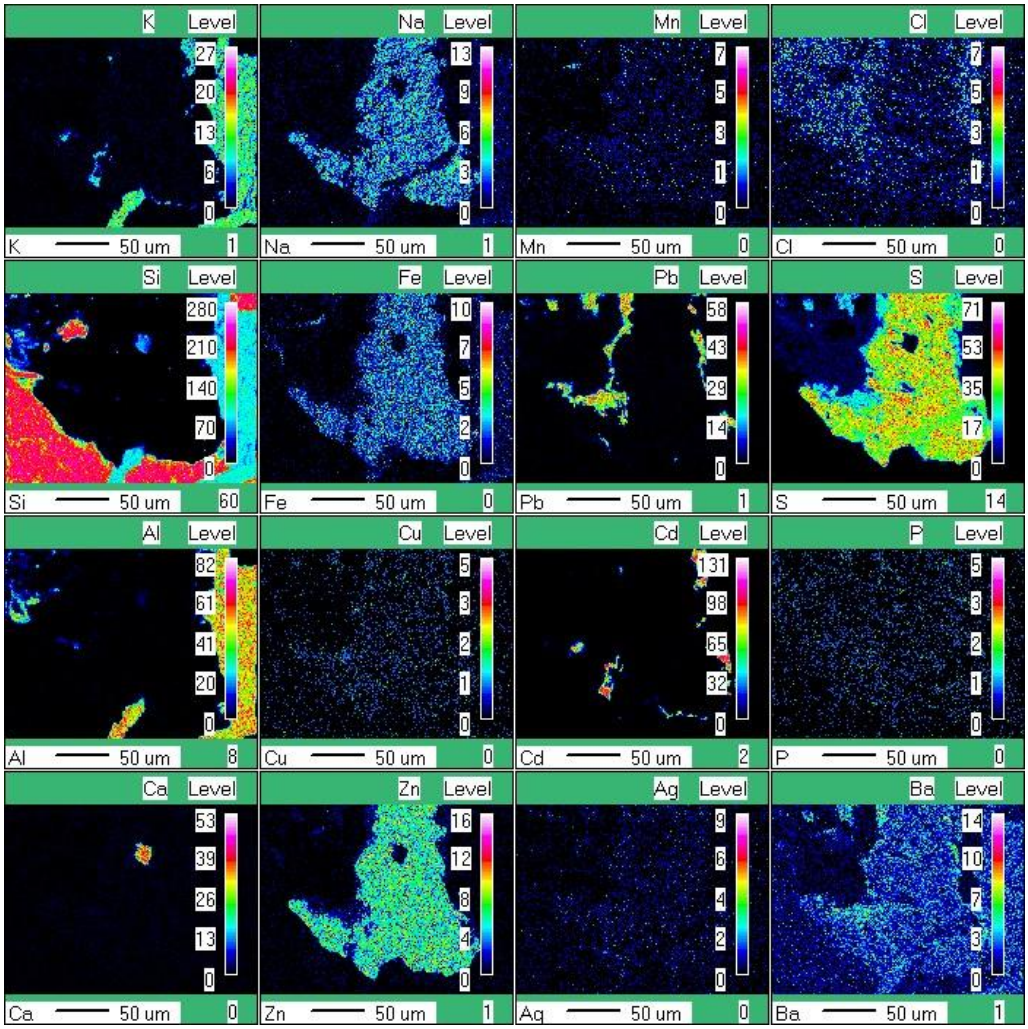

Figure 25: Galena within metasiliciclastics growing along sphalerite; Greenockite also intergrown with galena around sphalerite; (The Y-axis is in X-ray Counts)

Graphitic Schist

The main lead phase in the graphitic schist is galena. It is intergrown with sphalerite, chalcocite and greenockite. Pyrite seems to be isolated and fairly disseminated. From the elemental map (**Figure *26***), sphalerite has grown first, then surrounded by greenockite which is then overgrown by galena. The intergrowth of these minerals is generally subhedral to sub-rounded and has grown in pore spaces within the clay minerals (**Figure 27**). Pyromorphite occurs within pore spaces, along grain boundaries as well as within veins of this rock type (**Figure 28**).

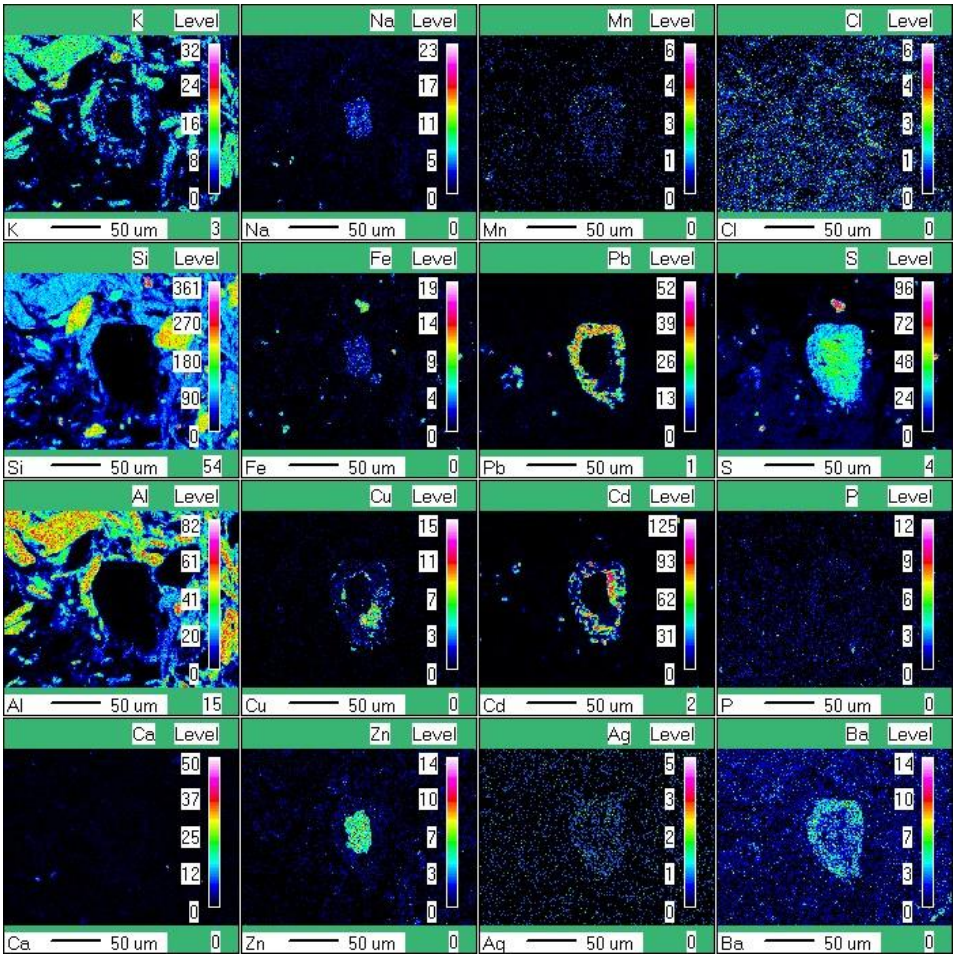

Figure 26: Element map of graphitic schist showing galena growing around sphalerite, and intergrown with chalcocite and greenockite; pyrite occurs as isolated grains ((The Y-axis is in X-ray Counts)

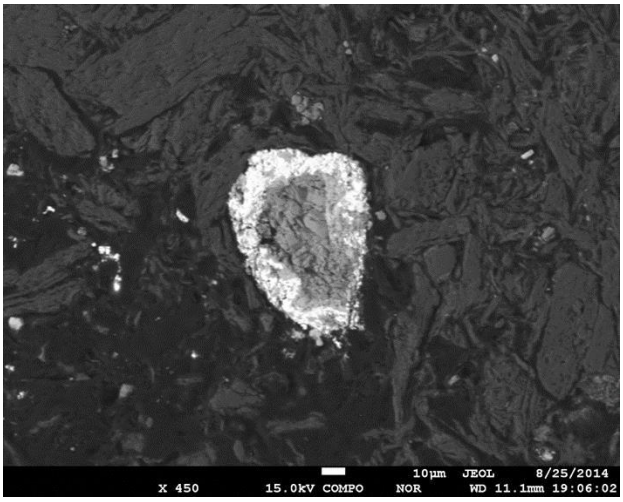

Figure 27: Backscatter image of element map in Figure 26

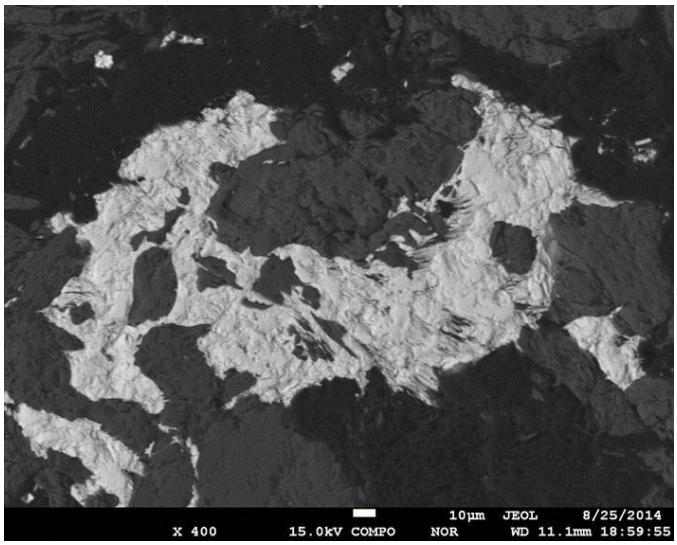

Figure 28: Pyromorphite in graphitic schist occurring in pore spaces as an anhedral phase

Carbonatized Sediment

Within the carbonatized sediment, lead occurs as pyromorphite. It grows around pyrite, and is in turn overgrown by smithsonite which is the dominant ore mineral in these samples. A barium bearing mineral and traces of chalcocite also occurs with pyromorphite. Pyromorphite grows within cracks of pyrite and as isolated fine grains. All these features are shown in (Figure 29).

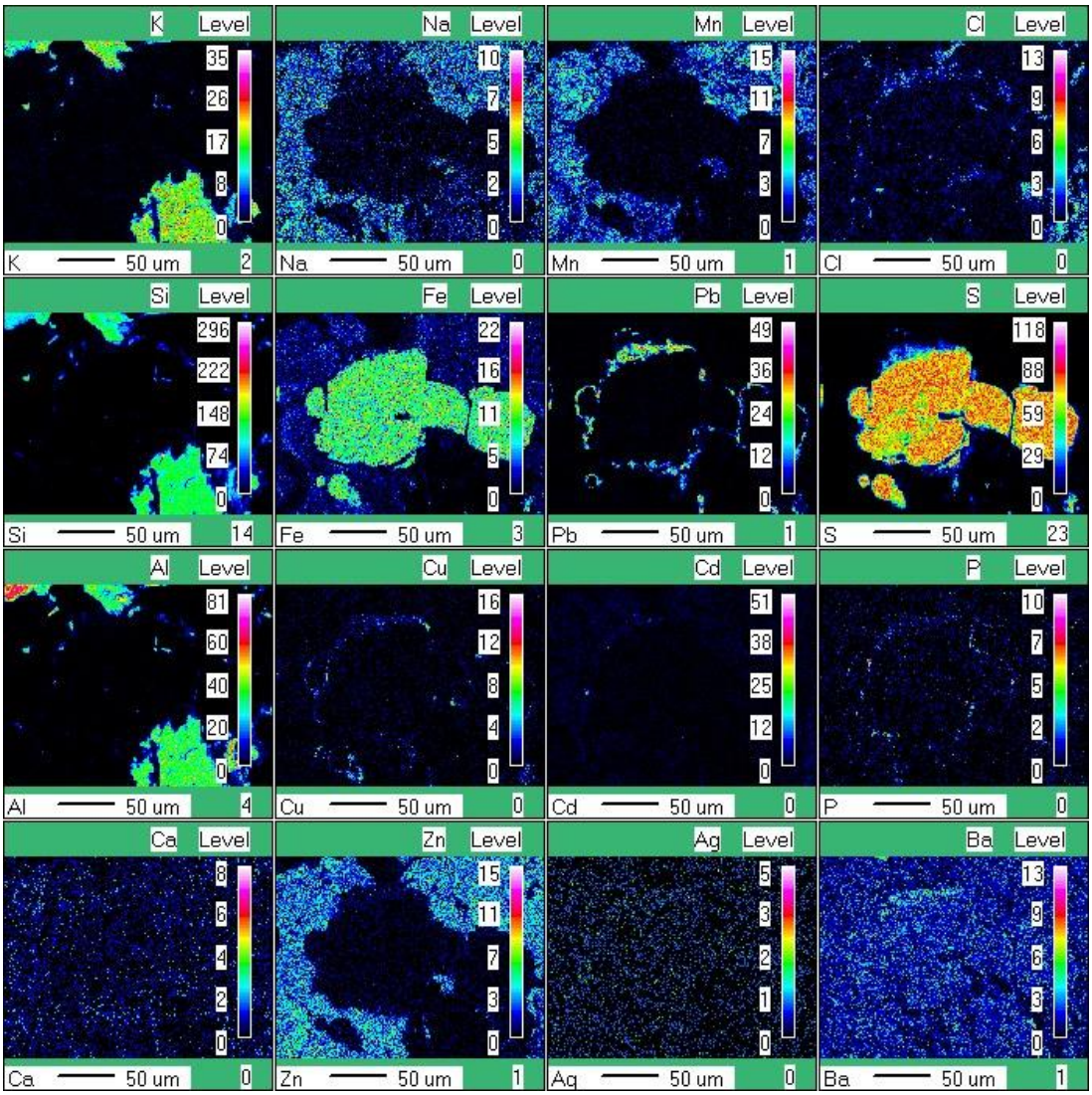

Figure 29: Element map of carbonatized sediment (showing pyromorphite textures and associated elements); (The Y-axis is in X-ray Counts)

4.3 Geochemistry

To understand the general spatial and statistical distribution of lead within the Skorpion deposit, a histogram and a cumulative probability diagram (Figure 30) was plotted and simple statistics were done on the samples with lead assays (Table 5). In addition to this, available geological, structural and borehole data was used to gain an understanding of the relationship of lead with various lithologies and major fault structures.

Figure 31 below shows the spatial distribution using mine digitized wireframes.

Table 5: Simple statistics for lead where data is available

Simple Statistics For Pb	
Minimum (%)	0.0001
Maximum (%)	12.35
Mode (%)	0.05
Mean (%)	0.08
Standard Deviation (%)	0.28
Variance	0.08
Mean on Statistical Cut-off (0.3%)	0.82
Mean on Statistical Cut-off (0.5%)	1.23
Number of Samples > 0.3%	2333
Number of Samples > 0.5%	1210
Number of Samples with Pb Assays	46407
Number of Database Samples	65535

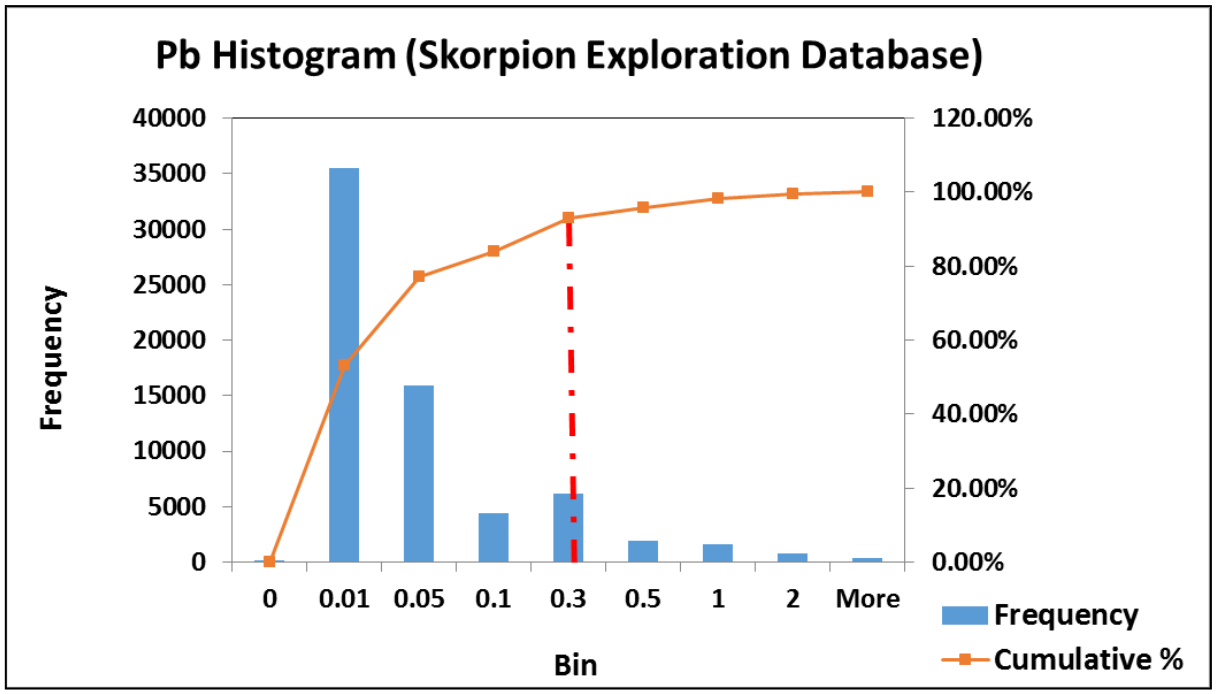

Figure 30: Histogram of Skorpion database lead and associated cumulative probability diagram; the red dotted line shows statistical cut-off of 0.3%

The histogram and cumulative probability diagrams above (Figure 30) indicate that more than 90% of the lead assays available lie below 0.3% and have a statistical cut-off of 0.3%. The mean at a 0.3% cutoff is 0.82%, which is very low. The mean calculated at 0.5% is 1.23%, which has a better future prospectivity.

Figure 31 below shows an east-west section through the Skorpion Deposit. The different rock types and major fault structures, as identified by various mapping campaigns, are indicated on the map as per the legend. The undifferentiated lead wireframe is also shown on the map. Undifferentiated metasiliciclastics are not shown on the map, but generally cover the entire open area west of the Zinc orebody, and including the Zinc orebody itself. Evident from the map as well as from the study samples, the bulk of the lead mineralization occurs within the felsic metavolcanic rocks, west of the Zinc orebody. Another significant portion of the mineralization occurs just above the felsic metavolcanics, within the metasiliciclastics. Negligible mineralization is associated with the mafic metavolcanic rocks. The lead mineralization occurs in very narrow veins that appear to be sub parallel to the major fault zones occurring within the felsic metavolcanics. Very high grades of lead have also been associated with faults within the exploration database.

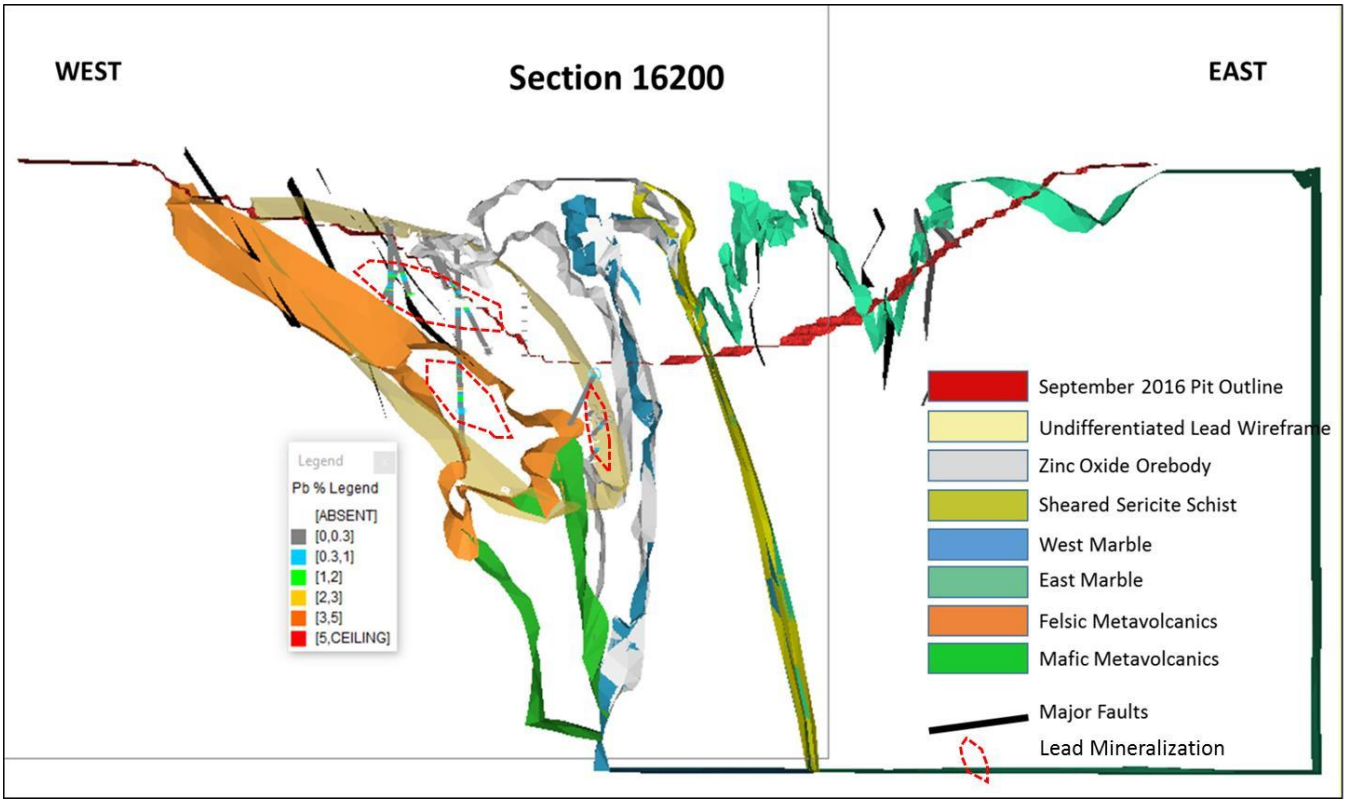

Figure 31: West-East Section through the Skorpion Zinc Pit, with the end September 2016 outline and the various rock type wireframes (adopted from various Skorpion Geologists' work) and Lead Wireframe digitized according to available data; Boreholes showing lead assays as per lead legend displayed are shown within the wireframe

Elemental associations were also studied using assays from the Skorpion Zinc Exploration Database and were plotted relative to their host lithologies. The lithologies were grouped into three main groups: metasiliciclastics, mafic metavolcanics and felsic metavolcanics. The distinction was based on geological logging in the database. Pearson's correlation diagrams were plotted, using the data analysis tool pack in excel, to try and understand the correlation coefficient of the various elements with each other, within each of the rock types. Moreover, histograms showing the distribution of lead in gossans and faults were plotted to show the variation within them. The plots were done for samples that have lead concentration greater than 0.1 to ensure that trends within the mineralized zones are not masked by barren samples. The conclusions from the observations are limited by the amount of lead assays within the database and drill holes drilled within these lead mineralization zones of the deposit.

	Ba_%	Cd_%	Co_%	Cu_%	Fe_%	Mn_%	Zn_%	S_%	Ag_%	Ni_%	Pb_%
Ba_%	1.00										
Cd_%	(0.11)	1.00									
Co_%	0.27	0.09	1.00								
Cu_%	0.09	0.01	0.07	1.00							
Fe_%	0.21	(0.01)	0.03	0.16	1.00						
Mn_%	0.60	(0.01)	0.35	0.14	0.24	1.00					
Zn_%	(0.15)	0.36	0.01	(0.05)	(0.12)	(0.08)	1.00				
S_%	0.00	0.10	0.01	(0.00)	0.06	0.04	(0.05)	1.00			
Ag_%	0.03	0.00	0.03	0.04	0.02	0.03	(0.01)	(0.00)	1.00		
Ni_%	(0.12)	0.24	0.17	0.02	(0.14)	(0.05)	0.57	(0.05)	0.05	1.00	
Pb_%	0.18	0.06	0.05	0.13	0.22	0.25	(0.11)	0.05	0.01	(0.12)	1.00

Figure 32: Diagram of Pearson's correlation coefficients within the clastic metasiliciclastics; Based on available data (Negative correlation is shown as brackets)

In the metasiliciclastics (Figure 32) lead shows a poor correlation with most of the elements. The highest correlation, which are both positive, are with iron and manganese. The highest elemental correlations within this lithology are seen between barium and manganese, zinc and nickel, zinc and cadmium as well as cobalt and manganese. These correlations are typical of oxidation zones of base metal deposits, particularly in gossanous zones.

	Mn_%	Cd_%	Co_%	Cu_%	Fe_%	Ba_%	Ag_%	Ni_%	Pb_%	Zn_%	S_%
Mn_%	1.00										
Cd_%	0.08	1.00									
Co_%	0.17	0.04	1.00								
Cu_%	0.06	0.04	(0.02)	1.00							
Fe_%	0.06	0.03	0.22	0.10	1.00						
Ba_%	0.23	(0.06)	0.44	(0.02)	0.15	1.00					
Ag_%	0.02	0.12	0.01	0.00	0.01	0.02	1.00				
Ni_%	0.04	(0.00)	0.40	(0.04)	0.05	0.23	(0.01)	1.00			
Pb_%	0.05	0.33	(0.00)	0.04	0.07	0.03	0.52	(0.01)	1.00		
Zn_%	0.01	0.03	0.01	0.00	0.03	0.01	(0.01)	0.05	0.00	1.00	
S_%	0.00	0.05	0.04	0.03	0.16	(0.05)	(0.01)	(0.04)	(0.02)	0.03	1.00

Figure 33: Diagram of Pearson's correlation coefficients within the felsic metavolcanics; Based on available data (Negative correlation is shown as brackets)

Silver shows the best positive correlation with lead in the felsic metavolcanics (Figure 33). This is indicative of primary lead mineralization, which is normally associated with silver. Lead also shows a positive correlation with cadmium. Other elements that correlate well are cobalt and barium as well as cobalt and nickel. These are both positive correlations.

	Ba_%	Cd_%	Co_%	Cu_%	Fe_%	Mn_%	Ag_%	Ni_%	Pb_%	Zn_%	S_%
Ba_%	1.00										
Cd_%	(0.10)	1.00									
Co_%	0.11	0.16	1.00								
Cu_%	(0.12)	0.17	(0.21)	1.00							
Fe_%	0.07	0.11	0.23	0.37	1.00						
Mn_%	(0.07)	0.16	0.07	(0.02)	0.14	1.00					
Ag_%	0.04	0.08	0.09	0.16	0.08	0.06	1.00				
Ni_%	(0.06)	0.20	0.34	(0.11)	0.27	0.12	0.01	1.00			
Pb_%	(0.05)	0.33	0.07	0.12	(0.05)	(0.02)	0.10	(0.01)	1.00		
Zn_%	0.02	0.20	0.18	(0.01)	0.12	0.01	0.00	0.17	0.03	1.00	
S_%	(0.10)	(0.00)	0.02	0.01	0.08	(0.04)	0.06	0.00	0.02	(0.06)	1.00

Figure 34: Pearson's Correlation coefficients diagram for mafic metavolcanics; Based on available data (negative correlation is shown as brackets)

The mafic metavolcanics (Figure 34) show poor correlations for all the elements. The best correlations are seen between lead and cadmium, as well as cobalt and nickel. These are both positive correlations.

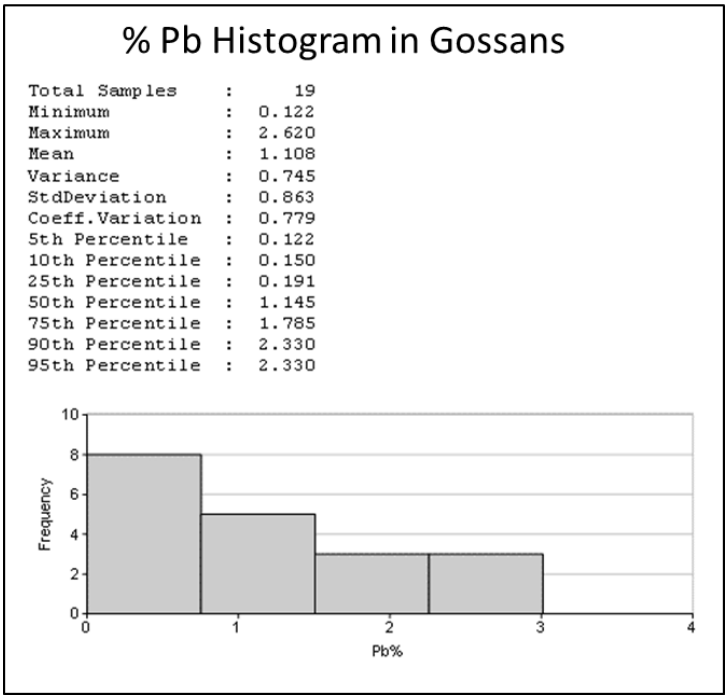

Figure 35: Histogram of samples within the gossanous zones

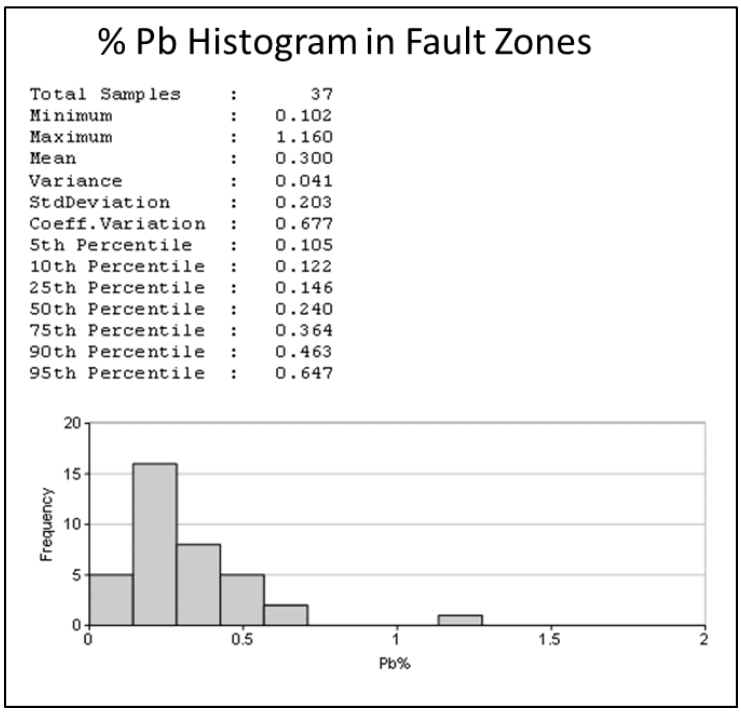

Figure 36: Histogram of samples within the fault zones

The simple statistics done on what has been logged as gossans and fault zones indicate a low coefficient of variance which implies a single population and therefore presumably a distinct mineralization genesis. Moreover, the mean in these two zones is significantly high at 0.300 % and 1.108% lead within the faults and gossans respectively. Additionally, as depicted by the 50th percentile in the gossanous zone, 50% of the samples in the zone have an average above 1.145% lead, which is a significant concentration when compared to the resource grade of a producing mine such as the Rosh Pinah Mine (Figure 36).

4.4 Lead Isotopes

For the plotting of the lead isotope study results, a distinction was made between samples containing non-sulphide lead mineralization, from those that contain galena as the lead mineral. The non-sulphide mineralization is generally hosted by metasiliciclastics whereas the sulphide mineralization is prominent in the felsic metavolcanics. This distinction was done to ensure that any obvious trends are identified easily.

As evident in (Table 6), the lower grade lead samples have high $^{206}Pb/^{204}Pb$ ratios, with the exception of sample MBHPb05 and MBHPb07. These samples have ratios that resemble samples with greater than 3 wt.% Pb. The two highest grade samples (Pb12 and Pb01) have ratios lower than 17.18. Although they both contain very high lead concentrations (4.6 wt.% and 5.8 wt.% respectively), they are markedly different in terms of lithology and mineralogy.

Table 6: Lead isotopes results and lead concentrations per sample

SAMPLE	$^{206}Pb/^{204}Pb$	$^{207}Pb/^{204}Pb$	$^{208}Pb/^{204}Pb$	$^{208}Pb/^{206}Pb$	$^{208}Pb/^{207}Pb$	$^{206}Pb/^{207}Pb$	Pb	Pb
	Unity	Unity	Unity	Unity	Unity	Unity	ppm	wt.%
MBHPb01	17.17	15.56	37.23	2.168	2.393	1.103	>10000	5.8
MBHPb12	17.18	15.52	37.18	2.164	2.396	1.105	>10000	4.6
MBHPb11	17.20	15.52	37.01	2.152	2.385	1.104	>10000	3
MBHPb09	17.29	15.61	37.36	2.162	2.394	1.105	>10000	2.7
MBHPb02	17.28	15.63	37.62	2.177	2.407	1.107	>10000	2.1
MBHPb06	17.31	15.67	37.66	2.176	2.403	1.106	>10000	1.9
MBHPb04	17.31	15.63	37.41	2.162	2.394	1.105	9160	0.9
MBHPb10	17.33	15.61	37.38	2.158	2.394	1.108	7300	0.7
MBHPb07	17.26	15.6	37.45	2.17	2.401	1.106	5730	0.6
MBHPb05	17.21	15.53	37.32	2.169	2.403	1.107	2650	0.3
MBHPb08	17.29	15.63	37.61	2.176	2.406	1.107	2640	0.3
MBHPb03	17.32	15.65	37.85	2.185	2.417	1.109	1310	0.1

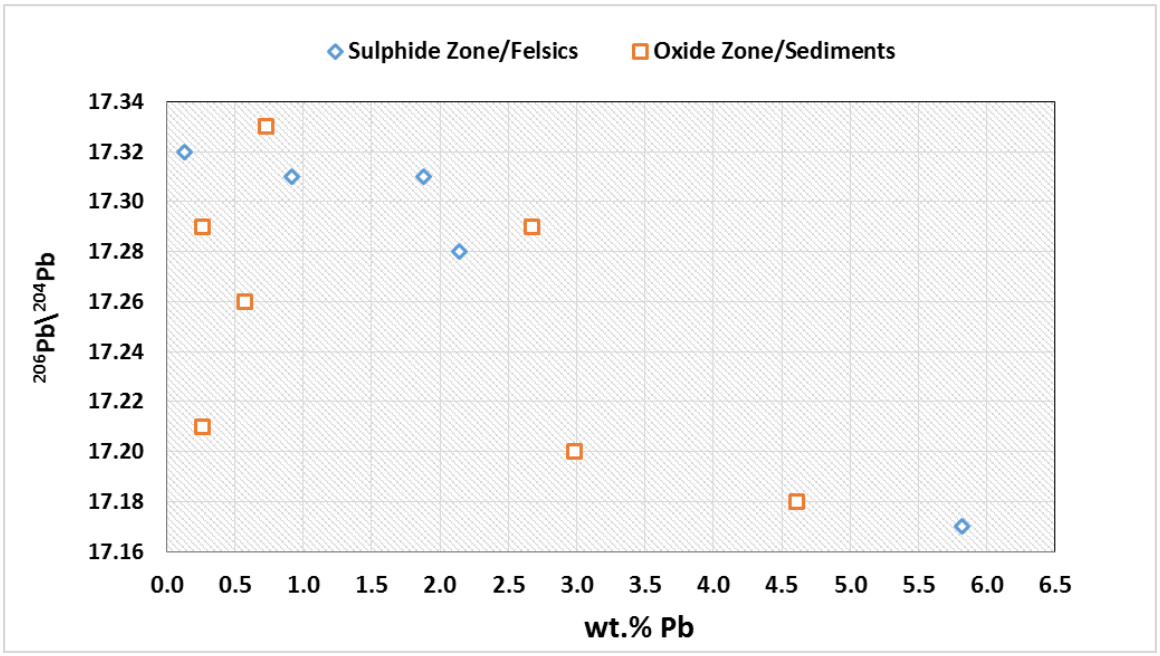

Figure 37: Sample lead concentrations in weight % plotted against 206Pb/204Pb

Majority of the non-sulphide lead samples contain $^{208}Pb/^{206}Pb$ ratios ranging between 2.150 and 2.170, with the exception of one sample (MBHPb08). Their $^{206}Pb/^{207}Pb$ ratios range between 1.104 and 1.108. The sulphide zone samples have a wider range of $^{206}Pb/^{207}Pb$, ranging from 1.103 to 1.109. Their $^{208}Pb/^{206}Pb$ are generally above 2.170 with the exception of MBHPb01. MBHPb01 is the sample with the highest Pb concentration (Table 6).

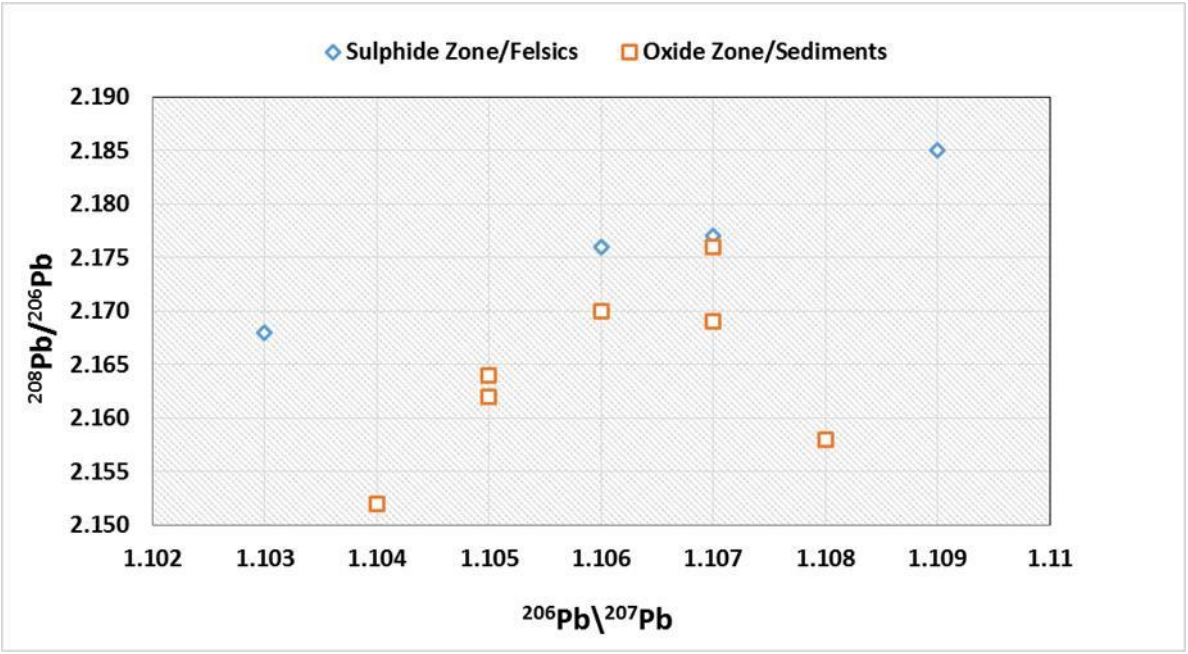

Figure 38: $^{206}Pb/^{207}Pb$ against $^{208}Pb/^{206}Pb$

With the $^{206}Pb/^{204}Pb$ vs $^{208}Pb/^{204}Pb$ plot, the ranges for the two different groups are not very distinct but samples from both groups seem to cluster in two different groups. The sulphide group has higher ratios of both $^{206}Pb/^{204}Pb$ and $^{208}Pb/^{204}Pb$ whereas the oxide group has lower ratios of both $^{206}Pb/^{204}Pb$ and $^{208}Pb/^{204}Pb$ (Figure 40). A similar scenario applies for the $^{207}Pb/^{204}Pb$ vs $^{206}Pb/^{204}Pb$ ratio plot (Figure 40). Two distinct groups of both mineralization types are also visible, however, the majority of the sulphide mineralization samples plot within the high $^{207}Pb/^{204}Pb$, $^{206}Pb/^{204}Pb$ and $^{208}Pb/^{204}Pb$ groups.

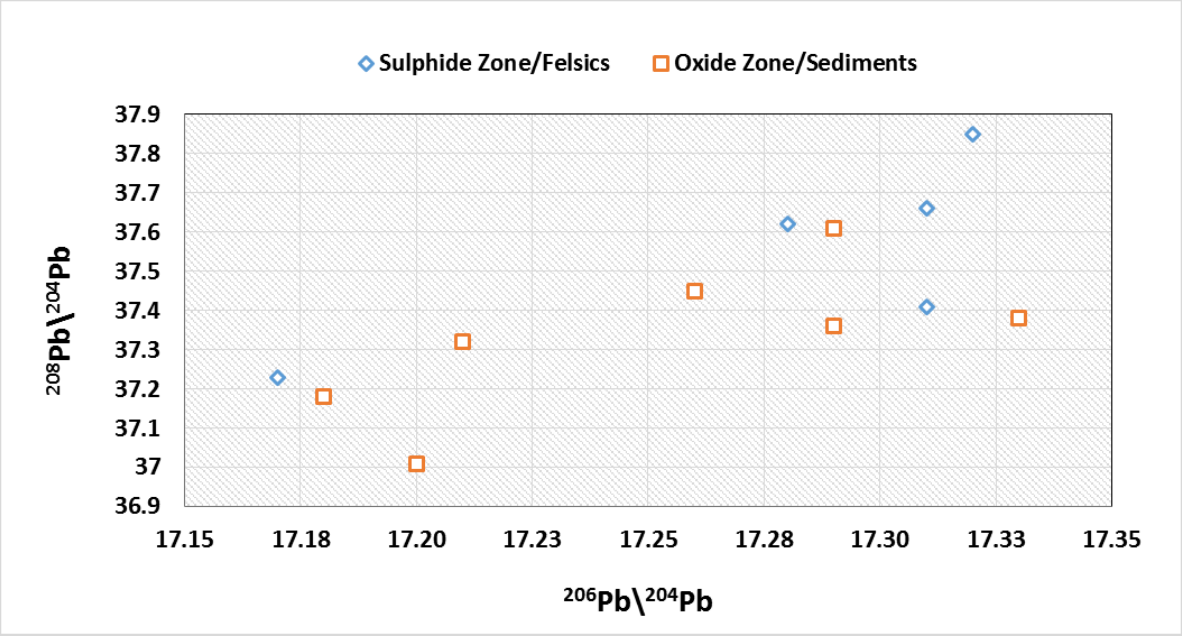

Figure 39: $^{206}Pb/^{204}Pb$ against $^{208}Pb/^{204}Pb$ (Thorogenic Diagram)

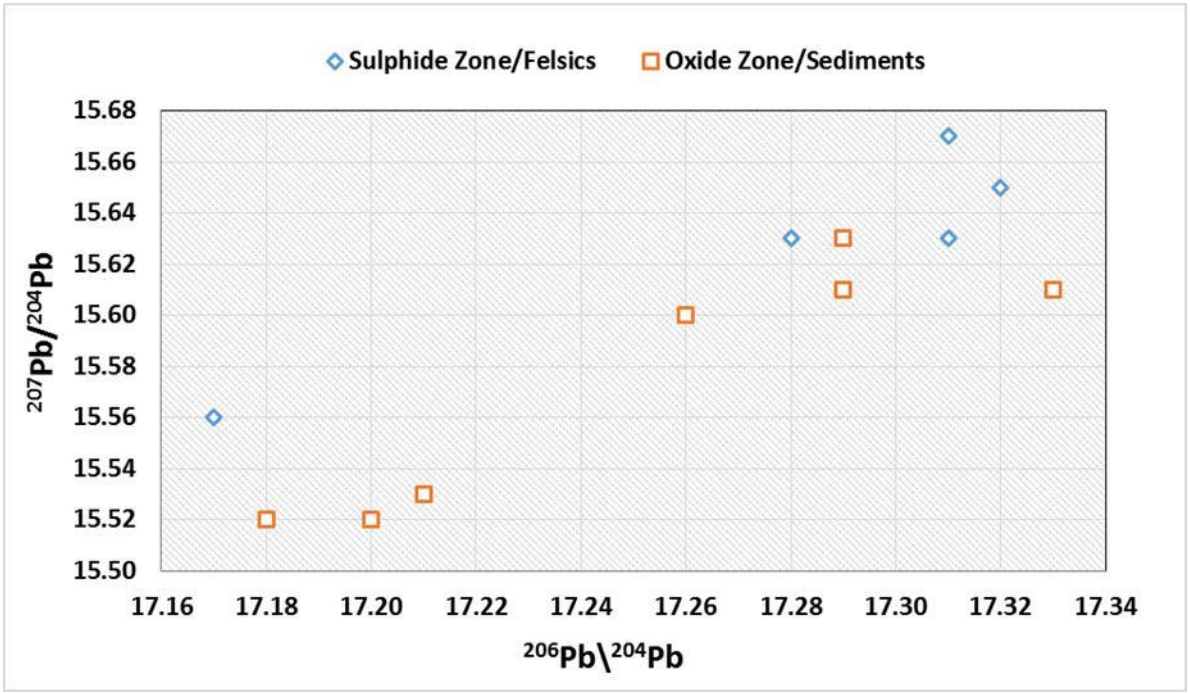

Figure 40: $^{206}Pb/^{204}Pb$ against $^{207}Pb/^{204}Pb$ (Uranogenic Diagram)

5 Discussion

5.1 Host Lithologies

The main host lithologies of lead identified from the 12 study samples, and the rest of the Skorpion Exploration Database data, are the felsic metavolcanic and metasiliciclastics. Subordinate amounts are hosted by the graphitic schists. These lithologies represent the rift and low energy environment that the Skorpion Zinc proto ore is believed to have formed (Kärner, 2003). All the identified lithologies are fine grained, highly quartz, muscovite, kaolinite, lizardite and orthoclase rich. This mineral composition is typical of felsic rocks that have undergone weathering of feldspars. Generally, the metasiliciclastics also contain a similar mineral composition. The differences between the two rock types arise in their textures.

Felsic metavolcanics are the main host rocks of the lead mineralization. Although the mineral composition and the appearance of the felsic metavolcanics justify their interpretation as having a felsic protolith, the presence of lithic fragments and graded bedding in some portions of the rock contradict this protolith. Moreover, the presence of thin bends of mafic minerals alternating with felsic minerals as well as the preferred orientation of the lithic fragments show that the rock may have undergone a certain degree of metamorphism. The major characteristics of this rock correlate well with the petrographic descriptions of the massive felsic lavas described and characterized by Allen et al. (1996). These rocks are locally known as quartz sericite schists and are believed to be metamorphosed felsic lavas that generally do not possess any primary volcanic features and can easily be mistaken for sedimentary rocks (Kärner, 2006). According to TAS diagrams by Kärner (2006), the felsic metavolcanics plot mainly as rhyolites and very few plot as andesites and dacites (Figure 41). Moreover, the felsic
metavolcanics plot in the ‘within plate’ zone on the Zr vs Zr/Y diagram. Kärner (2006) also indicated that the sulphur isotopes of sulphide mineralization within these rocks indicate a submarine felsic volcanic environment comparable to that of the Iberian Pyrite Belt. Although not much lead had been identified from the mafic metavolcanics, Kärner (2016) also showed that the amphibolite weathered equivalents were derived from basalts which were also formed in a ‘within plate’ environment.

The second major lead host rock are the metasiliciclastics. The fine grained nature of the rock imply sedimentation in a low energy environment, such as a deep sea environment. This implies that sedimentation of these rocks occurred during advanced stages of rifting. In comparison to the felsic metavolcanics, this rock should be stratigraphically younger. The presence of detrital zircon in this rock justifies its sedimentary nature. However, the presence of iron oxides in veins and within box work

structures indicate that the rock has undergone extensive fracturing due to deformation followed by high temperature fluid flow through the fractures that resulted in extensive oxidization of iron sulphides to form oxides. In addition to this, the interlocking quartz texture visible in some areas indicate that the rock has undergone a certain degree of metamorphism. However, the augen quartz and the banding show that metamorphism was followed by deformational events that put these rocks under strain. This has also been shown by workers such as Kärner (2006).

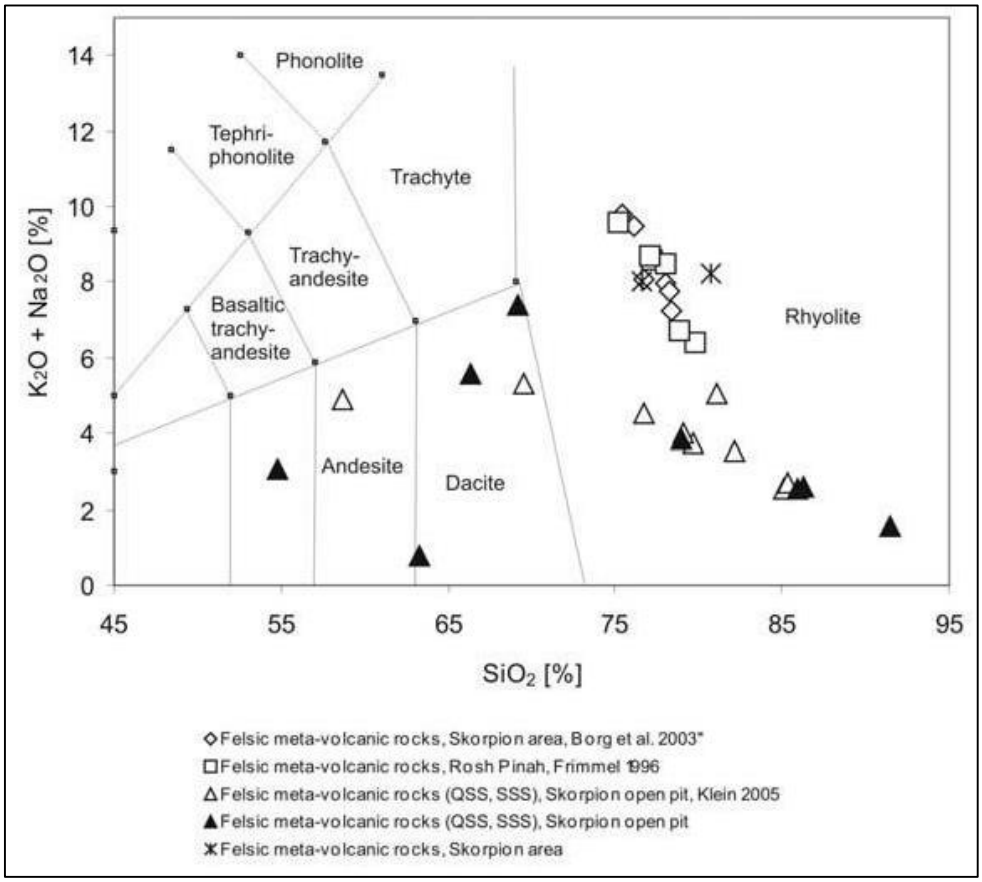

.

Figure 41: TAS diagram for Skorpion Felsic Metavolcanics (adapted from Kärner, 2006)

Other rocks that host lead are the calcified metasediment and the graphitic schist. Both these rocks contain a mineralogical compositions similar to that of the metasiliciclastics (Figure 42). However, the carbonatized metasediment contains a significant amount of smithsonite which is probably due to the carbonatization of a clastic sediment by carbonate rich mineralizing fluids that had reacted with a marble buffer and promoted the precipitation of zinc, copper and lead carbonates in porous rocks. The graphitic schist,

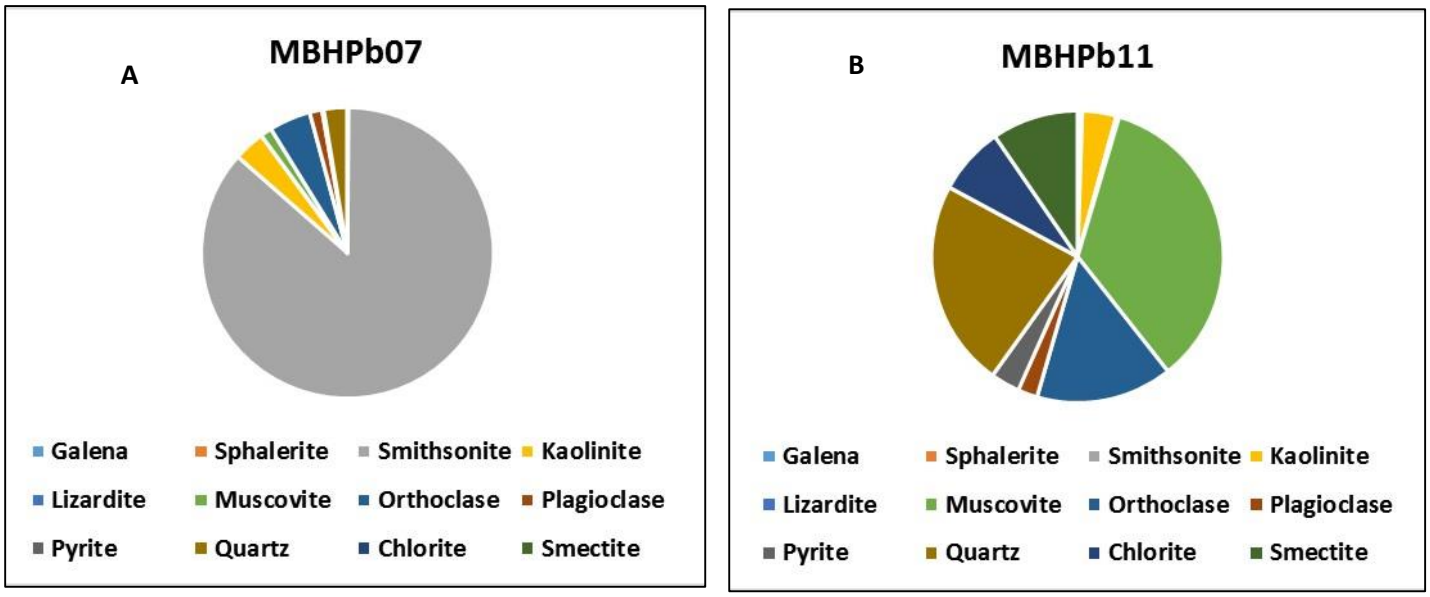

Figure 42: Mineral composition of the sample MBHPb07 showing the carbonatized metasediment composition (A) and sample MBHPb11 showing the graphitic schist composition (B)

contrary to the other rocks, contains smectites and chlorite which makes it much more clay mineral rich. Muscovite, which defines the schistosity, is the most abundant mineral in the rock. The black staining caused by the hand specimen is most probably a result of graphite flakes that may have formed from the metamorphism of organic material in the photolith (Simandl et al., 2015). This was most likely a sedimentary rock. The presence of organic matter within paleosoils of the Skorpion area has been proven by carbon isotope analysis done on smithsonite samples and compared to calcite in the ore bordering the marble horizon (Boni and Mondillo, 2015).

5.2 Lead Mineralization Distribution, Textures and Genesis

Textural analysis of the thin sections and elemental maps show that most of the galena occurs as anhedral grains growing around pyrite, sphalerite, and is intergrown with greenockite and chalcocite within the felsic metavolcanics. Some anhedral chalcocite grains also occur within galena. The textures indicate that galena may have been dissolved during supergene weathering and reprecipitated around partially dissolved pyrite grains. Moreover, the precipitation of anhedral galena around sphalerite, and intergrown with greenockite and chalcocite implies that galena was reprecipitated after sphalerite but coincident with greenockite and chalcocite. Galena also fills cracks within pyrite indicating that it may have been remobilized and reprecipitated within cracks resulting from brittle deformation events. The remobilization of lead is also evident from the occurrence of pyromorphite within the metasediments. This mainly occurs within fractures, intergrown with clay minerals and iron oxides. The presence of pyromorphite in metasediments imply that galena had been oxidized to anglesite and cerrusite, which are both unstable in acidic conditions and normally dissolve and reprecipitate the lead as pyromorphite.

This is a sign that EH, pH conditions changed during the remobilization of metals such as galena. This was also suggested by Kärner (2006) who attributed it to the dissolution of feldspars by acidic meteoric fluids as well as the presence of carbonate from the subsequent dissolution of the western and eastern marble. Moreover, the presence of elevated lead concentrations within the gossans and fault zone justify the dissolution and remobilization of galena and associated minerals. Lead occurs mainly as secondary phases, mainly as pyromorphite in the gossans due to the dissolution of galena caused by an increase in pH and Eh. The change in pH and Eh can be attributed to the dissolution of pyrite as it got exposed to oxygenated fluids. As indicated by the Eh, pH diagrams (Figure 43) galena dissolves fast but does not stay long in solution and reprecipitates as secondary sulphates carbonates or phosphate depending on the available ions in the solution (Anon, 2012). Although not very mobile, dissolved lead was transported through faults possibly from the primary felsic metavolcanic host into the metasediments. The extent of the transport of the lead is an indication of fast moving fluids possibly due to a high hydrological potential. Considering the current morphology of the lead mineralization within the Skorpion deposit, the postulated hypothesis by Kärner (2006) of leaching and reprecipitation having occurred due to meteoric waters flowing from WNW to ESE through faults as well due to fluctuations of the water table correlates with the observations.

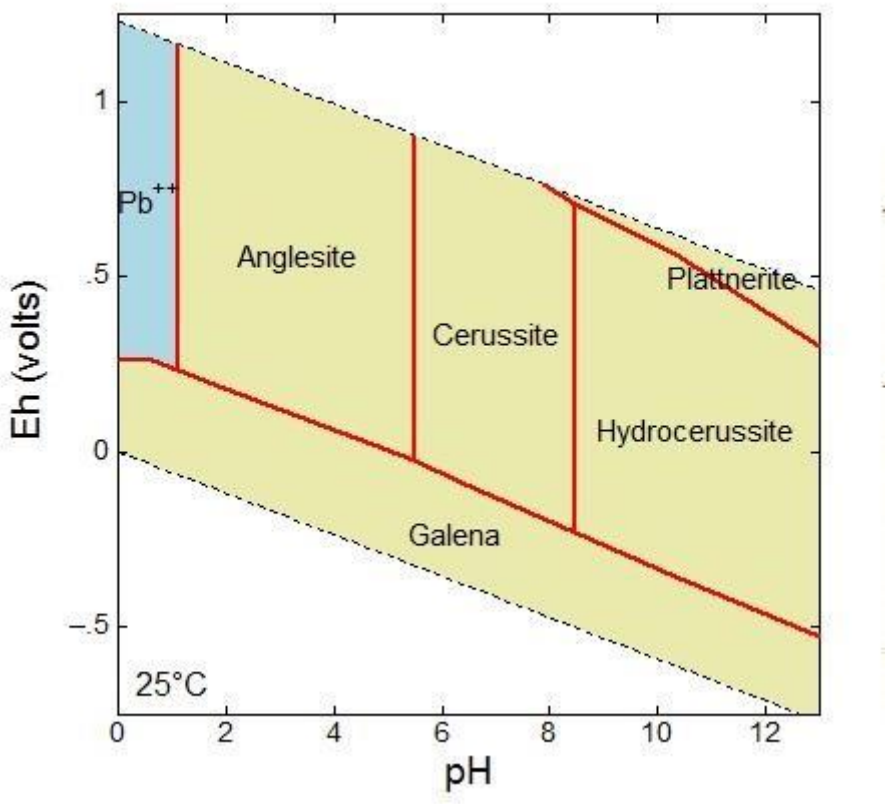

Figure 43: Eh, pH diagram of galena (Anon, 2012)

5.3 Elemental Associations and Implications

Spatially, the lead mineralization occurs in the most western zone of the Skorpion Zinc deposit, west of both the copper and zinc mineralization. Poor correlations between lead, zinc and copper can be established from the bulk of the study data. The poor correlations are particularly demonstrated by the EMPA results, the correlation diagrams, the XRD results as well as from scatter plots of the entire Skorpion Exploration database, plotted using Datamine software statistics function (Figure 44).

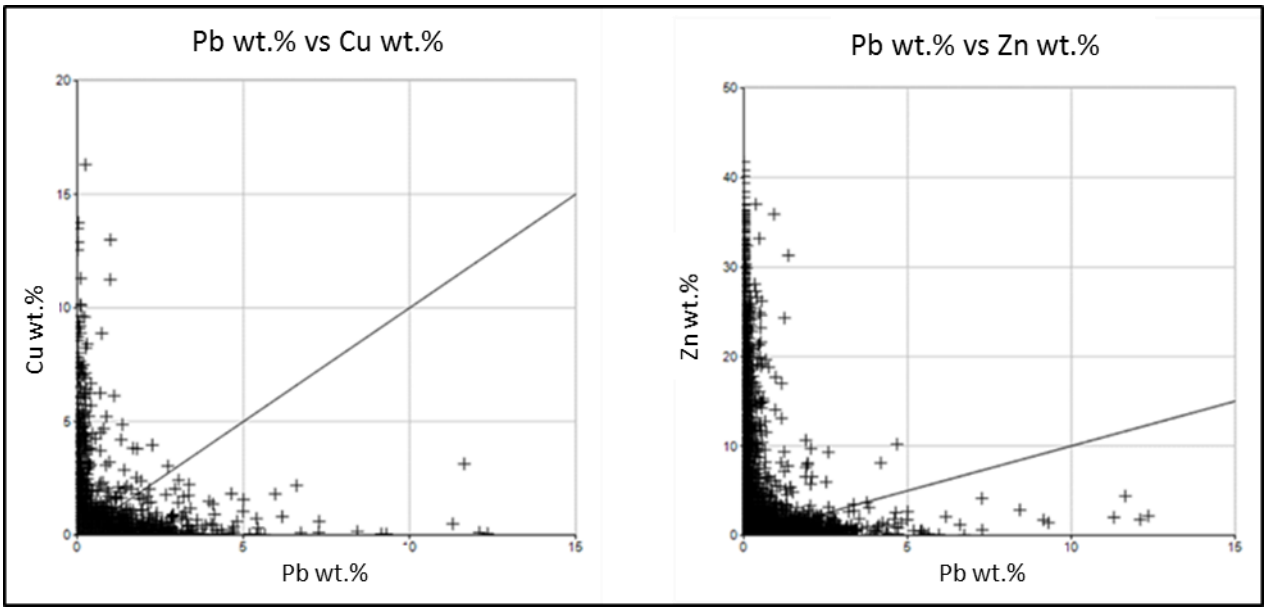

Figure 44: Scatter plots for Zn wt. % vs Pb wt.% and Cu wt.% vs Pb wt.%; both showing poor correlation

The poor correlation between lead and copper and lead and zinc can be attributed to the mode of formation of VMS deposits. Adapted from (Anon, 2017) Figure 45, shows that VMS deposits generally form in layers that are dominated by the four base metals, namely iron, lead, copper and zinc. Iron occurs in the bottom most layer, followed by lead and zinc in one zone, then lastly by a copper rich zone which is generally less horizontally extensive.

The host sequence deformation during the closure of the Adamastor Ocean, followed by the dissolution and remobilization of these metals in the original host rocks, is what has resulted in the current zoning seen in image B in Figure 46. Contrary to copper and zinc, lead is relatively immobile in acidic conditions and normally tends to reprecipitate close to or within the host lithology (Reddy et al., 1995). Therefore, the metals were reprecipitated in different zones in the flow direction of the dissolution fluids and in order of mobility. Zinc, being the most mobile of these elements, was deposits the furthest away from the proto ore location.

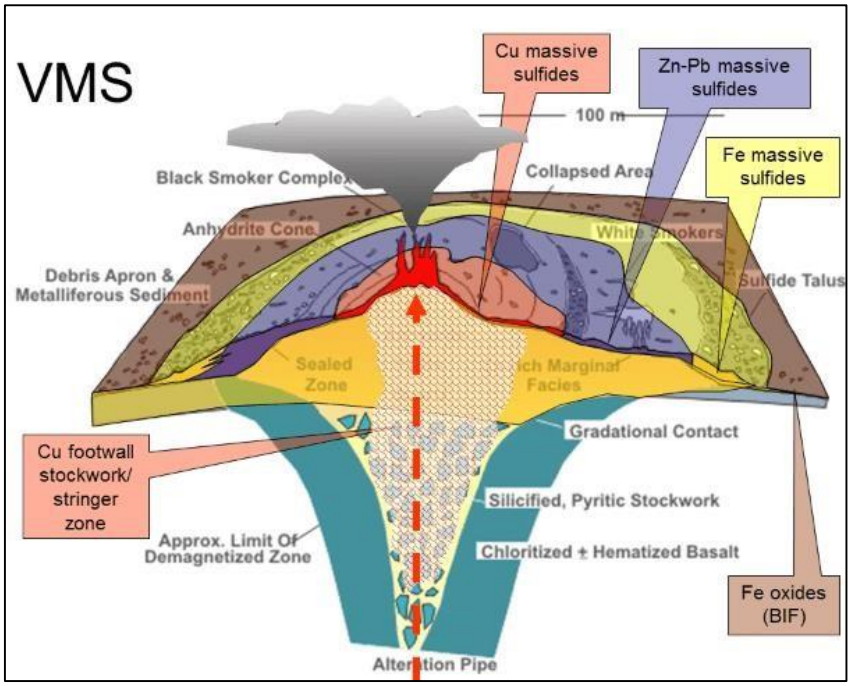

Figure 45: Image showing general morphology of VMS deposits; Zoning of Fe, Pb, Zn and Cu prior to secondary alterations are indicated in the image (adapted from Anon, 2017)

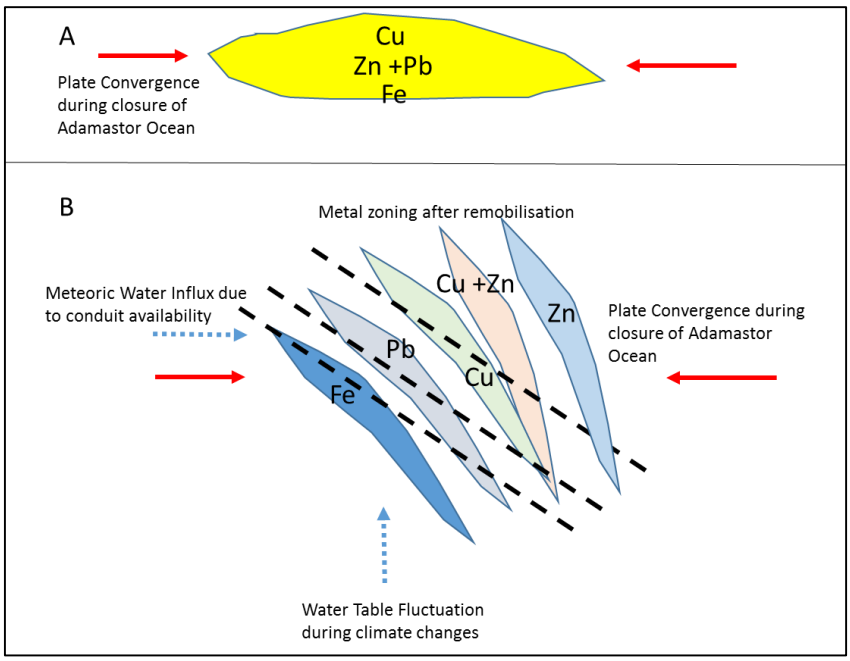

Figure 46: Illustration of changes in metal zonation from A (prior to deformation, alteration and metal remobilisation) before closure of the Adamastor Ocean; B shows current metal zonation that occurred after closure of the Adamastor Ocean as a result of Meteoric Waters percolating through faults (black dashed lines) as well as changes in the fluctuating water table

However, the correlation diagrams and EMPA results show that lead is associated with manganese and iron in the metasiliciclastics, and with silver and cadmium in the felsic metavolcanics. Barium also shows a good correlation with manganese within the metasiliciclastics, but not with lead. In the mafic

volcanics, lead shows a good correlation with cadmium, but not with silver. In addition to this, the best correlations in the mafic volcanics are evident between copper and iron, iron and cobalt, nickel and cobalt as well as iron and nickel.

The correlation between Ni, Co and Cu is expected of mafic volcanics, which are generally enriched in compatible elements (Winter, 2010). Small low-valence elements such as Ni, Cu, Co, Zn and Fe are compatible and get incorporated in the first solids and therefore appear to be more enriched in mafic volcanics as opposed to the felsic volcanics (Ridley, 2010). However, the poor correlation of Zn with the other compatible elements in the mafic volcanics could be an indication of secondary processes that may have leached and mobilized it to other rock types. Oxidation processes responsible for the formation of supergene ores tend to have a low pH which enhances the leaching and mobilization of Zn in the sulphide proto ore relative to other elements (Skarpelis & Argyraki, 2009). The low pH is generated by the presence of pyrite (Large, 2001) which is easily dissolved in oxygenated environments to form Fe^{2+} ions and H^{+}. This increases acidity (Eggleston et al., 1996) and promotes dissolution of metal sulphides, such as sphalerite, chalcocite and galena. Zn^{2+} has been proven to be more mobile in acidic ionic solutions than Pb^{2+} ions and Cu^{2+} and can therefore be transported by acidic fluids much further away from the proto ore than the other two metals (Reddy et al., 1995).

Silver and cadmium show the best positive correlation with lead in the felsic metavolcanics. The presence of Ag or Ag minerals within galena has been discussed by Zeng et.al (2000). Silver ions can substitute Pb^{2+} during crystallization and a variety of silver minerals can also be incorporated as inclusions within galena. However, this occurrence could not be proven by the EMPA conducted for the study. A study done by Saayman (2014) indicated the presence of Ag in galena from several Skorpion Zinc samples within the meta-sediments. The presence of Ag minerals in the meta-sediments can be a result of the dissolution of galena and possibly primary silver minerals and subsequent transport and precipitation of various secondary sliver bearing minerals, such as iodargyrite and cryptomelane, as proven by Saayman (2014). Cadmium is mildly incompatible and its fractionation can vary (Wang et al., 2016). Moreover, the mobility of cadmium is similar to that of zinc in acidic environments. This explains why cadmium shows a positive correlation with lead in the mafic volcanics, in the felsics as well as with zinc in the metasiliciclastics.

Although poor, lead shows the best positive correlations with manganese and iron in the metasiliciclastics. Better positive correlations are seen between manganese and barium, and zinc and nickel. The EMPA and thin sections indicate the presence of pyromorphite in the metasiliciclastics. Pyromorphite is a lead, manganese phosphate. This implies that the metasiliciclastics are the main host of the oxidation zone of the lead mineralization. The lead oxidation zone may have resulted from leaching and transport of the lead from the source felsic volcanics and possibly from primary sulphides within the metasiliciclastics. Moreover, the lack of correlation of the lead and zinc in the metasiliciclastics could be a result of the relative mobilities and implies that the two metals where not

precipitated in the same zone. The presence of high lead concentrations within the gossanous zones and fault zones (Figure 35 and Figure 36) is evidence of lead sulphide dissolution and transport through faults zones. Lead is relatively immobile in acidic conditions and normally tends to reprecipitate close to or within the host lithology (Reddy et al., 1995).

5.4 Lead Isotope Implications on Mineralization

The lead isotope data obtained from the 12 study samples show a good correlation with data presented by Frimmel et al. (2004) in terms of the age of the lead mineralization and the source rock. The average lead isotope ratios of $^{206}Pb/^{204}Pb$ (17.26), $^{207}Pb/^{204}Pb$ (15.60) and $^{208}Pb/^{204}Pb$ (37.42) resemble results provided by Frimmel (2004) for both the Skorpion and Rosh Pinah deposits. For the Skorpion samples from Frimmel (2004) had the following average ratios: $^{206}Pb/^{204}Pb$ (17.29), $^{207}Pb/^{204}Pb$ (15.59) and $^{208}Pb/^{204}Pb$ (37.51). The Rosh Pinah samples had the following average ratios: $^{206}Pb/^{204}Pb$ (17.17), $^{207}Pb/^{204}Pb$ (15.61) and $^{208}Pb/^{204}Pb$ (37.45).

Frimmel et al. (2004) showed that the elevated $^{207}Pb/^{204}Pb$ in the Rosh Pinah sulphide ore and Skorpion oxide ore within the sedimentary host rocks are in agreement with 2.0 Ga Eburnean pre-Gariep basement. This basement has thus been interpreted as the source rock for the host Rosh Pinah formation felsic metavolcanics. The similarities between data presented by Frimmel et al. (2004) and data from the study samples imply that Skorpion sulphides lead may have been derived from Gariep basement rock, most probably by partial melting during the rifting stages of the opening of the Adamastor Ocean (Frimmel et al., 2004). The melting provided the felsic melts that incorporated incompatible elements such as Pb, Th and U. This melt was extruded as the felsic volcanic rocks that host the primary Skorpion lead sulphides mineralization. Isotopic compositions of the metasediments, that incorporate majority of the lead oxide zone, show similar signatures as the felsic metavolcanic hosted sulphides. In addition to this, lead mineral textures within both the metasediments and most of the felsic metavolcanics show a degree of remobilization and concentration in veins and pore spaces. This could imply that most of the primary lead from the original felsic volcanics may have been remobilized into highly weathered and fractured rocks during and after deformation. As shown by Frimmel et al. (2004), the possibility of the sediments of the Rosh Pinah formation metasediments to have been sourced from the basements rock is also high.

Stacey and Kramers two stage models plotted by Frimmel et al. (2004), indicate that the Rosh Pinah deposit Pb mineralization is older the Skorpion lead mineralization and has slightly lower the $^{206}Pb/^{204}Pb$ isotopic ratios. This could imply that, although the mineralization is from the same source, the Rosh Pinah deposit hydrothermal mineralizing cells were much longer lived and sourced a deeper less evolved source, probably through deeper seated faults. This is in agreement with the nature of formation of SEDEX deposits (Evans, 1993).

Due to the change of Pb isotopes as a result of thorium and uranium decay series, $^{206}Pb/^{204}Pb$ ratios are used to discriminate the age of mineralization whereas the $^{207}Pb/^{204}Pb$ discriminate the extent of crustal and primitive magma input to the mineralization (Ceyhan, 2003). According to the plumbotectonic curves of Doe and Zartman (1981), adopted from Tao Liu et. al (2017) , the $^{208}Pb/^{204}Pb$ vs $^{206}Pb/^{204}Pb$ plot indicate that subvolcanic rocks are the source of the Skorpion lead, whereas the $^{207}Pb/^{204}Pb$ vs

$^{206}Pb/^{204}Pb$ plot indicates that the source might be the upper crust (Figure 47). However, the lead isotope plots presented by Frimmel et al., 2004 indicate that the Rosh Pinah deposit show a similar but slightly wider range isotopic composition which can imply a slightly longer lived mineralization event compared to the Skorpion deposit (Figure 48).This correlates well with Frimmel et al. (2004). With the Skorpion lead mineralization plotting on the upper crust curve as well as on the subvolcanic rocks zone (Figure 47), it can be hypothesized that the felsic melt derived from the Eburnean pre-Gariep basement may have been contaminated by upper crustal rocks.

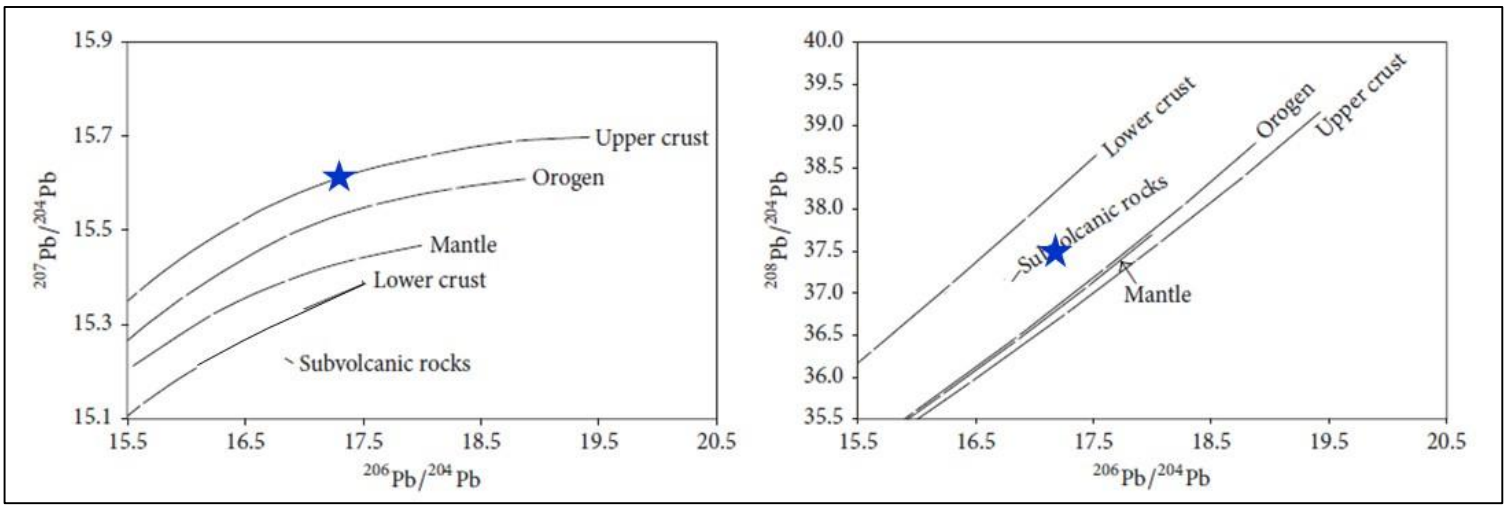

Figure 47: Studied galena lead isotope average shown as blue stars, plotted on Zartman and Doe (1981) Mantle Growth Curves adapted from Tao Liu et. al, 2017; The $^{206}Pb/^{204}Pb$ is 17.26; The $^{207}Pb/^{204}Pb$ is 15.60; The $^{208}Pb/^{204}Pb$ is 37.42

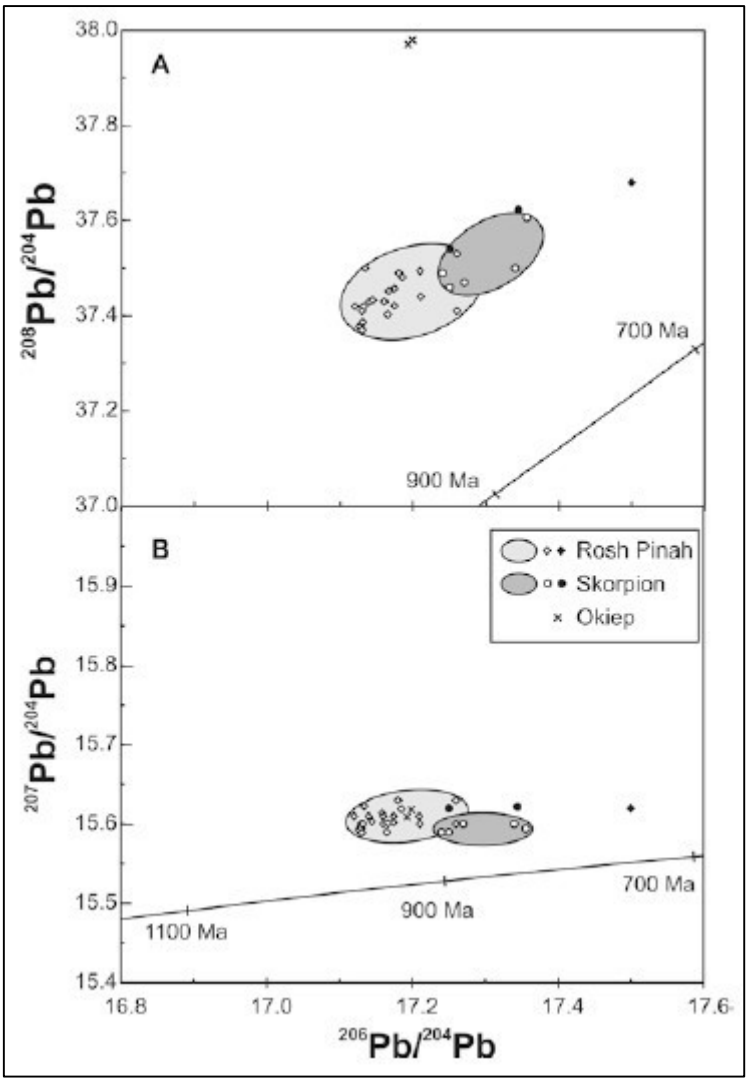

Figure 48: Galena derived Lead Isotopes Plot for Rosh Pinah, Skorpion and Hoits Mine near Okiep (adapted from Frimmel et.al, 2004 and including Stacey and Kramers (1975) Growth Curves); Open symbols represent primary galena whereas the filled symbols represent remobilised, secondary galena.

5.5 Postulated Mineralization Genesis and Related Tectonics

As evidenced by the lead isotopic signatures of the study samples, the mafic and felsic metavolcanic rocks were a result of the partial melting of the 2.0 Ga Eburnean pre-Gariep basement during the initial stages of rifting. These rocks were extruded into the failed Rosh Pinah graben and carried some of the lead mineralization and associated metals. Partial melting of subvolcanic rocks, influenced by a degree of upper crustal contamination, resulted in the observed slightly elevated isotopic signatures. Moreover, the narrow range seen in the Skorpion isotopic signatures could indicate a short lived, and or fast magmatism that may have had an early influence of sedimentation. Frimmel et al. (2004) indicated that smaller, syn-orogenic base metal deposits within the Rosh Pinah area seem to have been more influenced by surrounding country rock during the movement of orogenic fluids. These fluids introduced more radiogenic lead as seen with the elevated lead ratios of the study.

Uplift and erosion caused by the thinning of the crust during the D1 rifting, provided the sediments for the Rosh Pinah formation metasediments which are currently the main host rocks of the Skorpion supergene deposit. The Rosh Pinah deposit may have formed during the sedimentation period which may have lasted long and resulted in the much bigger deposit than the Skorpion deposit. The Skorpion deposit however also formed during this period but was highly influenced by felsic volcanism within a smaller subsea graben, within which sedimentation occurred faster and influenced the smaller nature of the deposit. This also justifies the occurrence of sulphides within the metasediments. Although both deposits where sourced from the 2.0 Ga Eburnean pre-Gariep basement, the Rosh Pinah deposit seems to have had a deeper seated conduit which allowed the mineralizing hydrothermal fluids to leach greater parts of the basement and provide more lead and zinc rich mineralization as compared to the Skorpion deposit. The relative mobility of the metals such as zinc, lead and copper as well as the proximity of the conduits to the source seems to have influenced the amount of metal deposited as the primary sulphides mineralization. Due to its relatively higher mobility, zinc was transported further and faster by the hydrothermal fluids and therefore managed to attain high concentrations despite the short lived mineralization event of the Skorpion sulphides proto ore. The presence of higher concentrations of copper within the Skorpion deposit compared to the Rosh Pinah deposit may imply that the Skorpion mineralization event had a magmatic influence. This is also justified by the presence of mafic metavolcanics just below the host felsic metavolcanics.

Mineralization had begun to cease in the Skorpion deposit bearing graben by the time the youngest carbonates where deposited in a shallowing water environment. Deposition of the carbonates was then followed by closure of the Adamastor Ocean which characterizes the D2 transpressional event and SSE directed thrusting. Compressional tectonics (D3) imparted by the collision of the South African and South American plates led to brittle-ductile deformation and the development of the major shear zones and faults that eventually facilitated the supergene alteration of the Skorpion sulphides proto-ore. The

lower greenschist to upper amphibolite facies metamorphism recorded within the area was also experienced during this time. Extensional tectonics related to the opening of the Atlantic Ocean (D4 event) led to the development of NW-NE trending faults which also provided more conduits.

These deformational events led to the structure that facilitated the supergene alteration of the sulphides proto ore by meteoric fluids as well as by the fluctuating water table. The steeply dipping sulphide proto ore that was highly affected by folding and faulting was later exposed to supergene enrichment. The exposure of pyrite bearing felsic metavolcanics to the oxygenated meteoric fluids and the fluctuating water table resulted in the acidification of the fluids and thereby the consequent dissolution of ore minerals such as chalcocite, sphalerite and galena. This liberated the constituent metal phases which were then transported along weak zones such as fault and shear zones and reprecipitated as the pH and Eh of the fluids changed due to dissolution of buffering minerals such as calcite. The mobility of the different metals determined how far they were transported and reprecipitated (Reddy et al., 1995). Zinc, being the most mobile between Fe, Mn, Pb and Cu, was transported the furthest, followed by Cu, then Pb, and then Fe and Mn. This metal distribution event, which was also explained by Kärner, 2006, implies that the meteoric fluids moved from WNW to ESE as well as bottom to top as a result of a fluctuating water table. Figure 49, adapted from Van Schalkwyk (2016) displays the current structure of the Skorpion orebody and related lead and copper mineralization. The sulphide proto ore original location is also indicated.

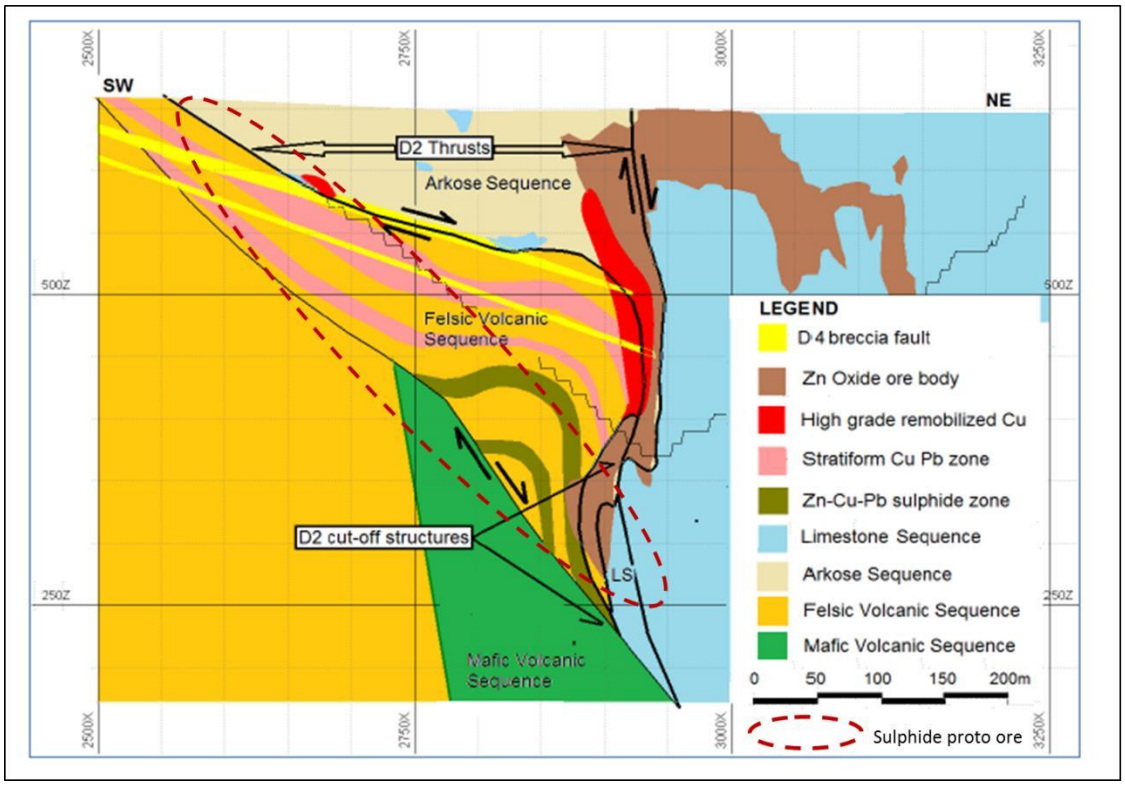

Figure 49: South West - North East Cross Section through the Skorpion Zinc Deposit, with illustrations of the D4 breccia faults, the different mineralization zone and lithologies; the sulphide proto ore is indicated by the dashed red oval (adapted from Van Schalkwyk, 2016)

6 Conclusions

The majority of the lead mineralization is hosted by the felsic metavolcanics as galena and in the metasiliciclastics as pyromorphite, a lead manganese phosphate. Subordinate, although elevated lead mineralization also occurs in graphitic schists, within gossans and along fault zones. The major host lithologies represent a rift environment followed by a low energy sedimentary environment. In terms of the mineral textures, the lead minerals appear to be mainly secondary phases that have been remobilized and reprecipitated as secondary galena in pyrite cracks, around pyrite and intergrown with chalcocite and greenockite. Galena and, predominantly, pyromorphite have reprecipitated in veins and are concentrated along fault zones. Moreover, elevated pyromorphite concentrations occur within gossanous zones in close association with iron and manganese oxides. These textures represent supergene enrichment of a sulphide proto ore. However, in contrast to Cu and Zn mineralization, Pb was not remobilized far from the proto-ore, as a function of its poor mobility in acidic fluids (Reddy et al., 1995). The poor correlation observed between lead, zinc and copper in the felsic metavolcanics is justified by the relative mobilities of the three metals. Texture of the major host lithologies, lead mineralization textures as well as the metal correlations imply the following genesis for the depositional environment and mineralization:

1) Submarine felsic volcanism induced by rifting and consequent partial melting of the upper crustal rocks during opening of the Adamastor Ocean

2) Submarine sulphide precipitation coincident with moderate to low energy sedimentation

3) Late stage lacustrine, particularly limestone, deposition during closure of the Adamastor Ocean

4) Deformation caused by closure of the Adamastor Ocean which eventually resulted in extreme faulting, folding and metamorphism

5) This was followed by uplift, erosion and oxidation of the primary sulphide mineralization by acidic fluids flowing through fault conduits

6) Oxidation of pyrite promoted dissolution of primary galena, chalcopyrite, chalcocite, sphalerite and feldspars

7) Remobilization and reprecipitation of the dissolved metals as the pH and Eh conditions changed

The average lead isotope ratios of $^{206}Pb/^{204}Pb$ (17.26), $^{207}Pb/^{204}Pb$ (15.60) and $^{208}Pb/^{204}Pb$ (37.42) resemble results provide by Frimmel (2004) for both the Skorpion and Rosh Pinah deposits. For the Skorpion samples from Frimmel (2004) had the following average ratios: $^{206}Pb/^{204}Pb$ (17.29), $^{207}Pb/^{204}Pb$ (15.59) and $^{208}Pb/^{204}Pb$ (37.51). The Rosh Pinah samples had the following average ratios: $^{206}Pb/^{204}Pb$ (17.17), $^{207}Pb/^{204}Pb$ (15.61) and $^{208}Pb/^{204}Pb$ (37.45). Lead isotopic signatures of the mineralization

indicates lead derivation from the lower 2.0 Ga Eburnean pre-Gariep basement in agreement with Frimmel et al. (2004). The host felsic metavolcanics might have been derived from melting of the basement rocks during the formation of the Adamastor Ocean with upper crustal contamination. Compared to the Rosh Pinah deposit lead isotope signatures, the Skorpion lead isotopes overlap with the Rosh Pinah deposit isotopes, but have a much narrower range. This is an indication of a much shorter lived and potentially fast mineralization event contrary to the SEDEX type Rosh Pinah deposit. The smaller nature of the Skorpion deposit, its poorer lead concentrations and the elevated radiogenic lead substantiates this theory. Moreover, SEDEX deposits are generally fed by deep seated conduits that allow more leaching of metals from the underlying basement rocks with minor influence from upper crustal rocks. This allows for richer and larger deposits to be formed. Frimmel et al. (2004) indicated that smaller, syn-orogenic base metal deposits within the Rosh Pinah area seem to have been more influenced by surrounding country rock during the movement of orogenic fluids. These fluids introduced more radiogenic lead as seen with the elevated lead ratios of the study.

7 Recommendations

To realize the potential of the lead mineralization of the Skorpion deposit in the near future, the following is recommended:

- With the aid of further drilling within the western zones of the deposit, a resource estimation should be conducted to better define the extent of the mineralization as well as identify further hot spots (the fault zones are currently the main hot spots identified)
- A detailed mineralogical analysis and leaching potential of the identified hot spots should be conducted to determine what methods can be used to treat the lead
- Additionally, the lead content of the stockpiled copper rich material should be assessed and its leachability should also be determined
- It is also recommendable to initiate with the analysis of lead within the Grade Control samples with the onsite laboratory in order to have more closer spaced data for better and prompt decision making
- Moreover, routine estimation of lead within the Grade Control Model is recommended once the lead analysis by the onsite laboratory commences

8 References

Alchin DJ and JM Moore. (2005). A review of the Pan-African, Neoproterozoic Rosh Pinah Zn-Pb deposit, south western Namibia. South African Journal of Geology Volume 108, 71-86.

Anon. (2012, February 1). http://www.coalgeology.com/lead-geochemistry-eh-ph-solubility-and-remedial-technologies/21720.

Anon. (2018, February). https://www.lme.com/Metals/Non-ferrous/Lead#tabIndex=2.

Anon. (2018). https://www.trevali.com/operations/gergarub.

Anon. (2018). https://www.trevali.com/operations/rosh-pinah-zinc-mine.

Boni, M. (2003). Non-sulphide Zinc Deposits: a new-(old) type of Economic Mineralisation. SGA News, 15.

Borg G., Kärner K., Buxton M., Armstrong R. & Van der Merwe S.W. (2003). Geology of the Skorpion Zinc Deposit, Southern Namibia. Economic Geology, 749-771.

Borg, G. (2000). Regional controls on sediment-hosted Pb-Zn (Ba-Cu) occurances within the Pan African orogeic belts in Namibia. Communs geol Surv. Namibia , pp. 239-249.

Borg, G., Kärner, K. & Klein, E. (2005): Structural control on the localisation and deep oxidation of the Skorpion supergene zinc deposit, Namibia. Abstract Volume, 8th Biennial SGA Meeting, Beijing, August 18 – 21, 2005.

Ceyhan, N. (2003). Lead Isotope Geochemistry of Pb-Zn Deposits from Eastern Taurides, Turkey. MSc, Department of Geological Engineering.

Churchman, G.J and Lowe, D,J. (2012). Alteration, Formation and Occurence of Minerals in Soils. Handbook of Soil Sciences.

Corrans RD, Gewald H , Whyte R M and Land B N. (1993). The Skorpion SZ Secondary Zinc Deposit- South Western Namibia.Skorpion Zinc Mine Internal Report.

Coward MP and Davis C. (1982). The structural evolution of the Gariep Arc in southern Namibia. Precambr. Res, 173-198.

Dirks P.H.G.M. (2004). A Structural Geological Framework for the Skorpion Zn Deposit; Implications for Pit Design and Ore Body Genesis. Skorpion Zinc Mine Internal Report.

Eggleston, C.M., Ehrhardt, J.J. and Stumm, W. (1996). Surface structural controls on pyrite oxidation kinetics: An XPS-UPS, STM, and modelling study. American Mineralogist Volume 81, 1036-1056.

Evans, A. M. (1993). Ore Geology and Industrial Minerals: An Introduction. Blackwell Science Ltd. .

Frimmel H E and Board W S . (2000). Fluid evolution in and around the Rosh Pinah massive sulphide deposit in the external Pan-African Gariep Belt, Namibia. South African Journal of Geology 103, 191-206.

Frimmel H E and Lane K. (2005). Geochemistry of carbonate beds in the Neoproterozoic Rosh Pinah Formation, Namibia: Implications on depositional setting and hydrothermal ore formation. South African Journal of Geology 108, 5-18.

Frimmel H.E, Hartnady CJH and Koller F. (1996). Geochemistry and Tectonic Setting of Magmatic Units in the Pan-African Gariep Belt, Namibia. Chemical Geology 130, 101-121.

Frimmel Hartwig E, Jonasson Ian R , Mubita P. (2004, April 2). An Eburnean base metal source for sediment-hosted zinc-lead deposits in Neoproterozoic units Namibia: Lead isotopic and geochemical evidence. Mineralium Deposita, pp. 328-343.

Frimmel H., Klotzli U. and Siegfried P. (1996). New Pb-Pb Single Zircon Age Constraints on the Timing of Neoproterozoic Glaciation and Continental Break-up in Namibia. The Journal of Geology, 459-469.

Frimmel HE and Frank W. (1998). Neoproterozoic tectono-thermal evolution of the Gariep Belt and its basement, Namibia and South Africa. Precambrian Research, 1-28.

Frimmel HE (2008) Neoproterozoic Gariep Orogen: The Geology of Namibia, Chapter 14 pg.1-39,

Gutzmer, J. (2004). Characterization of supergene manganese oxihydroxidses from the Skorpion Mine, Namibia. Johannesburg: Technical Report, Anglo American Plc.

Kärner, K. (2006). The Metallogenisis of the Skorpion Non-sulphide Zinc Deposit, Namibia . Dissertation Submitted to the University of Martin Luther, Halle-Wittenberg

Large, D. (2001). The geology of non-sulphide zinc deposits: An Overview. Erzmetall 54 , 264-276.

Mondillo, M and Boni N. (2015). The “Calamines” and the “Others”: The great family of supergene. Ore Geology Reviews 67, 208-233.

Boni, M. & Large, D. (2003): Non-sulfide zinc mineralisation in Europe: An Overview.

Economic Geology, 98, 4, 715 – 729.

Reddy, K.J ,Wang, L. and Gloss, S.P. (1995). Solubility and mobility of copper, zinc and lead in acidic environments. Plant and Soil 171, 53-58.

Ridley, W. I. (2010). Volcanogenic Massive Sulfide Occurrence Model. U.S. Department of the Interior and U.S. Geological Survey.

Rozendaal A, Stalder M and Alchin D. (2005). Wall rock alteration and lithogeochemical haloes associated with the sediment-hosted Rosh Pinah Zn-Pb-Ag deposit in the Pan-African Gariep Belt, south western Namibia. South African Journal of Geology 108, 119-134.

Saayman, D. F. (2011). Silver Mineralization in the Skorpion Zinc Ore Body. University of Stellenbosch (Unpublished).

Simandl, G. J. , Paradis, S. and Akam, C. (2015). Graphite deposit types, their origin, and economic. Symposium on critical and strategic materials. British Columbia Geological Survey Paper.

Sitoka, S. (2012). Gergarub Zn Sulphide Mineralization Model: VMS vs SEDEX. Honours Thesis-Rhodes University (Unpublished)

Skarpelis, N. and Argyraki, A. (2009). Geology and Origin of Supergene Ore at the Lavrion. Resource Geology Vol 59, 1-14.

Theron, S.J and Carter, L.M. (2001). Preliminary Report: Mineralogical and Geochemical Examination of sixteen rock samples from the Skorpion Area, Namibia. Anglo American Internal.

Theron, S.J and Carter, L.M. (2001). Preliminary Report: Mineralogical and Geochemical Examination of Sixteen Rock Samples from the Skorpion Area, Namibia. Anglo American Internal.

Van Schalkwyk CL. (2016). Notes on the Geology of the Skorpion Pit. Skorpion Zinc Mine Internal Report

Wang, Z. ,Laurenz, V., Petitgirard, S. and Becker, H. (2016). Earth's Moderately Volatile Element Composition May not be Chondritic: Evidence from In, Cd and Zn. 47th Lunar and Planetary Science Conference.

Winter, J. (2010). Principles of Igneous and Metamorphic Petrology. Pearson Prentice Hall .

Zartman, R.E. and Doe, B.R. (1981) Plumbotectonics – The Model. Tectonophysics, 135-162

Zeng, N., Izawa, E. , Motomura, Y. and Lai, L. (2000). Silver Minerals and Paragenesis in the Kangjiawa Pb-Zn-Ag-Au Deposit of the Shuikoushan Mineral District, Hunan Province, China. The Canadian Mineralogist Volume 38, 11-22.

Appendix 1: Samples used for the study

Study Samples Descriptions and indication of samples used for Thin Sections and/ or Polished Sections

Original Sample	Sample ID	Description	Thin Section/Plolished Section
Pb01	Pb01-A	Grey rock with some irregular veins of white and grey fine grained mineral, minor dissiminated pyrite grains	Polished Section
	Pb01-B	Grey rock with some irregular veins of white and grey fine grained mineral	Thin Section
Pb02	Pb02-A	White grey rock with black mineral withing a vein, quartz and muscovite	Polished Section
	Pb02-B	White grey rock with black mineral more stubby and slightly elongated, quartz and muscovite	Thin Section
Pb03	Pb03-A	Light grey rock with dark mininerl and dessiminated pyrite	Thin Section
	Pb03-B	Grey rock, minor dissiminated pyrite grains,dark grey metallic mineral in aggregates	Polished Section
Pb04	Pb04-A	Light grey quartz and muscovite rock with tiny dissiminated pyrite	Polished Section
	Pb04-B		
Pb05	Pb05-A	Redish brown rock with iron oxides,massive and irregular	Thin Section

Original Sample	Sample ID	Description	Thin Section/Plolished Section
Pb05	Pb05-B	Banded rock brown rock with iron oxides	Thin Section
Pb06	Pb06-A	Whitish grey rock with dark grey mineral and minor dissiminated pyrite	Thin Section
	Pb06-B	Whitish grey rock with dark grey mineral and minor dissiminated pyrite	Polished Section
Pb07	Pb07-A	Very hard light grey rock with vugs filled with an earthy crystalline mineral	Thin Section
	Pb07-B	Very hard light grey rock with vugs filled with an earthy crystalline mineral, however much less of the earthy mineral and with some pyrite grains	Polished Section
	Pb07-C	Very hard light grey rock with vugs filled with an earthy crystalline mineral, however with some iron oxide staining on earthy mineral	Thin Section
Pb08	Pb08-A	Light brown orange rock with some oxidized minerals	Thin Section
	Pb08-B	Light brown orange rock with some oxidized minerals	Polished Section
Pb09	Pb09-A	Whitish pink rock with pinkish mineral vein, medium grained	Thin Section
	Pb09-B	Iron and manganese rich rock, massive and dark brown, fine grained	Polished Section

Original Sample	Sample ID	Description	Thin Section/Plolished Section
Pb09	Pb09-C	Iron and manganese rich rock, massive and dark brown, fine grained, with aggregates of manganese mineral	Thin Section
Pb10	Pb10-A	Dark brown rock with clasts of a white rock, and thin dark veins	Thin Section
	Pb10-B	Iron and manganese rich rock, massive and dark brown, fine grained	Thin Section
	Pb10-C	Black brown rock with whitish veinlet	Thin Section
Pb11	Pb11-A	Fine grained dark grey graphitic rock, tiny dissiminated pyrite	Thin Section
	Pb11-B	Fine grained dark grey graphitic rock, tiny dissiminated pyrite, some whitish talcy mineral	Polished Section
Pb12	Pb12-A	Iron and manganese rich rock, massive and dark brown, fine grained	Polished Section
	Pb12-B	White with dark brown black bands	Thin Section

Appendix 2: Wavelength Dispersive Spectrometry Scans

Pb01-A and B (SK_204 @ 166 to 167): Confirmed presence of sphalerite and galena

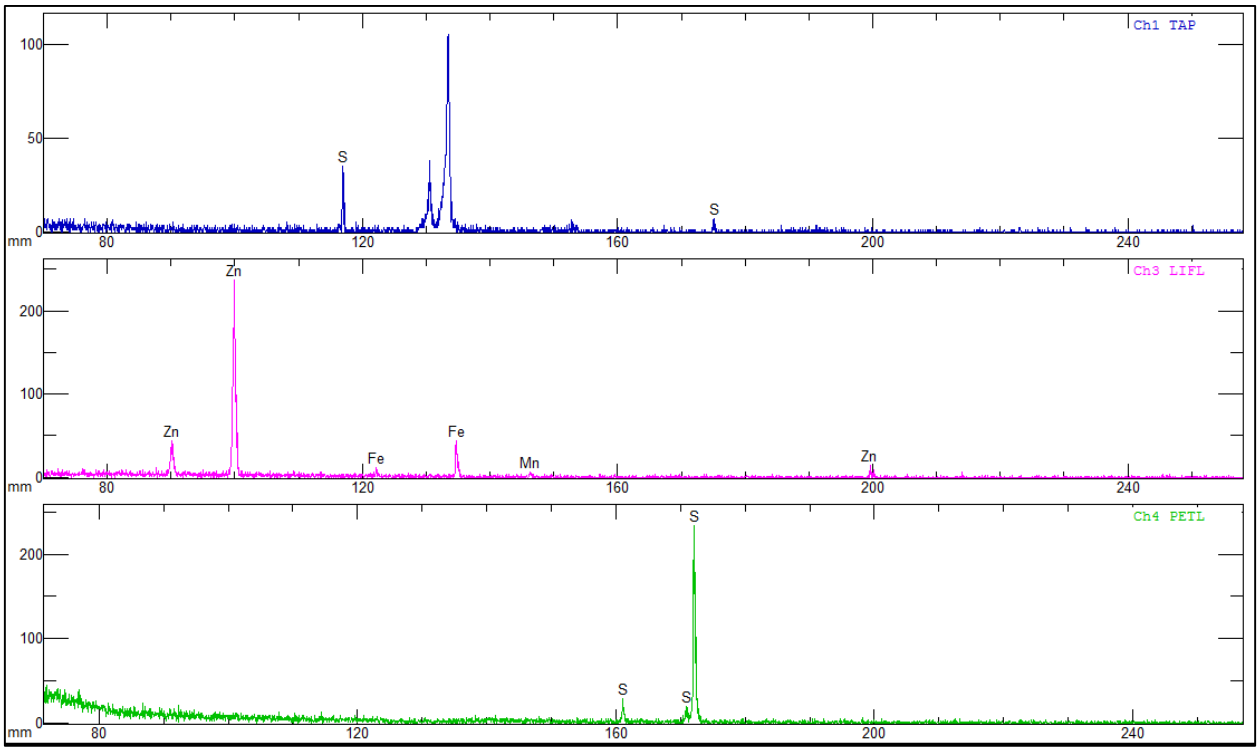

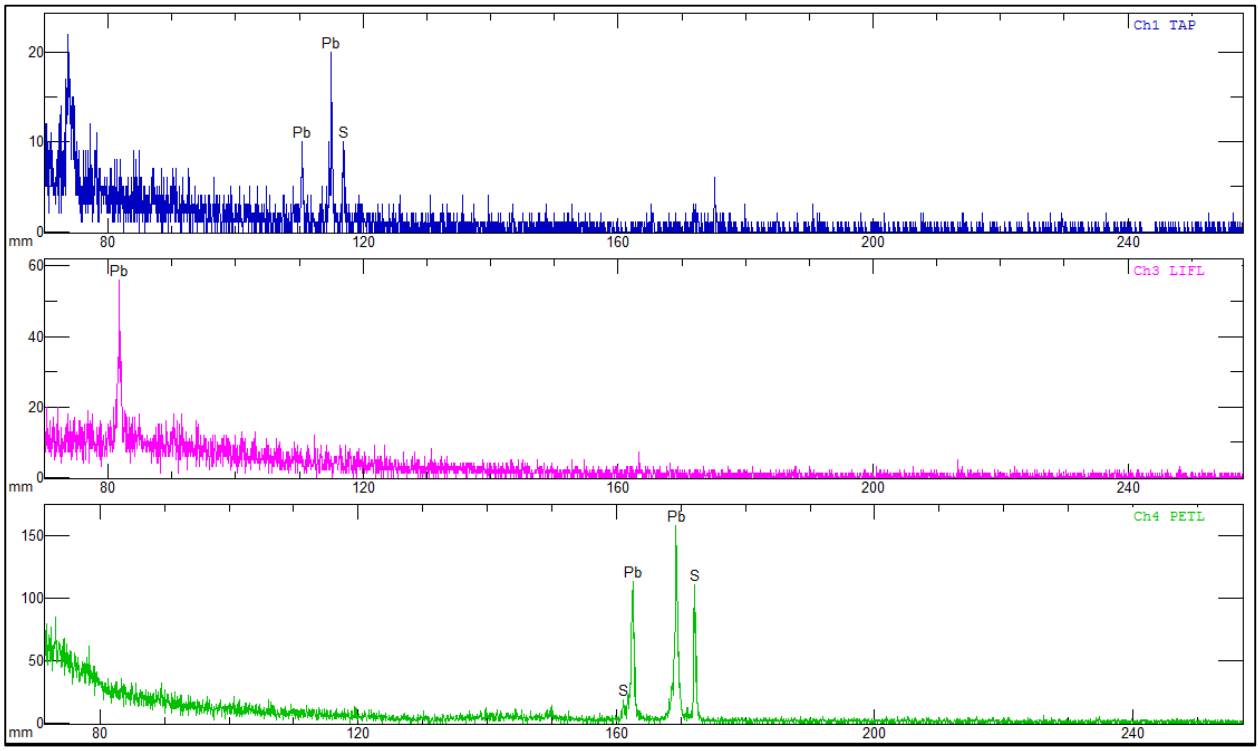

Pb04-A and B (SK_203): Confirmed presence of sphalerite and galena

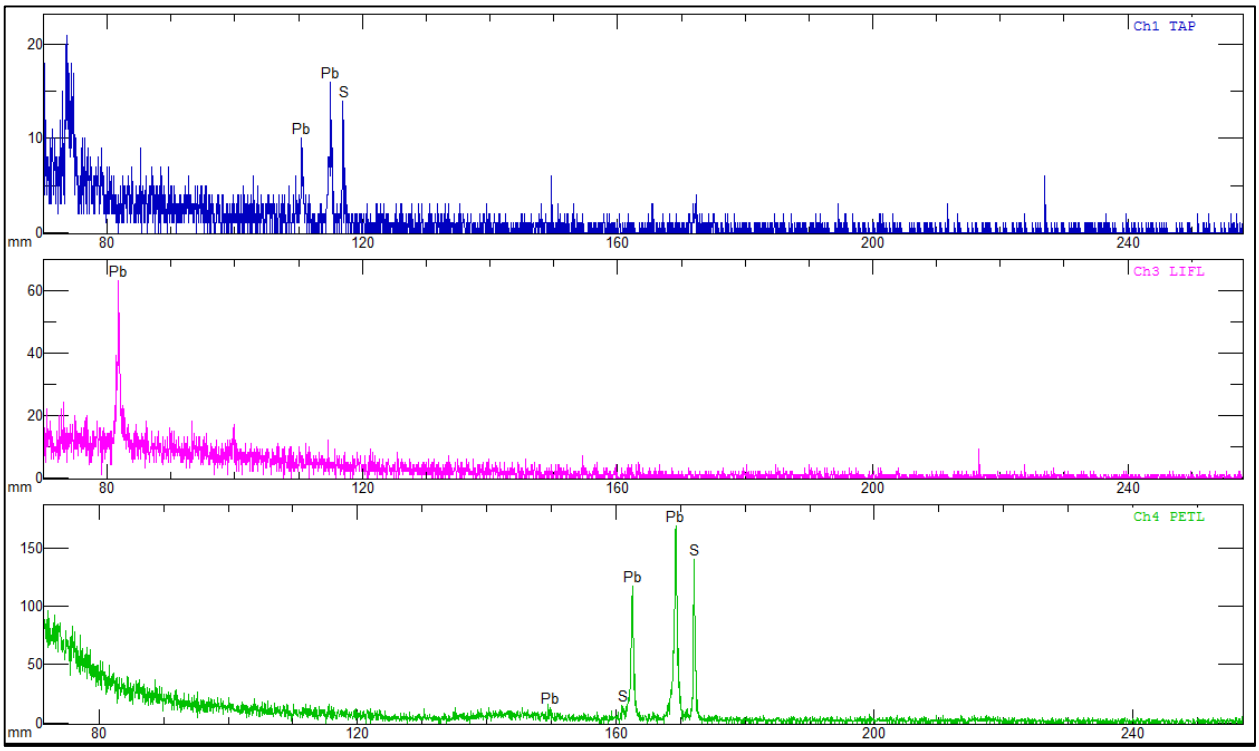

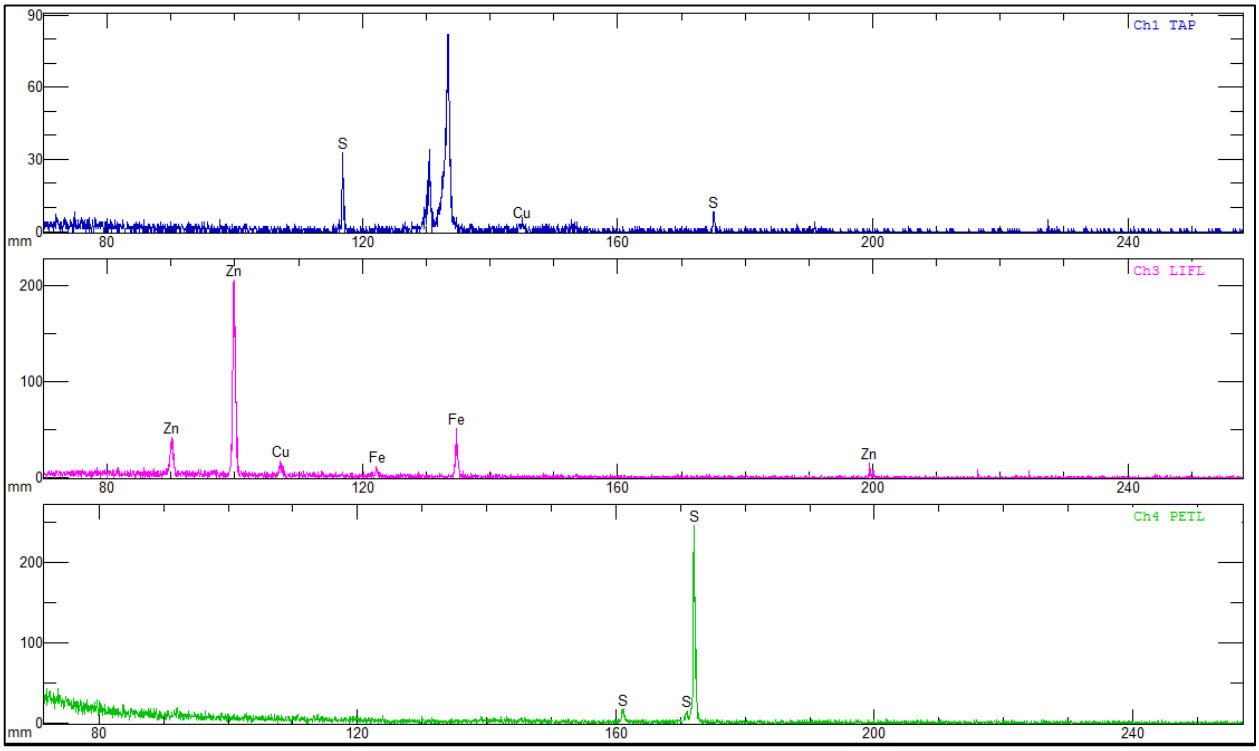

Pb07-A and B (SK_204 @ 225to 227): Confirmed the presence of pyromorphite

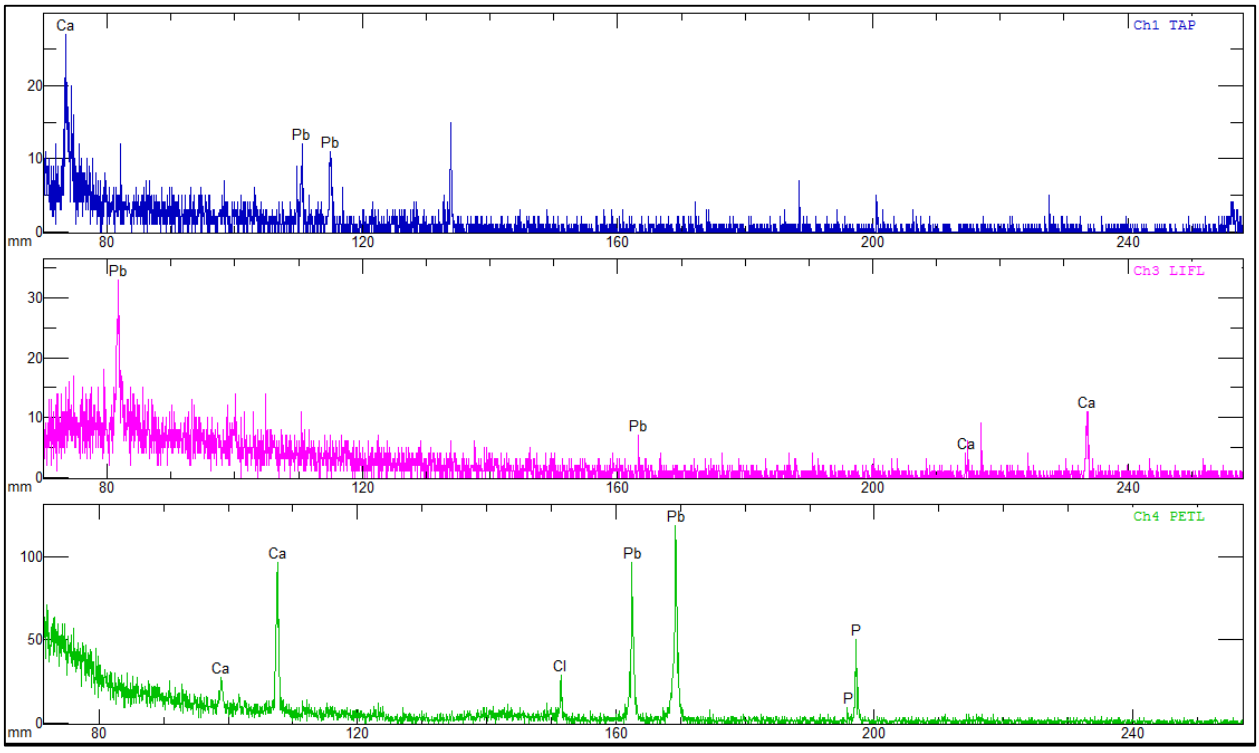

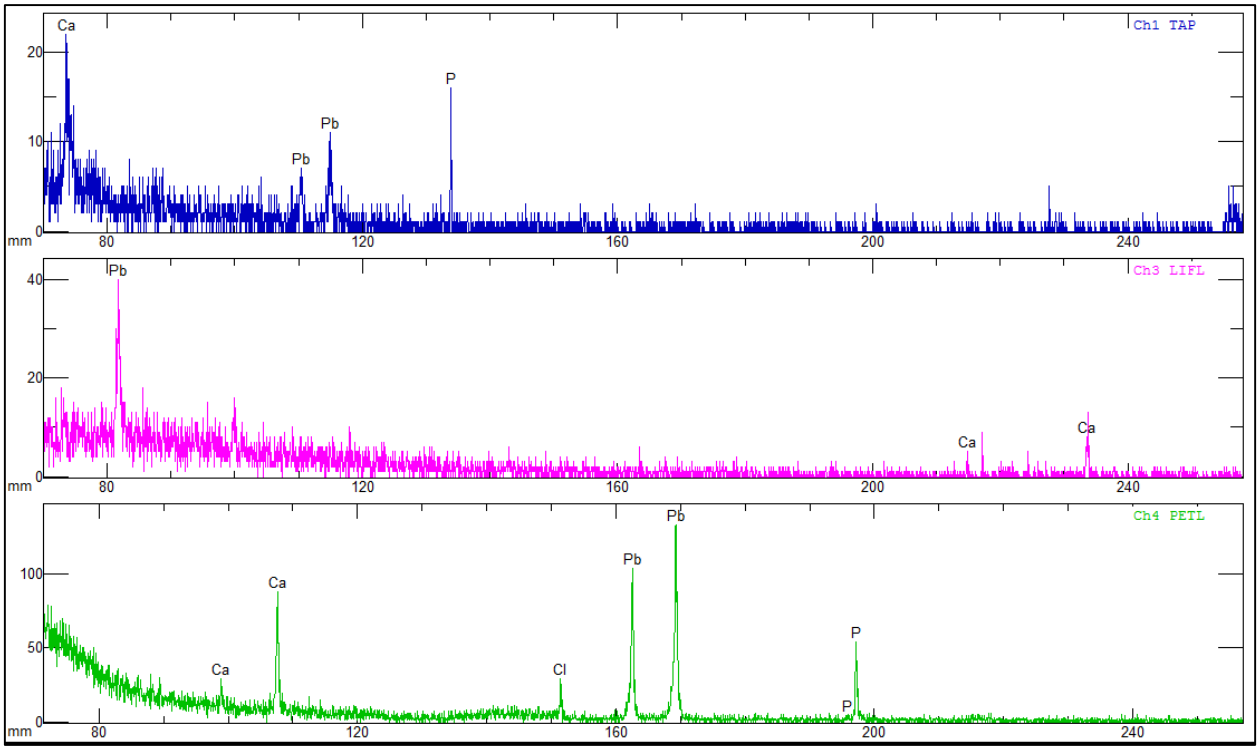

Pb010-A and B (SKSDD05 @ 343 to 347): Confirmed the presence of zircon